Optical Properties of Semiconductors

Jérôme Faist

Eidgenössische Technische Hochshule Zürich

Zürich, May 2008

Contents

List of Figures

List of Tables

variables used

Physical constants:

ϵ_0	vaccuum permettivity
q	electron charge
k	Boltzmann constant
m_0	Electron mass
P	Kane's matrix element
E_P	Kane energy

Variables:

α	absorption coefficient
E	Energy
ε	Energy
$\mathcal{E}$	Electric field
ϵ	Dielectric constant
μ	Chemical potential (energy units)
$|\psi\rangle, \psi(x)$	Electron wavefunction
τ	Lifetime
n_{refr}	Refractive index

Chapter 1

Introduction

These are the notes of a lecture given in the spring semester of 2008, entitled "optical properties of semiconductors". The goal of this lecture was to give a broad overview of the basic physical processes that govern the interaction between the light and semiconductor. My goal was to show the richness of the topic and to show the thread connecting the original research of the sixties and today's litterature. Whenever possible, I tried to show the connection between the fundamental aspects and the applications in today's devices. At this stage, these lecture notes are rather patchy and are not trying to substitute for a complete text.

1.1   bibliography

1.1.1   Introductory texts

Here I mention introductory textbooks that have a section on optical properties of semiconductors.

C. Kittel "Introduction to solid state physics" . Chapts 1-3 treat elementary aspects of optical properties of solids

Ashcroft & Mermin,"Solid state physics" .(Saunders College) In this classic Solid State physics reference textbook, chapter 28 and 29 summarize the semiconductor general properties in an fairly elementary level.

K. Seeger "Semiconductor Physics, an introduction" (Springer). Contains numerous derivations of analytical expressions. Chapt 11-13 treat optical properties.

M. Balkanski and R.F. Wallis, "Semiconductor Physics and Applications" (Oxford). Very good treatement, includes some fairly advanced treatements of the optical properties (Chapt 10,11,14,17)

1.1.2   Advanced treatements

This list contains the references I used to prepare the lecture.

E. Rosencher and B. Winter "Optoelectronics" . Very good presentation, more oriented towards devices.

H. Haug and S.W. Koch "Quantum Theory of the Optical and Electronic Properties of S (World Scientific). Advanced treatements of the semiconductor optical properties, more oriented towards theory.

Yu and Cardona "Fundamentals of semiconductor" (Springer) Excellent reference book, geared more towards the fundamental aspects of the optical properties.

G. Bastard "Wave mechanics applied to semiconductor heterostructures" (Les editions de physique). Very good description of the computation of electronic state in semiconductor heterostructures.

P. Zory "Quantum well lasers" (Wiley?) Contains some good chapters on quantum well semiconductor lasers, especially one written by S. Corzine.

1.2   Notes and acknowledgements

Under this form, this script is meant for "internal use" since it does not always give proper credit to the figures, especially for the ones taken from the books cited above. The author would like to acknowledge Giacomo Scalari for his help in preparing this lecture, as well as the one from Profs L. Degiorgi, Prof. B. Devaud-Pledran, Prof. A. Fiore who nicely volonteered with some of their data. Tobias Gresch prepared the artwork of the cover.

Chapter 2

Introduction to Semiconductors

In this chapter, we would like to rapidely review the key concepts on semiconductors. See Chapter 28 of Ashcroft and Mermin's book.

2.1 Crystalline structure and symmetries

A perfect crystal is invariant under the translational symmetry

$$\vec{r} \to \vec{r} + u\vec{a} + v\vec{b} + w\vec{c} \tag{2.1.1}$$

where u,v,w are integers.

The crystalline structure of GaAs is displayed in Fig. 2.1, and is of the ZincBlende type. It consists of two interpenetrated diamond lattices.
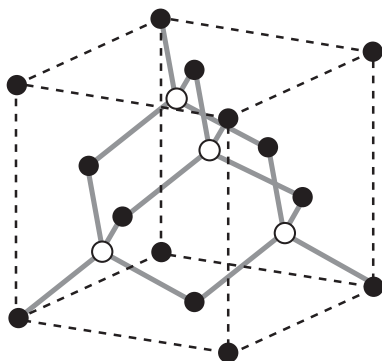
Figure 2.1: Zinc-blende crystalline structure
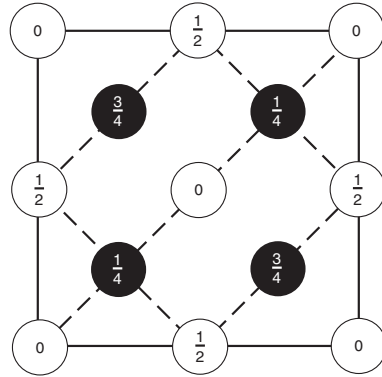
Figure 2.2: Zinc-blende crystalline structure

$Nb\,of\,atoms\,per\,cell$

$$
\begin{aligned}
&= \frac{Nb\,summets}{8} + \frac{Nb\,atomes\,faces}{2} + Nb\,atomes\,interieurs \\
&= \frac{8}{8} + \frac{6}{2} + 4 \\
&= 8
\end{aligned} \tag{2.1.2}
$$

per cell.

The structure does not posess any center of symmetry. The basis of this zinc-blende structure are thetrahedrical bonds Si-Si or Ga-As. Each atom is the origin of a double bond towards its nearest neighbors, as shown in Fig. 2.3. The absence of inversion symmetry is also apparent on these tetrahedric bonds.
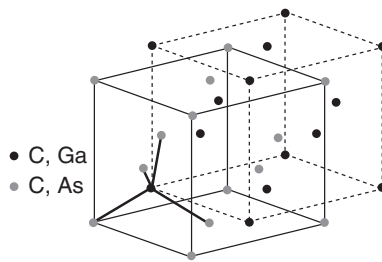
Figure 2.3: Terahedrical bond of the zinc-blende

2.1.1   Wigner-Seitz cell

A Wigner-Seitz cell is the region of the space that is closer to a specific point of the lattice than to any other point of the lattice.A primitive Wigner-Seitz cell is constructed by taking the perpendicular bisector planes of the translation vectors from the chosen centre to the nearest equivalent lattice sites.

2.1.2 Reciprocal lattice

The set of all wave vectors $\vec{K}_n$ that yield plane waves with the periodicity of a given Bravais lattice is known as its reciprocal lattice. The bases vectors of the reciprocal lattice are given by:

$$\vec{A} = \frac{2\pi}{\vec{a} \cdot (\vec{b} \times \vec{c})} \vec{b} \times \vec{c} \tag{2.1.3}$$

and by rotation of indices. The reciprocal space exhibits translational periodicity with all equivalent reciprocal wavevectors spanned by the set of integers h,k,l

$$\vec{G} = h\vec{A} + k\vec{B} + l\vec{C} \tag{2.1.4}$$

The set of wavevectors $\vec{G}$ is a basis into which the crytal potential may be expanded:

$$V(\vec{r}) = \sum_{\vec{G}} V_{\vec{G}} \exp(i\vec{G}\vec{r}) \tag{2.1.5}$$

2.2 Wavefunctions of the crystal, Bloch Theorem

The Hamiltonian of a semiconductor crytal has the translation symmetry

$$H(\vec{r} + \vec{R}) = H(\vec{r}) \tag{2.2.6}$$

with $\vec{R}$ being a reciprocal lattice vector.

The Bloch theorem states that the wavefunctions have two "good" quantum numbers, the band index n and a reciprocal vector $\vec{k}$ such that the wavefunctions of the crystal may be written as:

$$\psi_{nk}(\mathbf{r}) = e^{i\mathbf{k}\cdot\mathbf{r}} u_{nk}(\mathbf{r}) \tag{2.2.7}$$

where $u_{nk}(\mathbf{r} + \mathbf{R}) = u_{nk}(\mathbf{r})$ exhibits the periodicity of the crystal.

It may also be written as:

$$\psi_{nk}(\mathbf{r} + \mathbf{R}) = e^{i\mathbf{k}\cdot\mathbf{r}} \psi(\mathbf{r}). \tag{2.2.8}$$

2.2.1 Proof of Bloch's theorem

Ashcroft & Mermin, chapt 8
Translation operator

$$T_{\mathbf{R}}\psi(\mathbf{r}) = \psi(\mathbf{r} + \mathbf{R}). \tag{2.2.9}$$

If $\mathbf{R}$ belongs to the Bravais lattice, the operator will commute with the Hamiltionian

$$\begin{aligned} T_{\mathbf{R}} H \psi(\mathbf{r}) &= H(\mathbf{r} + \mathbf{R})\psi(\mathbf{r} + \mathbf{R}) \\ &= H(\mathbf{r})\psi(\mathbf{r} + \mathbf{R}) = H T_{\mathbf{R}}\psi(\mathbf{r}) \end{aligned} \tag{2.2.10}$$

and therefore

$$T_{\mathbf{R}} H = H T_{\mathbf{R}}. \tag{2.2.11}$$

These two operators form a common set of commuting observable, we can therefore write the wavefunctions using eigenfunctions of both:

$$H\psi = E\psi T_{\mathbf{R}}\psi = c(\mathbf{R})\psi. \tag{2.2.12}$$

Considérons maintenant les propriétés de $c(\mathbf{R})$

$$T_{\mathbf{R}}T_{\mathbf{R}'} = T_{\mathbf{R}+\mathbf{R}'} \tag{2.2.13}$$

et donc

$$c(\mathbf{R})c(\mathbf{R}') = c(\mathbf{R} + \mathbf{R}'). \tag{2.2.14}$$

To simplify somewhat the notation, a_i with $i = 1, 2, 3$ the basis vectors of the primitive Bravais lattice, and b_i the basis vector of the reciprocal lattice. We can always define (because $c(a_i)$ is always normalized to unity:

$$c(a_i) = e^{2\pi i x_i}. \tag{2.2.15}$$

If now $\mathbf{R}$ is a translation of the Bravais lattice, it can be written as

$$\mathbf{R} = n_1 a_1 + n_2 a_2 + n_3 a_3, \tag{2.2.16}$$

then, using 2.2.15

$$
\begin{aligned}
c(\mathbf{R}) = c(n_1\mathbf{a_1} + n_2\mathbf{a_2} + n_3\mathbf{a_3}) \\
= c(\mathbf{a_1})^{n_1} c(\mathbf{a_2})^{n_2} c(\mathbf{a_3})^{n_3} \\
= \sum_{i=1..3} e^{2\pi x_i n_i}.
\end{aligned}
\tag{2.2.17}
$$

Using the orthogonality relations between the direct and reciprocal basis vectors, written as

$$\mathbf{a_i} \cdot \mathbf{b_j} = 2\pi\delta_{ij}. \tag{2.2.18}$$

Considering the product between the vector $\mathbf{R}$ of the real space and the vector k of the reciprocal space, written in the basis of the $\mathbf{b_i}$:

$$\mathbf{k} = \sum_{i=1..3} k_i\mathbf{b_i}, \tag{2.2.19}$$

and then

$$\mathbf{k} \cdot \mathbf{R} = 2\pi(k_1 n_1 + k_2 n_2 + k_3 n_3). \tag{2.2.20}$$

It was in fact the result we had obtained for $c(\mathbf{R})$, that was written as:

$$
\begin{aligned}
c(\mathbf{R}) = \exp(2\pi i(x_1 n_1 + x_2 n_2 + x_3 n_3) \\
= \exp(i\mathbf{k} \cdot \mathbf{R})
\end{aligned}
\tag{2.2.21}
$$

setting naturally $x_i = k_i$. The wavefunctions may well be written as:

$$
\begin{aligned}
T_{\mathbf{R}}\psi = \psi(\mathbf{r} + \mathbf{R}) \\
= c(\mathbf{R})\psi = e^{i\mathbf{k}\cdot\mathbf{R}}\psi(\mathbf{r})
\end{aligned}
\tag{2.2.22}
$$

that is one of the equivalent formulations of the Bloch theorem.

2.3 Electronic states: formation of bands and gaps

Bragg reflection and the perturbed electron

2.4 Band structure of III-V and group IV semiconductors

Look at the band structure of Si, GaAs, InP

2.4.1 Group IV semiconductors (Si,Ge)

The band structure of these semiconductors is very similar because:

1. They do crystallize in the same crystallographic structure (diamond)

2. they have similar electronic outer orbitals

The structure of silicon is purely covalent. The last orbital of atomic silicon has the electronic configuration $3s^2p^2$. There are therefore 4 electrons ($2s$ et $2p$) sharing an orbital that could contain 8 (2 for the s orbital, 6 for the p orbital). Silicon has therefore 4 valence bands. The band structure of silicon and germanium, two most important semiconductors formed using the column IV of the periodic table, is shown in Fig. 2.4.
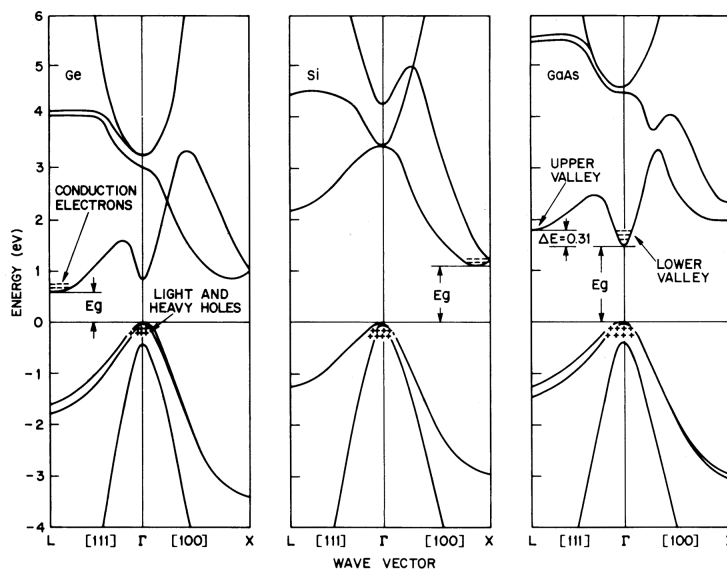
Figure 2.4: Germanium (left), Silicon (center) and Gallium Arsenide (right) band structures.

The valence band maximum is at $k = 0$ and is degenerate with the heavy and light hole bands. A third important valence band is the "spin-split" called this way because it is split

by the spin-orbit interaction. Finally, most important in the band structure of Silicon and Germanium is the fact that the minimum of the conduction band does not coincide with the maximum of the valence band. The semiconductor is called "indirect" (See Fig. 8.1.

The conduction band minimum in silicon is in the direction $[010]$ and, as a result, also in the directions $[0\bar{1}0], [001], [00\bar{1}], [100], [\bar{1}00]$ for a total of six minima.
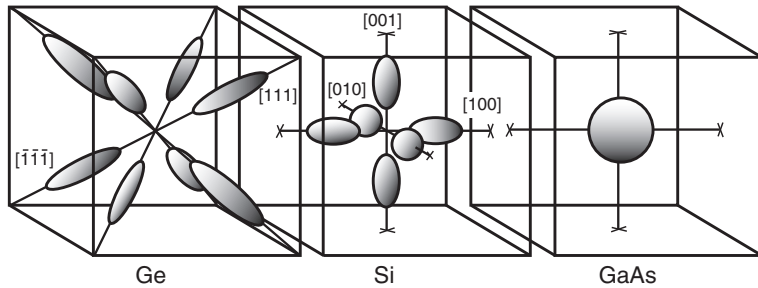
Figure 2.5: Minima of the conduction band of Si, Ge and GaAs

In Germanium, in contrast, the conduction band minimum is in the directions corresponding to the cube's diagonal, and we have therefore 8 conduction band minima.

2.4.2 III-V Semiconductors (GaAs, InP, ..)

The band structure of III-V semiconductors is similar since the tetrahedral bonds have the same structure as the ones in Silicon or Germanium. In fact, the missing electron of the group III with the electron configuration $4s^2 4p$ (for example Gallium) is provided by the column V element (for example Arsenic) of configuration $4s^2 4p^3$ and these bonds have a low ionicity.
For a large number of III-V semiconductors, the bandgap is direct.
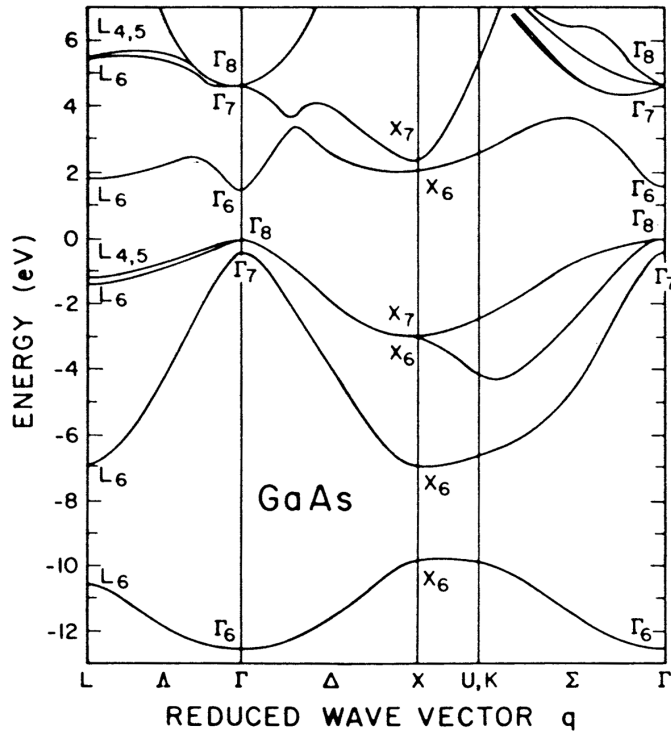
Figure 2.6: Structure de bande du GaAs

As an example, the computed band structure of GaAs is shown in Fig. 2.6.

2.5 Effective mass approximation

2.5.1 Band extrema, effective mass

Even though the band structure of semiconductors is in general very complex, as apparent in Fig. 2.6, the fact that the Fermi level lies in the middle of the forbidden bandgap enables us to consider the band structure in a region close to the band extrema. In that case, the band dispersion can be expanded $\epsilon(k)$ into a second order Taylor series:

$$\epsilon(k) = \epsilon_0 + \sum_{i=1..3} \frac{\partial^2 \epsilon}{\partial k_i^2} \cdot (k_i - k_0)^2. \tag{2.5.23}$$

The equation 2.5.23 is written in the simplified case that the energy ellipsoid are aligned with the x, y and z axis of the coordinate system; in the general case terms of the form $\frac{\partial^2 \epsilon}{\partial k_i \partial k_j}$ must be added.

By analogy with the free electron case, the term of the expansion can be identified with the inverse of an effective mass:

$$\frac{1}{m^*_{x,y,z}} = \frac{1}{\hbar^2} \frac{\partial^2 \epsilon}{\partial k^2_{x,y,z}}. \tag{2.5.24}$$

2.5.2 Semiclassical electron dynamics

The analogy may be pushed further: the group velocity of the electron is:

$$v_g = \frac{1}{\hbar}\frac{\partial(\hbar\omega)}{\partial k} = \frac{1}{\hbar}\frac{\partial\epsilon}{\partial k}. \tag{2.5.25}$$

and the electron will obey the semiclassical electron dynamics given by:

$$\vec{F} = \hbar\frac{d\vec{k}}{dt} \tag{2.5.26}$$

where

$$\vec{F} = -q\mathcal{E} - q\vec{v}\times\vec{B} \tag{2.5.27}$$

is the classical force on the electron

2.5.3 The hole

The motion of the electrons in a not completely filled band with negative mass can be interpreted with a particle called the hole, that has the following properties:

- Its mass is positive and given by $\frac{1}{m_h^*} = -\frac{1}{\hbar^2}\frac{\partial^2\epsilon}{\partial k^2}$

- Its wavevector is the opposite of the one of the missing electron: $k_h = -k_e$

- Its charge is positive and the opposite of the one of the electron $q_h = -q_e$

2.6 Density of states in 3, 2 and 1 dimensions

2.6.1 3D

Wavefunction

$$\psi(x,y,z) = Ae^{i(k_x x + k_y y k_z z)}. \tag{2.6.28}$$

In a finite volume, Born-von Karman periodic boundary conditions, $\psi(x+L, y, z) = \psi(x, y, z)$ imply:

$$\begin{aligned} k_x &= n_x 2\pi/L \\ k_y &= n_y 2\pi/L \\ k_z &= n_z 2\pi/L \end{aligned} \tag{2.6.29}$$

Using for the energy:

$$E = \frac{\hbar^2 k_{max}^2}{2m^*}. \tag{2.6.30}$$

and the number of state as a function of k_{max}

$$N(k_{max}) = \frac{\frac{4}{3}\pi k_{max}}{(2\pi/L)^3}. \tag{2.6.31}$$

we have

$$N(E) = \frac{2}{6\pi}\left(\frac{2m^*E}{\hbar^2}\right)^{3/2}L^3.$$

(2.6.32)

Differentiating with respect to the energy:

$$D(E) = \frac{dN(E)}{dE} = \frac{3}{2}\frac{2}{6}\frac{1}{\pi^2}\left(\frac{2m^*}{\hbar^2}\sqrt{E}\right) = \frac{1}{2\pi^2}\frac{(2m^*)^{3/2}}{\hbar^3}\sqrt{E}.$$

(2.6.33)

2.6.2   2D

$$D(E) = \frac{m^*}{\pi\hbar^2}$$

(2.6.34)

2.6.3   1D

$$D(E) = \frac{1}{\pi}\frac{\sqrt{2m^*}}{\hbar}\frac{1}{\sqrt{E}}.$$

(2.6.35)

2.7   Phonons

optical phonon, acoustic phonon

2.8   Doping

Impurities may act either as deep level, shallow levels or alloy.

2.8.1   Hydrogenoid donors

Same energy spectrum as the Hydrogen atom but renormalized by the dielectric constant
and the effective mass

2.9   Carrier statistics

2.9.1   Ferm-Dirac Statistics

The probability of finding an electron a energy E in a bath at temperature T is:

$$f(E, \mu, T) = \frac{1}{\exp\left(\frac{E-\mu}{kT}\right) + 1}$$

(2.9.36)

where k is Boltzmann's constant and μ is the chemical potential.
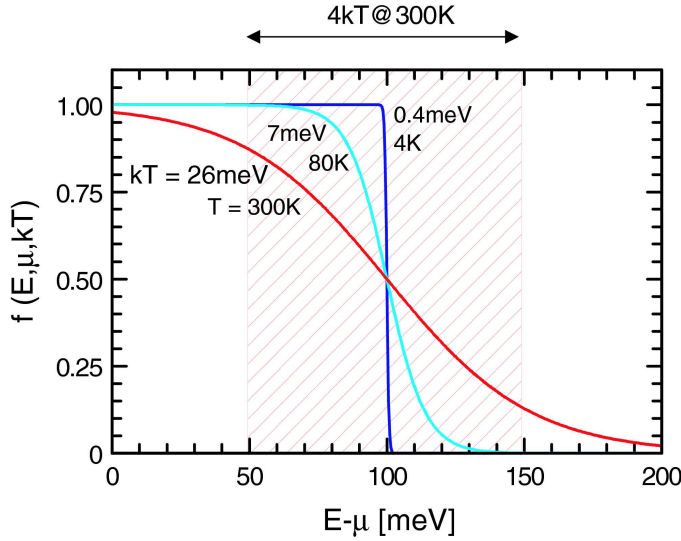
Figure 2.7: Fermi-Dirac distribution for various temperatures

The total number of electrons in the structure is the integral of the product of the density of state and the Fermi-Dirac distribution function.

$$N_{tot} = \int_{E=0}^{\infty} D(E) \frac{1}{\exp\left(\frac{E-\mu}{kT}\right) + 1} dE. \tag{2.9.37}$$

2.9.2 Holes

Distribution of holes: for the holes, one applies the rule (hole = no electrons) and then

$$f_h(E, \mu, kT) = 1 - f_e(E, \mu, kT) = \frac{\left(\frac{E-\mu}{kT}\right)}{\exp\left(\frac{E-\mu}{kT}\right) + 1} = \frac{1}{\exp\left(\frac{\mu-E}{kT} + 1\right)}. \tag{2.9.38}$$

2.9.3 Classical limit

In the case where $E - \mu >> kT$, the Fermi distribution can be simplified because $\exp\left(\frac{E-\mu}{kT}\right) >> 1$ and then

$$f(E, \mu, kT) \approx \exp\left(\frac{\mu - E}{kT}\right). \tag{2.9.39}$$

This corresponds to a probability of occupation much below unity and therefore is called the classical limit.
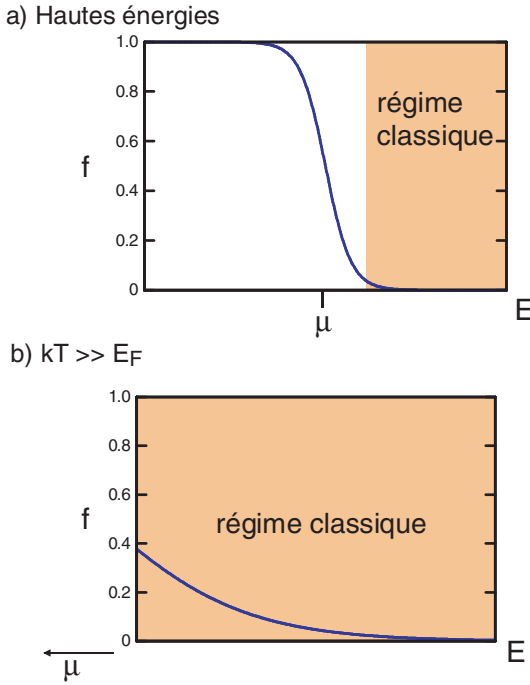
Figure 2.8: Regimes in which the classical limit can be used. a) High energies in a metal. b) Low doped semiconductor

In this approximation, the total number of electron can be computed in the bulk case:

$$n = \int_{E_G}^{\infty} \frac{1}{2\pi^2} \frac{(2m^*)^{3/2}}{\hbar^3} \sqrt{E - E_G} \exp\left(-\frac{E - \mu}{kT}\right) dE$$

$$n = \frac{1}{2\pi^2} \frac{(2m^*)^{3/2}}{\hbar^3} \exp(\mu kT) \int_{E_G} \infty \sqrt{E - E_G} \exp\left(-\frac{E}{kT}\right) dE. \tag{2.9.40}$$

To carry out the intégrale 2.9.40, we use a change of variable:

$$x = \frac{E - E_G}{kT}, dx = \frac{1}{kT} dE$$

$$\int_{E_G}^{\infty} \sqrt{E - E_G} \exp\left(-\frac{E}{kT}\right) dE = \sqrt{kT} \int_{x=0}^{\infty} x^{1/2} \exp(-x) \exp\left(-\frac{E_G}{kT}\right) dx kT \tag{2.9.41}$$

$$n = \frac{1}{2\pi^2} \frac{(2m^* kT)^{3/2}}{\hbar^3} \exp\left(\frac{\mu - E_G}{kT}\right) \int_{x=0}^{\infty} x^{1/2} \exp(-x) dx$$

The last integral is performed using Cauchy's formulai:

$$\int_{x=0}^{\infty} x^{1/2} \exp(-x) dx = \sqrt{\frac{\pi}{2}} \tag{2.9.42}$$

On obtains then finally:

$$n = 2\left(\frac{m_e k_B T}{2\pi \hbar^2}\right)^{3/2} \exp\left(\frac{\mu - E_G}{kT}\right). \tag{2.9.43}$$

The same approach can be carried over for the holes:

$$f_h \approx \exp\left(-\frac{\mu - E}{kT}\right). \tag{2.9.44}$$

Assuming that the zero of energy is on the top of the valence band:

$$p = \int_{-\infty}^{\infty} D_h(E) f_h(E) dE = 2\left(\frac{m_h k_B T}{2\pi \hbar^2}\right)^{3/2} \exp\left(\frac{-\mu}{kT}\right). \tag{2.9.45}$$

The product between electron and hole concentration yields:

$$n \cdot p = 4\left(\frac{kT}{2\pi \hbar^2}\right)^3 (m_e m_h)^{3/2} \exp\left(-\frac{E_G}{kT}\right). \tag{2.9.46}$$

The produt $n \cdot p$ depends only on the crystal nature and its temperature.

The number of electrons in the band is also written in terms of the quantum concentration for the conduction n_c and the valence band n_v (also called effective density of states in some texts):

$$\begin{aligned} n &= n_c \exp\left(\frac{\mu - E_G}{kT}\right) \\ p &= n_v \exp\left(-\frac{\mu}{kT}\right) \end{aligned} \tag{2.9.47}$$

where

$$\begin{aligned} n_c &= 2\left(\frac{m_e kT}{2\pi \hbar^2}\right)^{3/2}, \\ n_v &= 2\left(\frac{m_h kT}{2\pi \hbar^2}\right)^{3/2} \end{aligned} \tag{2.9.48}$$

depend on temperature T and effective mass m^*. In virtually all IIII-V semiconductors, the valence band consists of a heavy hole and a light hole band, the concentration for each band must be summed together: :

$$\begin{aligned} p &= \int D_{hh} f_h + D_{lh} f_{lh} \\ &= 2\left(\frac{m_{hh} k_B T}{2\pi \hbar^2}\right)^{3/2} \exp\left(\frac{-\mu}{kT}\right) + 2\left(\frac{m_{lh} k_B T}{2\pi \hbar^2}\right)^{3/2} \exp\left(\frac{-\mu}{kT}\right) \end{aligned} \tag{2.9.49}$$

that can be written as 2.9.45 if one sets:

$$m_v^{3/2} = m_{hh}^{3/2} + m_{lh}^{3/2} \tag{2.9.50}$$

which is called "density of state effective mass).

Note that the product $n \cdot p$ is constantt:

$$np = n_c n_v \exp\left(-E_G/kT\right) = n_i^2. \tag{2.9.51}$$

n_i is called the intrinsic concentration and is:

$$n_i = \sqrt{n_c n_v} \exp\left(-\frac{E_G}{2kT}\right). \tag{2.9.52}$$

It is the thermal concentration of carriers in undoped semiconductors.
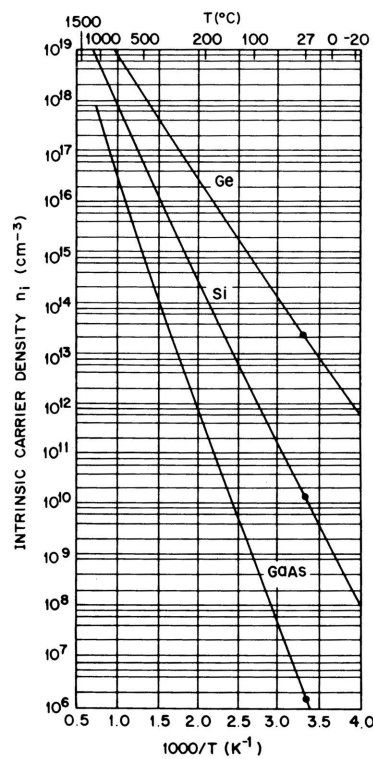
Figure 2.9: Intrinsic concentration for Ge, Si, et GaAs as function of reciprocal temperature

Chapter 3

Light-matter interaction

3.1 Oscillator model

Solving the equation for a (classical) harmonic motion with damping:

$$m_0\ddot{x} + 2m_0\gamma\dot{x} + m_0\omega_0 x = -q\mathcal{E}(t) \tag{3.1.1}$$

yields a polarization $P(\omega)$ at angular frequency ω given by:

$$P(\omega) = -\frac{n_0 q^2}{m_0} \frac{1}{\omega^2 + 2i\gamma\omega - \omega_0^2}\mathcal{E}(\omega) \tag{3.1.2}$$

Remembering the definition of the susceptibility as:

$$P(\omega) = \epsilon_0 \chi(\omega)\mathcal{E}(\omega) \tag{3.1.3}$$

the latter is then

$$\chi(\omega) = -\frac{n_0 q^2}{m_0 \epsilon_0} \frac{1}{\omega^2 + 2i\gamma\omega - \omega_0^2} \tag{3.1.4}$$

The above equations can be rewritten in terms of the sum of two poles

$$P(\omega) = -\frac{n_0 q^2}{m_0 \omega_0'}\Big[\frac{1}{\omega - \omega_0' + i\gamma} - \frac{1}{\omega - \omega_0' + i\gamma}\Big] \tag{3.1.5}$$

with $\omega_0' = \sqrt{\omega_0^2 - \gamma^2}$

3.2 Dielectric function

The dielectric function can be then derived as:

$$\epsilon = \epsilon_0\Big(1 - \frac{\omega_p^2}{2\omega_0'}\big(\frac{1}{\omega - \omega_0' + i\gamma} - \frac{1}{\omega + \omega_0' + i\gamma}\big)\Big) \tag{3.2.6}$$

17

where $\omega_p = \sqrt{\frac{n_0 q^2}{\epsilon_0 m_0}}$ is the plasma frequency.

The dielectric function can be written separately for the real and imaginary parts (neglecting the negative frequency pole):

$$\chi' = \epsilon_r' - 1 = -\frac{\omega_p^2}{2\omega_0} \frac{\omega - \omega_0}{(\omega - \omega_0)^2 + \gamma^2} \qquad (3.2.7)$$

and for the imaginary part:

$$\chi'' = \epsilon_r'' = \frac{\omega_p^2}{4\omega_0} \frac{2\gamma}{(\omega - \omega_0)^2 + \gamma^2} \qquad (3.2.8)$$
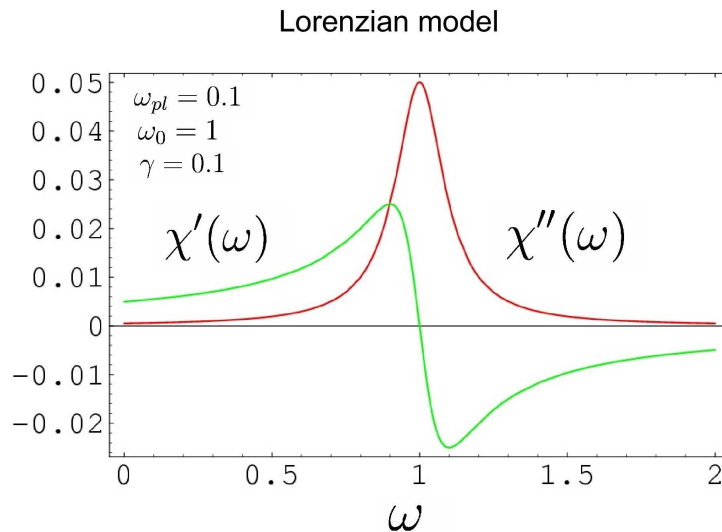
Figure 3.1: Real and imaginary part of the susceptibility in the Lorenzian model.

3.3   Effective medium approximation

Taking into account the effect of other resonances in the susceptibility:

$$\epsilon = \epsilon_\infty \left(1 - \frac{\epsilon_0}{\epsilon_\infty} \frac{\omega_p^2}{2\omega_0'} \Big(\frac{1}{\omega - \omega_0' + i\gamma} - \frac{1}{\omega + \omega_0' + i\gamma} \Big) \right) \qquad (3.3.9)$$

The only trick is to remember to add the polarization. Because of the form of Equ. 3.3.9, one is then lead to redefine the plasma frequency as:

$$\omega_p = \sqrt{\frac{n_0 q^2}{\epsilon_\infty m_0}} \qquad (3.3.10)$$

Example of "classical" dynamics and plasmon oscillations: subpicosecond plasmon excitations in doped semiconductors (Kersting, C. Unterrainer et al., PRL 1997). As shown in figure 3.2, the excitation is done by a femtosecond Ti:sapphire laser.
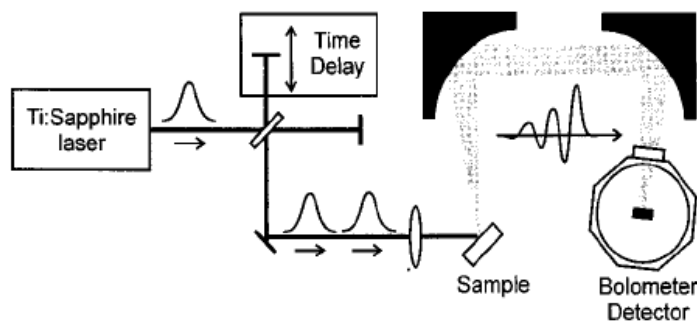
Figure 3.2: Ultrafast excitation of doped semiconductor.

Electron-hole pairs are created at the surface, and excite the plasmons of the doped layer.
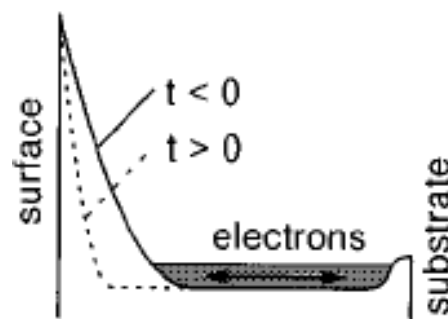
Figure 3.3: Schematic drawing of the sample.

As expected, oscillations are observed at the plasma frequency ω_p.
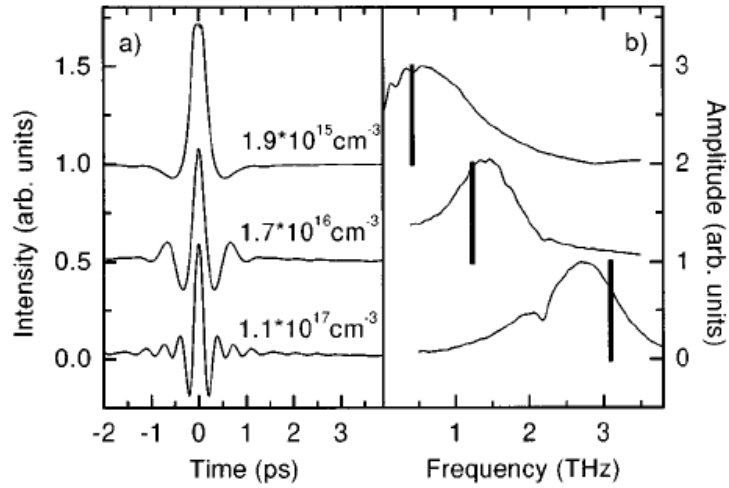
Figure 3.4: Spectrum of the oscillations as a function of doping.

For the example above, using $n = 1.710^{16} cm^{-3}$, $\epsilon_\infty = 13.1$, an effective mass of 0.065, a computed frequency of 1.2THz. is obtained.

3.4 Kramers-Konig relations

The susceptibility $\chi(t)$ has some important mathemtical features because it is a linear response function. The polarization at time t can be expressed as a function of electric field at past times through:

$$P(t) = \int_{-\infty}^{t} \chi(t - t')\mathcal{E}(t')dt' = \int_{0}^{\infty} \chi(\tau)\mathcal{E}(t - \tau)d\tau \tag{3.4.11}$$

where, because of causality, $\chi(\tau) = 0 if \tau < 0$ $\chi(\omega)$ is therefore analytic in the upper half plane. Using a Cauchy integral argument, it follows that

$$\chi(\omega) = P \int_{-\infty}^{\infty} \frac{\chi(\nu))}{i\pi(\nu - \omega - i\delta)}. \tag{3.4.12}$$

The latter equation implies a relationship between real and imaginary parts of the susceptibility, called the Kramers-Krönig relations:

$$\chi'(\omega) = P \int_{0}^{\infty} \frac{d\nu}{\pi} \frac{2\nu\chi''(\nu)}{\nu^2 - \omega^2} \tag{3.4.13}$$

$$\chi''(\omega) = -\frac{2\omega}{\pi} P \int_{0}^{\infty} d\nu \frac{\chi'(\nu)}{\nu^2 - \omega^2} \tag{3.4.14}$$
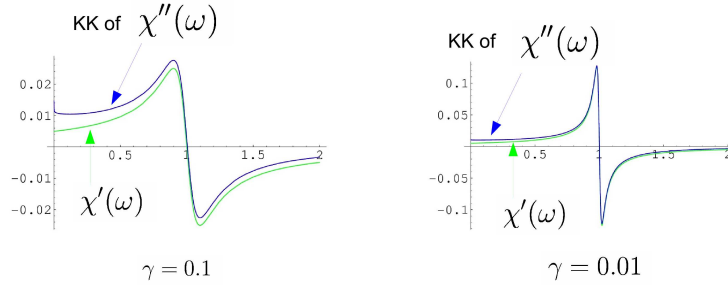
Figure 3.5: Comparison between the real part of the susceptilibity computed by a Kramers-Krönig transform of the imaginary part and by the expression given by 3.2.8. The difference arises from neglecting the negative frequency pole.

3.4.1   Sellmeir's equation

Approximating the imaginary part of the susceptibility by

$$\chi''(\omega) = \frac{\pi \omega_p^2}{\omega_0} \delta(\omega - \omega_0) \tag{3.4.15}$$

and using Kramers-Konig relations, we obtain for the real part of the susceptibility:

$$\chi'(\omega) = \frac{\omega_p^2}{\omega_0^2 - \omega^2} \tag{3.4.16}$$

which predicts the dispersion far away from the resonance. A simple generalization of this equation is referred as Sellmeir's equation for the refractive index, usually written as a function of the wavelength instead of the angular frequency:

$$n^2(\lambda) - 1 = a + \sum_i \frac{b_i}{\lambda^2 - \lambda_i^2} \tag{3.4.17}$$
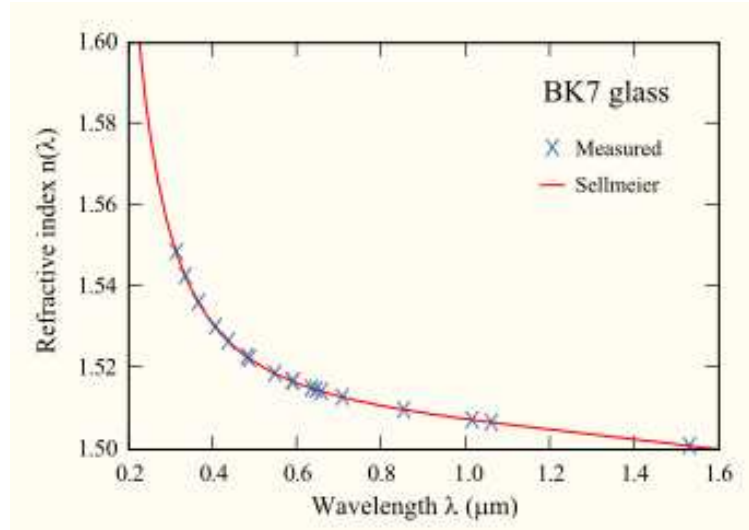
Figure 3.6: Comparison between a Sellmeir's equation with three resonances (two in the UV, one in the mid-infrared) and the experimental refractive index for BK7 glass.

3.5   Interaction between light and a quantum system

Depending on the result of the microscopic model, there are many ways to introduce the optical response.

3.5.1   Fermi's golden rule: a loss term to a propagating wave

Let us assume the interaction Hamiltonian

$$H_{int} = -q\vec{r} \cdot \vec{\mathcal{E}} \sin(\omega t) \tag{3.5.18}$$

the scattering rate, using Fermi's golden rule, writes:

$$R = \frac{1}{\tau} = \frac{\pi}{2\hbar} \sum |\langle i|H_{int}|f\rangle \rho(E_f - E_i - \hbar\omega). \tag{3.5.19}$$

The absorption of the electromagnetic wave by the quantum system is responsible for a decay of the latter with an absorption coefficient α, where

$$I(x) = I_0 \exp(-\alpha x) \tag{3.5.20}$$

The energy loss by the wave per unit volume is

$$P/v = I\alpha \tag{3.5.21}$$

and the intensity is related to the electric field by

$$I = \frac{1}{2}\epsilon_0 n_{refr} c \mathcal{E}^2 \tag{3.5.22}$$

where n_{refr} is the refractive index and c the light velocity. Balancing the energy loss of the EM field with the energy gained by the quantum system yields:

$$\alpha = \frac{2R\hbar\omega}{\epsilon_0 n_{refr} c \mathcal{E}^2} \tag{3.5.23}$$

therefore:

$$\alpha = \frac{\pi\omega}{\epsilon_0 n_{op} c} \sum_f |\langle i|D|f\rangle|^2 \rho(E_f - E_i - \hbar\omega) \tag{3.5.24}$$

3.5.2 A polarization field

As a polarization field $\vec{P}$ reacting to the incident field $\vec{E}$. The polarization is computed by evaluating the dipole operator in the time-dependent wavefunction:

$$P(t) = n_0 \langle \psi(t)|qx|\psi(t)\rangle \tag{3.5.25}$$

and using a first order, time dependent perturbation expansion for the wavefunction $\psi(t)$, the susceptibility $\chi(\omega)$ is

$$\chi(\omega) = -\frac{q^2 n_0}{\hbar} \sum_{m \neq l} |x_{Ml}|^2 \left(\frac{1}{\omega + \omega_{lm} + i\gamma} - \frac{1}{\omega - \omega_{lm} + i\gamma}\right) \tag{3.5.26}$$

that can also be rewritten using the oscillator strength, defined as:

$$f_{ml} = \frac{2m_0}{\hbar} |x_{ml}|^2 \omega_{ml} \tag{3.5.27}$$

in a fashion very reminiscent of the classical expression:

$$\chi(\omega) = -\frac{q^2 n_0}{2m_0} \sum_{m \neq l} \frac{f_{ml}}{\omega_{ml}} \left(\frac{1}{\omega + \omega_{lm} + i\gamma} - \frac{1}{\omega = \omega_{lm} + i\gamma}\right) \tag{3.5.28}$$

3.5.3 A current density j

As a current density $\vec{j}$ that is added to Maxwell's equations, in a crystal that has already a dielectric response $\epsilon(\omega)$:

$$\vec{\nabla} \times \vec{H} = \vec{j} + \frac{\partial \vec{D}}{\partial t} = \sigma\vec{E} - i\omega\epsilon\vec{E} \tag{3.5.29}$$

The equivalent dielectric function is written as:

$$\tilde{\epsilon}_r(\omega) = \frac{i\sigma(\omega)}{\epsilon_0 \omega} + \epsilon_r(\omega) \tag{3.5.30}$$

3.6 Momentum p and dipole z matrix elements: sum rule

3.6.1 Relation between p and z matrix elements

As the commutator between p and z is $[z, p] = i\hbar$, applying it to the kinetic term of the Hamiltonian one can derive the relation:

$$\langle \phi_n | p | \phi_m \rangle = i m_0 \omega_{nm} \langle \phi_n | z | \phi_m \rangle \tag{3.6.31}$$

3.6.2 Sum rule

Taking the completeness of the (eigen)states

$$\sum_n | \phi_n \rangle \langle \phi_n | = 1 \tag{3.6.32}$$

and the relationship between position and momentum matrix element, the sum rule for the oscillator strength can be derived:

$$\sum_n f_{nl} = 1 \tag{3.6.33}$$

The sum rule appears in a number of context. It can be expressed as the integral of the absorption strength. In the next graph, intersubband absorption for three different samples with various energy level ladder are compared. As expected, the integrated absorption is constant within experimental error.
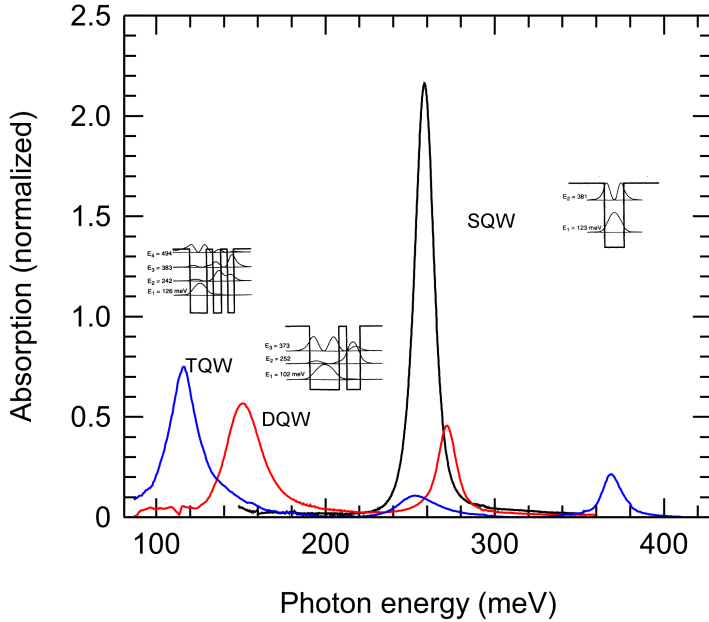
Figure 3.7: Comparison of the intersubband absorption for various structures, with energy levels schematically drawn close to the curves

3.7 Dipole or momentum matrix elements

Hamiltonian derived from

$$H = \frac{(\vec{P} - q\vec{A})^2}{2m} \tag{3.7.34}$$

Use Coulomb gauge ($\nabla A = 0$). For low intensity (neglect the term in A^2), we obtain as an interaction Hamiltonian:

$$H_I = -\frac{q}{m_0}\vec{A} \cdot \vec{P}. \tag{3.7.35}$$

Because of the large difference between the light wavelength and the atomic dimension, the spatial dependence of A(r) is neglected inside the matrix elements. This is called the dipole approximation. The ratio of the spatial frequency of the light wave $k_p h$ to the electronic part k_e is

$$\frac{k_{ph}}{k_e} = \sqrt{\frac{E_{ph}}{E_{rest}2(m^*/m_0)}} \tag{3.7.36}$$

where $E_{rest} = 550 keV$ is the rest mass of the electron. This ratio is $\approx 10^{-5}$ for 1eV photons. The form commonly used is then:

$$\langle\psi_i|H_I|\psi_j\rangle = \frac{-q\vec{A}(r)}{m}\langle\psi_i(r)|\vec{P}|\psi_j(r)\rangle \tag{3.7.37}$$

For a plane wave, $\vec{A}$ is paralell to $\vec{\mathcal{E}}$, for a wave polarized along z and propagating in the y direction:

$$\vec{A}(\vec{r}, t) = A_0 \vec{e}_z e^{i(ky - \omega t)} + A_0^* \vec{e}_z e^{-i(ky - \omega t)}. \tag{3.7.38}$$

It is convient to use A_0 being pure imaginary such both electric and magnetic fields are real: that yield $\mathcal{E} = 2i\omega A_0$ and $B = 2ikA_0$.

Chapter 4

Optical properties of semiconductors

4.1 Reflectivity measurements, ellipsometry

4.1.1 Reflectivity

Use a Kramers-Kronig relation to express the phase of the reflectivity from the spectrum of the intensity reflectivity:

$$\Theta(\omega) = -\frac{2\omega}{\pi} \int_0^\infty \frac{ln(\rho(\omega')d\omega'}{\omega'^2 - \omega^2} \tag{4.1.1}$$

4.1.2 Ellipsometry

There, the dielectric constant is obtained from a measurement of the ratio of the p to s reflectivity $\sigma = \frac{r_p}{r_s}$ through:

$$\epsilon(\omega) = \sin^2 \phi + \sin^2 \phi \tan^2 \phi \left[\frac{1 - \sigma}{1 + \sigma}\right]^2 \tag{4.1.2}$$
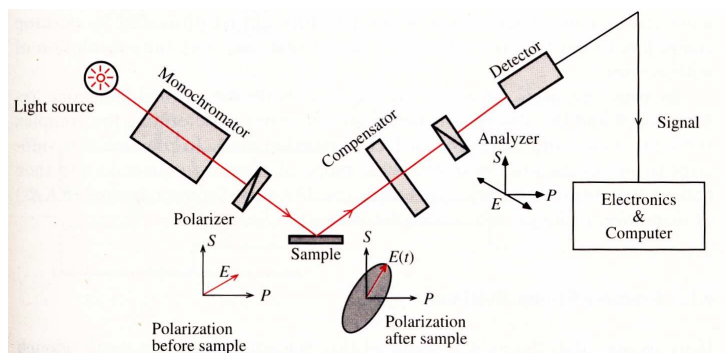
Figure 4.1: Schematic diagramm of an ellipsometer.
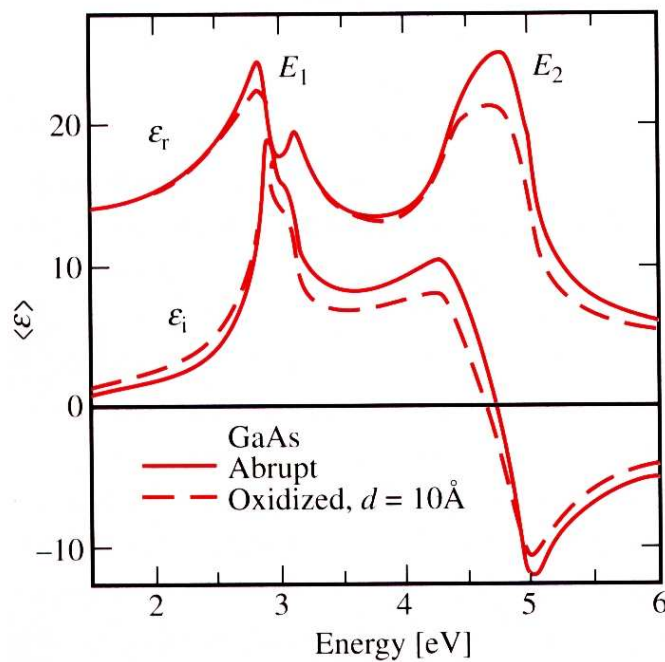
Figure 4.2: Dielectric function of GaAs. Note the influence of the surface oxide.
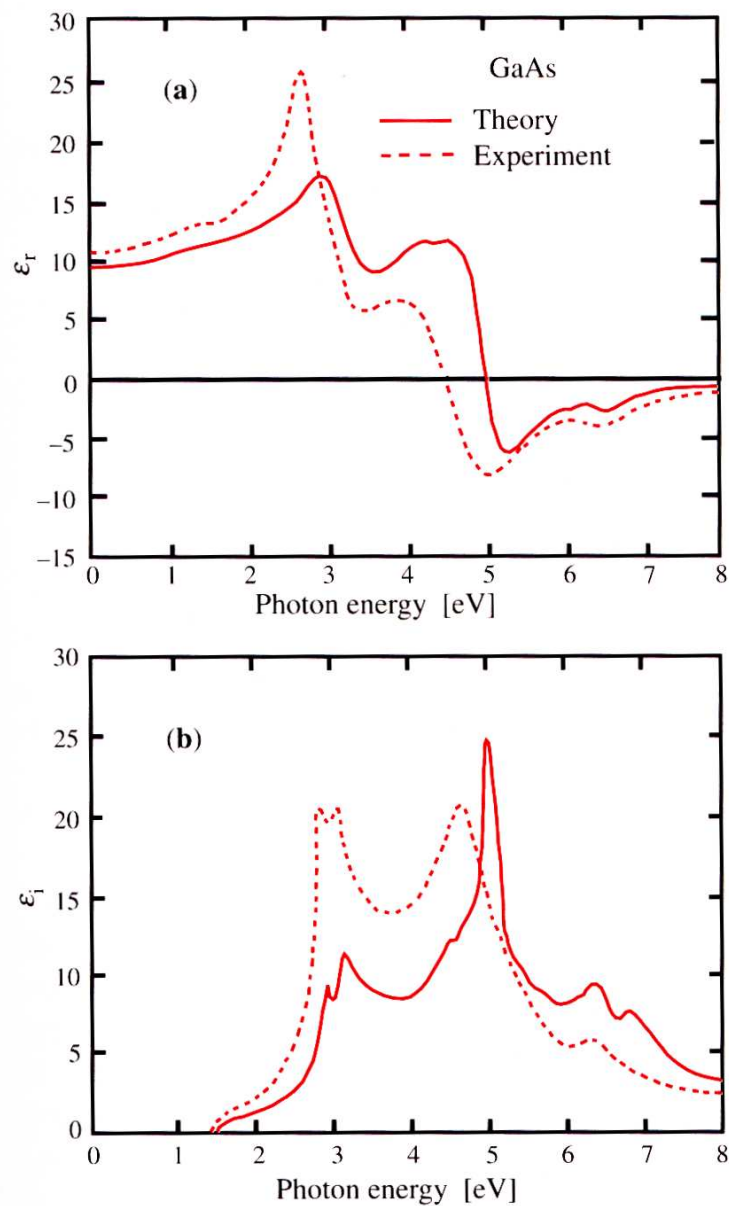
Figure 4.3: Dielectric function of GaAs including the gap.

4.2   Critical points and band structure, Van Hove singularities
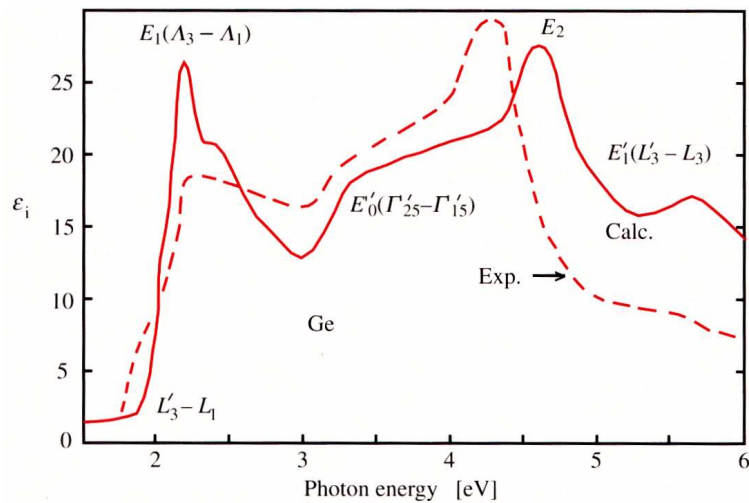
Figure 4.4: Dielectric function of Ge.compared with the computation.
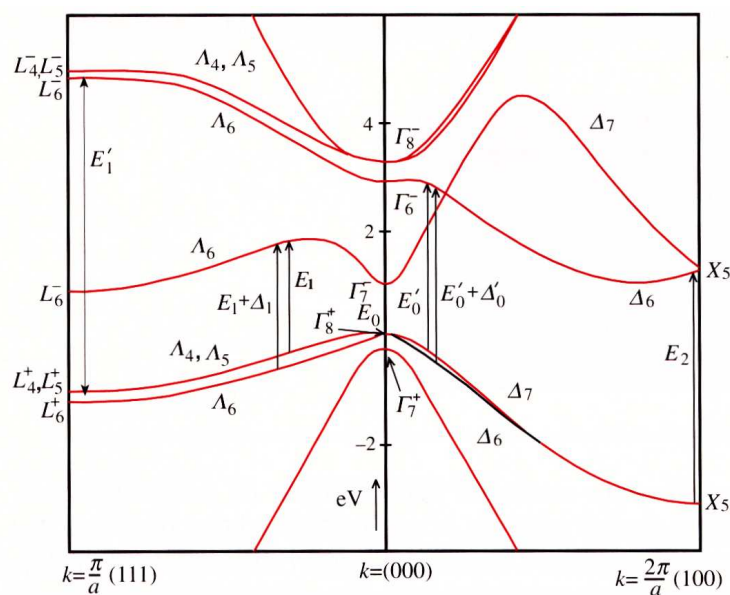
Figure 4.5: Germanium bandstructure with the critical points

Let us use the Fermi golden rule, and assuming the invariance of the matrix element with energy and wavevector. The transition rate is then given by:

$$R = C \int \frac{1}{8\pi^3} \frac{dS|e \cdot M_{vc}|^2}{|\nabla_k(E_c - E_v)|_{E_c - E_V = \hbar\omega}} \tag{4.2.3}$$

where dS is the element of surface in k space defined by the equation

$$E_c(k) - E_v(k) = \hbar\omega \tag{4.2.4}$$

and C is a prefactor given by

$$C = \frac{4\pi\hbar q^2}{m_0^2} A_0^2 \tag{4.2.5}$$

Expanding the energy around a critical point in a Taylor expansion:

$$E_c - E_v = E_0 + \sum_{i=1}^{3} a_i(k_i - k_{0i})^2 \tag{4.2.6}$$

enables a classification of the Van Hove singularities depending on the relative signs of the coefficients a_i: M_0 and M_3 if they have the same sign (positive, resp negative), M_1 and M_2 for saddle points. The shape of the absorption is shown in Fig. 4.6.

As an example, for a three dimensional crystal with the M_0, $\int dS = 4\pi k^2$ and $|\nabla_k(E_c - E_v)|_{E_c - E_V = \hbar\omega} = \frac{\hbar^2 k}{m_r}$ yields an absorption coefficient proportional to

$$(m_r)^{3/2}\sqrt{E - E_0} \tag{4.2.7}$$

Type		D_j	
		$E < E_0$	$E > E_0$
Three dimensions	M_0	0	$(E - E_0)^{1/2}$
	M_1	$C - (E_0 - E)^{1/2}$	C
	M_2	C	$C - (E - E_0)^{1/2}$
	M_3	$(E_0 - E)^{1/2}$	0
Two dimensions	M_0	0	C
	M_1	$-\ln(E_0 - E)$	$-\ln(E - E_0)$
	M_2	C	0
One dimension	M_0	0	$(E - E_0)^{-1/2}$
	M_1	$(E_0 - E)^{-1/2}$	0
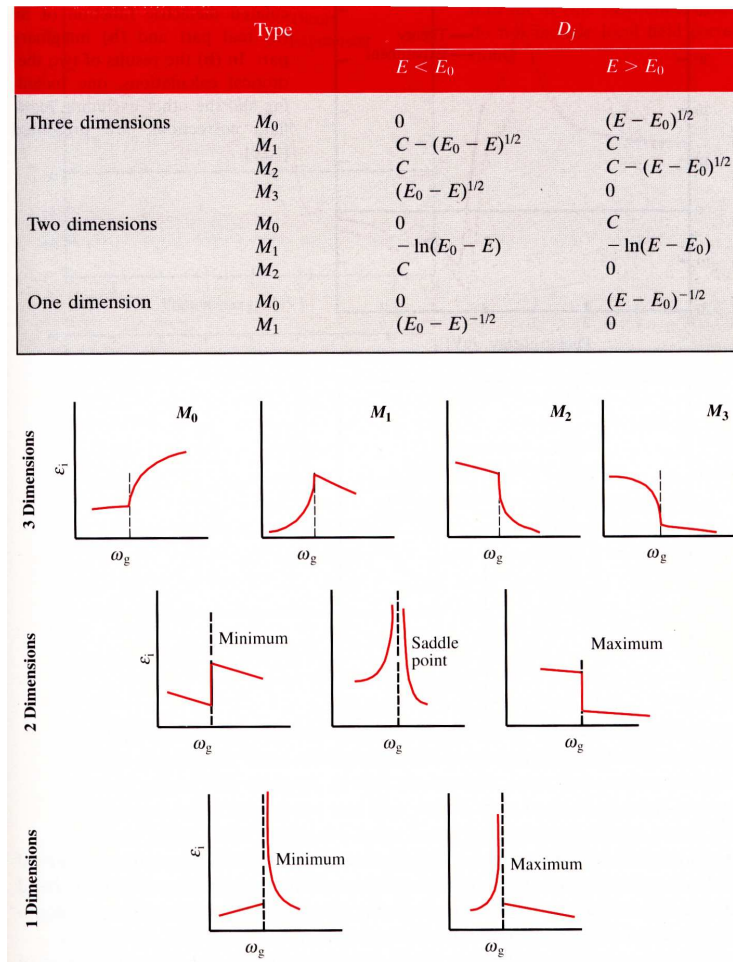
Figure 4.6: Van Hove singularities

The square-root shape of the absorption at the band edge is compared to the experiment for InSb in Fig 4.7.
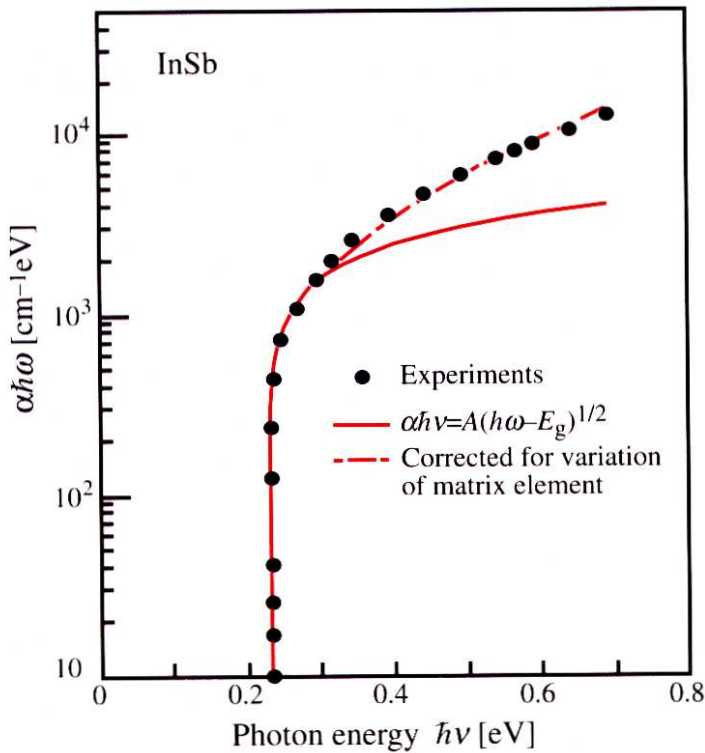
Figure 4.7: InSb absorption, compared with the computations assuming constant and non-constant matrix elements

4.3 Refractive index

For many devices, an accurate knowledge of the refractive index and its frequency dependence is very important. The Kramers Kronig relations, together with a modelisation of the imaginary part of the dielectric function, allow a phenomenological model of the refractive index dispersion of III-V direct semiconductor to be derived. Assuming the imaginary part of the dielectric function ϵ'' with the form:

$$\epsilon''(E) = \eta E^4 \tag{4.3.8}$$

between the bandgap energy E_G and a final cutoff energy E_f and zero elsewhere, as shown in Fig4.8
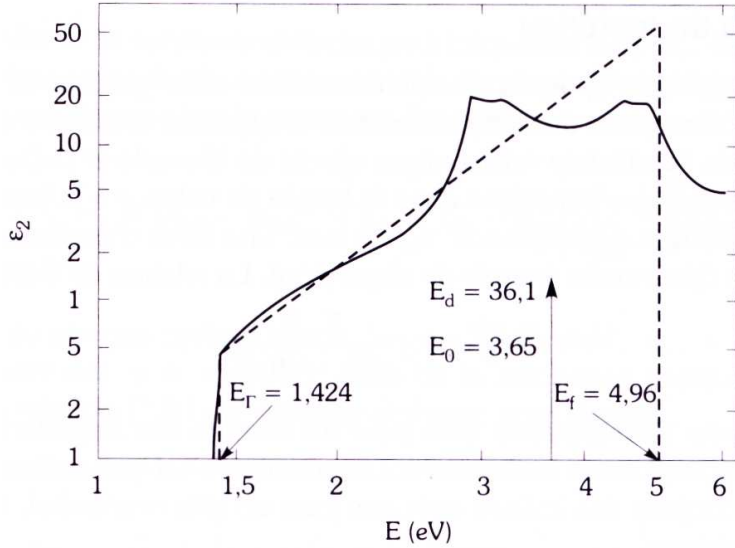
Figure 4.8: Imaginay part of the dielectric function for GaAs and the Aframowitz approximation

Because the dielectric response of the III-V materials cannot be easily represented by a finite sum of oscillators, this is a better approximation than a "normal" Sellmeir's equation. From a integration of the Kramers-Kronig equation, the refractive index is obtained as:

$$n^2(E) = 1 + \frac{\eta}{2\pi}(E_f^4 - E_G^4) + \frac{\eta}{\pi}E^2(E_f^2 - E_G^2) + \frac{\eta}{\pi}E^4 \ln\left(\frac{E_f^2 - E^2}{E_G^2 - E^2}\right) \tag{4.3.9}$$

where η, E_f and E_G fully characterize the material. In the litterature, the parametes are given in terms of parameters of a Sellmeir's equation

$$\epsilon'(E) = 1 + \frac{E_{oe}E_d}{E_{oe}^2 - E^2}. \tag{4.3.10}$$

These parameters are related to the ones of our model through

$$E_f = \sqrt{2E_{oe}^2 - E_G^2} \tag{4.3.11}$$

and

$$\eta = \frac{\pi}{2}\frac{E_d}{E_{oe}^3(E_{oe}^2 - E_G^2)}. \tag{4.3.12}$$

The experimental results for a few relevant III-V materials are shown in Fig. 4.9 and
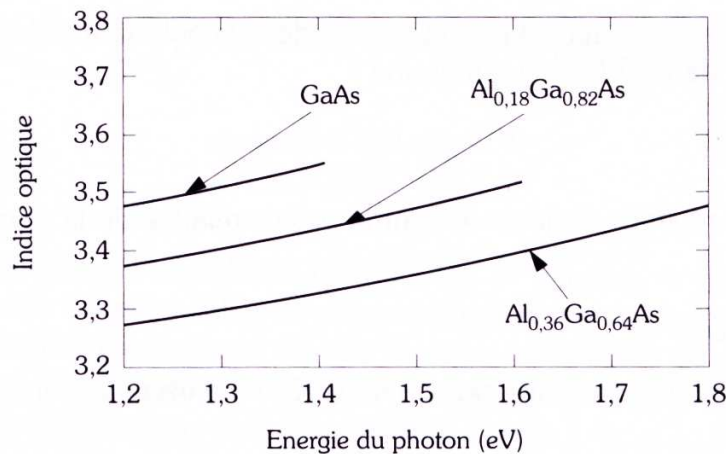
Figure 4.9: Computed dispersion of the refractive index

the relevant material parameters in Fig. 4.10.

	$Ga_{1-x}Al_xAs$	$GaAs_{1-x}P_x$	$Ga_xIn_{1-x}P$
E_{oe} (eV)	$3{,}65 + 0{,}871x + 0{,}179x^2$	$3{,}65 + 0{,}721x + 0{,}139x^2$	$3{,}391 + 0{,}524x + 0{,}595x^2$
E_d (eV)	$36{,}1 - 2{,}45x$	$36{,}1 + 0{,}35x$	$28{,}91 + 7{,}54x$
E_G (eV)	$1{,}424 + 1{,}266x + 0{,}26x^2$	$1{,}441 + 1{,}091x + 0{,}21x^2$	$1{,}34 + 0{,}668x + 0{,}758x^2$

Figure 4.10: Energy gaps for various III-V materials for the refrative index

Chapter 5

Bulk semiconductors: bandstructure and fundamental gap

5.1 k·p approximation

5.1.1 Basic approximations

Behind the effective mass approximation lies a very powerful approach to the computation of the band structure. It relies on the knowledge of the band structure at $k = 0$ and expanding the wavefunctions in this basis. The Schröedinger equation for a crystal writes:

$$\Big(\frac{p^2}{2m_0} + V(r) + \frac{\hbar^2}{4m_0^2 c^2}(\vec{\sigma} \times \vec{\nabla}V) \cdot \vec{p}\Big)\psi(\vec{r}) = E\psi(\vec{r}) \tag{5.1.1}$$

For simplicity, we drop the spin-orbit coupling term. The latter arises as a relativistic term: the motion of the electon in the field of the ion, the latter sees an equivalent magnetic field that operates on the angular momentum variable. Let us first compute the action of $\vec{p}$ on ψ, written in terms of Bloch wavefunctions so that

$$\psi_{n\vec{k}}(\vec{r}) = e^{i\vec{k}\vec{r}}u_{n\vec{k}}(\vec{r}), \tag{5.1.2}$$

we obtain:

$$\vec{p} \cdot (e^{i\vec{k}\vec{r}}u_{n\vec{k}}(\vec{r})) = -i\hbar\vec{\nabla} \cdot (e^{i\vec{k}\vec{r}}u_{n\vec{k}}(\vec{r})) \tag{5.1.3}$$

$$= \hbar\vec{k}e^{i\vec{k}\vec{r}}u_{n\vec{k}}(\vec{r}) + e^{i\vec{k}\vec{r}}\vec{p} \cdot u_{n\vec{k}}(\vec{r}) \tag{5.1.4}$$

$$= e^{i\vec{k}\vec{r}}(\vec{p} + \hbar\vec{k})u_{n\vec{k}}(\vec{r}). \tag{5.1.5}$$

Using the above relation, the Schrödinger equation is obtained for $u_{n\vec{k}}(\vec{r})$:

$$\Big(\frac{p^2}{2m_0} + \frac{\hbar}{m}\vec{k} \cdot \vec{p} + \frac{\hbar^2 k^2}{2m_0} + V(\vec{r})\Big)u_{n\vec{k}}(\vec{r}) = E_{nk}u_{n\vec{k}}(\vec{r}) \tag{5.1.6}$$

The Hamiltonian $H = H_0 + W(\vec{k})$ may be splitted into a k-independent

$$H_0 = \frac{p^2}{2m_0} + V(\vec{r}) \tag{5.1.7}$$

and k-dependent part

$$W(\vec{k}) = \frac{\hbar^2 k^2}{2m_0} + \frac{\hbar}{m}\vec{k}\cdot\vec{p}.$$ (5.1.8)

The solution of the the equation

$$H_0 u_{n0}(\vec{r}) = E_{n0} u_{n0}(\vec{r})$$ (5.1.9)

are the energies of the band structure at the Γ point $k = 0$. The fundamental idea of the $k \cdot p$ approximation is to use the $u_{n0}(\vec{r})$ as a basis for the expansion of the wavefunction and energies at finite k value. In the simplest cases, taking an interband transition across the gap and looking at the conduction band, taking the second-order perturbation expansion:

$$E_c(k) = E_c(0) + \frac{\hbar^2 k^2}{2m_0} + \frac{\hbar^2 k^2}{m_0}\sum_{m\neq c}\frac{|\langle u_{c,0}|p|u_{m,0}\rangle|^2}{E_c - E_m}$$ (5.1.10)

In the lowest order approximation, all other bands except for the valence band may be neglected, in which case the dispersion can be written as (taking the zero energy at the top of the valence band):

$$E_c(k) = E_G + \frac{\hbar^2 k^2}{2m_0} + \frac{\hbar^2 k^2}{m_0}\frac{p_{cv}^2}{E_G}$$ (5.1.11)

Defining the Kane energy $E_P = 2m_0 P^2$ such that

$$E_P = \frac{2}{m_0}|\langle u_{c,0}|p|u_{v,0}\rangle|^2$$ (5.1.12)

the dispersion of the conduction band can be written as:

$$E_c(k) = E_c + \frac{\hbar^2 k^2}{2m_0}\left(1 + \frac{E_P}{E_G}\right)$$ (5.1.13)

We then obtain the effective mass as:

$$(m^*)^{-1} = (m_0)^{-1}\left(1 + \frac{E_P}{E_G}\right)$$ (5.1.14)

The Kane energy is much larger than the gap $E_P >> E_G$ and is rather constant across the III-V semiconductors. As a result, the effective mass in inversly proportional to the band gap.
One should be careful that some authors use the definition

$$E_P = 2m_0 P^2$$ (5.1.15)

(Bastard, for example), while others (Rosencher) use

$$E_P = P^2.$$ (5.1.16)

At least they all use E_P having the dimension of energy!.

	InP	InAs	InSb	GaAs	GaSb
ε_0(eV)	1.4236	0.418	0.2352	1.5192	0.811
Δ(eV)	0.108	0.38	0.81	0.341	0.752
m_{Γ_6}/m_0	0.079	0.023	0.0139	0.0665	0.0405
E_p(eV)	17	21.11	22.49	22.71	22.88

Figure 5.1: Fundamental gap ε_0, Split-off energy Δ, conduction band effective mass and Kane energy E_P for various III-V semiconductors

In the above expressions, the spin-orbit term can be included by replacing the operator $\vec{p}$ by

$$\vec{\pi} = \vec{p} + \frac{\hbar}{4m_0 c^2}(\vec{\sigma} \times \vec{\nabla}V). \tag{5.1.17}$$

5.1.2 Beyond the perturbation expansion

A very powerful procedure is to expand formally the solutions of Equ. 5.1.6 in the solutions at $k = 0$, writing formally:

$$u_{nk}(r) = \sum_m c_m^{(n)}(k)u_{m,0}(r) \tag{5.1.18}$$

and restricting the sum to a limited relevant subset of bands. Improved accuracy can be achieved by introducing more bands. In this basis, and projecting the equation onto the state $u_{M,0}$, the Hamilton equation is written as:

$$\left(E_{M0} + \frac{\hbar^2 k^2}{2m_0} - E_n(k)\right)c_M^{(n)}(k) + \sum_{m \neq M} H_{Mm}^{kp} c_m^{(n)}(k) = 0 \tag{5.1.19}$$

where the kp Hamiltonian is

$$H_{Mm}^{kp} = \frac{\hbar}{m_0}k \cdot \langle u_{M,0}|p|u_{m,0}\rangle \tag{5.1.20}$$

To the extend the matrix elements are known, equation 5.1.19 can be solved.

5.1.3 Example: a two-band Kane model

Let us write explicitely a two-band Kane model. The latter can be a fairly realistic model if one is only interested at the effect of the valence band onto the conduction one, replacing the three spin-degenerate valence bands (heavy hole, light hole, split-off) by an effective valence band. The u_{nk} can then be expressed as:

$$u_{nk} = a_c u_{c0} + a_v u_{v0} \tag{5.1.21}$$

Replacing this expansion into Eq. 5.1.19, we obtain the following matrix equation:

$$\begin{pmatrix} E_c + \frac{\hbar^2 k^2}{2m_0} & \frac{\hbar}{m_0}\vec{k} \cdot \vec{p}_{cv} \\ \frac{\hbar}{m_0}\vec{k} \cdot \vec{p}_{cv}^* & E_v + \frac{\hbar^2 k^2}{2m_0} \end{pmatrix} \begin{pmatrix} a_c \\ a_v \end{pmatrix} = E \cdot \begin{pmatrix} a_c \\ a_v \end{pmatrix}. \tag{5.1.22}$$

Assuming $E_c = 0$, $E_v = -E_G$, the solution of the matrix equation satisfies:

$$(\frac{\hbar^2 k^2}{2m_0} - E)(-E_G + \frac{\hbar^2 k^2}{2m_0} - E) - \frac{\hbar^2}{m_0^2}|\vec{k} \cdot \vec{p}_{cv}|^2 = 0. \qquad (5.1.23)$$

This second order equation in E can be of course solved directly; it is however more instructive to write it under the form a pseudo effective mass equation (remember $E_P = \frac{2}{m_0}p_{cv}^2$:

$$E(k) = \frac{\hbar^2 k^2}{2m_0} \frac{E_P + E_G + 2E}{E + E_G}. \qquad (5.1.24)$$

For $k \to 0$ the above expression reduces itself to the result of the perturbation expansion:

$$(m^*)^{-1} = (m_0)^{-1}\big(1 + \frac{E_P}{E_G}\big). \qquad (5.1.25)$$

Equation 5.1.25 can be expressed in a somewhat simplified form:

$$m^*(E) = m^*(0)\big(1 + \frac{E}{E_G}\big) \qquad (5.1.26)$$

that is commonly used in the literature.

5.1.4   Realistic model

To have a realistic description of the band strucure, the following steps are taken.

In a first step, the valence band k=0 Bloch basis function are build using orbitals $|X, Y, Z \uparrow\downarrow\rangle$, in such a way as to build states that are eigenstates of the total angular momentum operator J^2 and J_z. Of course at this point the direction of quantification is totally arbitrary. The figure 5.3 gives this expansion explicitly. This expansion is done in two steps: first one should eigenstates of the orbital angular momentum as a function of the orbitals and then use the sum of angular momentum rules to get the total angular momentum (orbital plus spin).
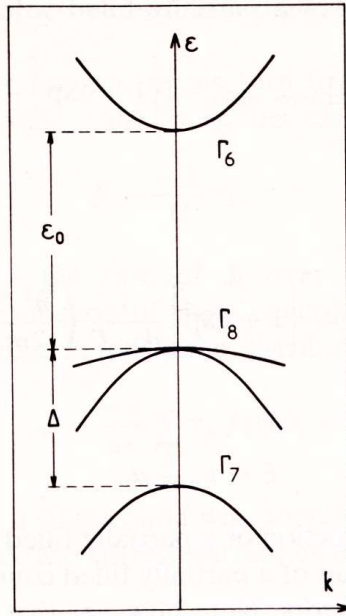
Figure 5.2: Schematic band structure

u_i	$\|J, m_J\rangle$	ψ_{J,m_J}	$\varepsilon_i(k=0)$
u_1	$\left\|\frac{1}{2}, \frac{1}{2}\right\rangle$	$i\|S\uparrow\rangle$	0
u_3	$\left\|\frac{3}{2}, \frac{1}{2}\right\rangle$	$-\sqrt{\frac{2}{3}}\|Z\uparrow\rangle + \frac{1}{\sqrt{6}}\|(X+iY)\downarrow\rangle$	$-\varepsilon_0$
u_5	$\left\|\frac{3}{2}, \frac{3}{2}\right\rangle$	$\frac{1}{\sqrt{2}}\|(X+iY)\uparrow\rangle$	$-\varepsilon_0$
u_7	$\left\|\frac{1}{2}, \frac{1}{2}\right\rangle$	$\frac{1}{\sqrt{3}}\|(X+iY)\downarrow\rangle + \frac{1}{\sqrt{3}}\|Z\uparrow\rangle$	$-\varepsilon_0 - \Delta$
u_2	$\left\|\frac{1}{2}, -\frac{1}{2}\right\rangle$	$i\|S\downarrow\rangle$	0
u_4	$\left\|\frac{3}{2}, -\frac{1}{2}\right\rangle$	$-\frac{1}{\sqrt{6}}\|(X-iY)\uparrow\rangle - \sqrt{\frac{2}{3}}\|Z\downarrow\rangle$	$-\varepsilon_0$
u_6	$\left\|\frac{3}{2}, -\frac{3}{2}\right\rangle$	$\frac{1}{\sqrt{2}}\|(X-iY)\downarrow\rangle$	$-\varepsilon_0$
u_8	$\left\|\frac{1}{2}, -\frac{1}{2}\right\rangle$	$-\frac{1}{\sqrt{3}}\|(X-iY)\uparrow\rangle + \frac{1}{\sqrt{3}}\|Z\downarrow\rangle$	$-\varepsilon_0 - \Delta$

Figure 5.3: Definition of the basis vector

Once this basis is defined, the matrix elements are taken between these basis states dropping the k-dependence of the spin-orbit term. Relativistic term such as the Darwin term are also

neglected. The only non-zero matrix elements between orbitals are

$$P = \frac{-i}{m_0}\langle S|p_x|X\rangle = \frac{-i}{m_0}\langle S|p_y|Y\rangle = \frac{-i}{m_0}\langle S|p_z|Z\rangle \tag{5.1.27}$$

between orbitals with the same spin because all others vanish by symmetry. The resulting matrix is shown in Fig 5.4.

	$|iS\uparrow\rangle$	$\left|\frac{3}{2},\frac{1}{2}\right\rangle$	$\left|\frac{3}{2},\frac{3}{2}\right\rangle$	$\left|\frac{1}{2},\frac{1}{2}\right\rangle$	$|iS\downarrow\rangle$	$\left|\frac{3}{2},-\frac{1}{2}\right\rangle$	$\left|\frac{3}{2},-\frac{3}{2}\right\rangle$	$\left|\frac{1}{2},-\frac{1}{2}\right\rangle$
$\langle iS\uparrow|$	$\frac{\hbar^2k^2}{2m_0}$	$-\sqrt{\frac{2}{3}}P\hbar k_z$	$P\hbar k_+$	$\frac{1}{\sqrt{3}}P\hbar k_z$	0	$-\frac{1}{\sqrt{3}}P\hbar k_-$	0	$-\sqrt{\frac{2}{3}}P\hbar k_-$
$\left\langle\frac{3}{2},\frac{1}{2}\right|$	$-\sqrt{\frac{2}{3}}P\hbar k_z$	$-\varepsilon_0+\frac{\hbar^2k^2}{2m_0}$	0	0	$\frac{P}{\sqrt{3}}\hbar k_-$	0	0	0
$\left\langle\frac{3}{2},\frac{3}{2}\right|$	$P\hbar k_-$	0	$-\varepsilon_0+\frac{\hbar^2k^2}{2m_0}$	0	0	0	0	0
$\left\langle\frac{1}{2},\frac{1}{2}\right|$	$\frac{1}{\sqrt{3}}P\hbar k_z$	0	0	$-\varepsilon_0-\Delta+\frac{\hbar^2k^2}{2m_0}$	$\sqrt{\frac{2}{3}}P\hbar k_-$	0	0	0
$\langle iS\downarrow|$	0	$\frac{P}{\sqrt{3}}\hbar k_+$	0	$\sqrt{\frac{2}{3}}P\hbar k_+$	$\frac{\hbar^2k^2}{2m_0}$	$-\sqrt{\frac{2}{3}}P\hbar k_z$	$P\hbar k_-$	$\frac{1}{\sqrt{3}}P\hbar k_z$
$\left\langle\frac{3}{2},-\frac{1}{2}\right|$	$-\frac{1}{\sqrt{3}}P\hbar k_+$	0	0	0	$-\sqrt{\frac{2}{3}}P\hbar k_z$	$-\varepsilon_0+\frac{\hbar^2k^2}{2m_0}$	0	0
$\left\langle\frac{3}{2},-\frac{3}{2}\right|$	0	0	0	0	$P\hbar k_+$	0	$-\varepsilon_0+\frac{\hbar^2k^2}{2m_0}$	0
$\left\langle\frac{1}{2},-\frac{1}{2}\right|$	$-\sqrt{\frac{2}{3}}P\hbar k_+$	0	0	0	$\frac{P}{\sqrt{3}}\hbar k_z$	0	0	$-\varepsilon_0-\Delta+\frac{\hbar^2k^2}{2m_0}$

Figure 5.4: Matrix equation for the $k \cdot p$ 8 band model

Solving the matrix equation shown in Fig. 5.4, one obtain an implicit equation for the dispersion given by:

$$\lambda(k) = -\epsilon_G \tag{5.1.28}$$

$$\lambda(k)\big[\lambda(k) + \epsilon_G\big]\big[\lambda(k) + \epsilon_G + \Delta\big] = \hbar^2 k^2 P^2\big[\lambda(k) + \epsilon_G + \frac{2\Delta}{3}\big] \tag{5.1.29}$$

where $\lambda(k)$ is defined by

$$\lambda(k) = \epsilon(k) - \frac{\hbar^2 k^2}{2m_0} \tag{5.1.30}$$

Equation 5.1.29 is the one of the heavy particule (at this level, they display a positive (i.e. electron-like) dispersion, and the equation 5.1.29 the light particules. The computed bands, with GaAs band parameters, are shown in Fig. 5.5.
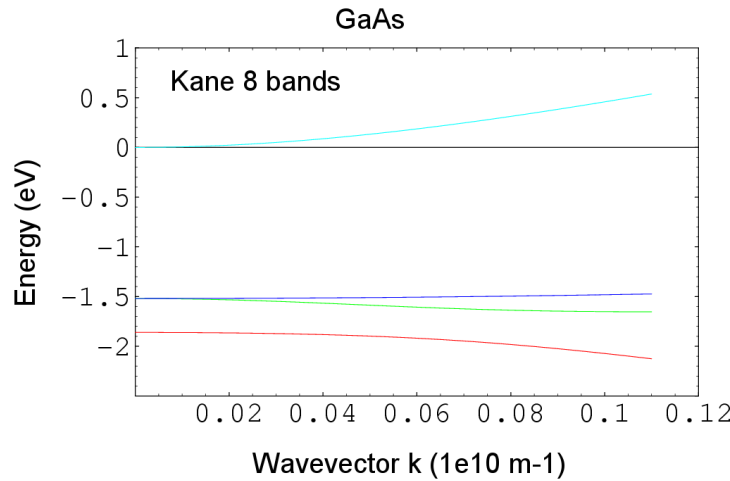
Figure 5.5: Computed band structure of the GaAs using the 8 band model

The structure of the valence band is shown in more detail in Fig. 5.6.
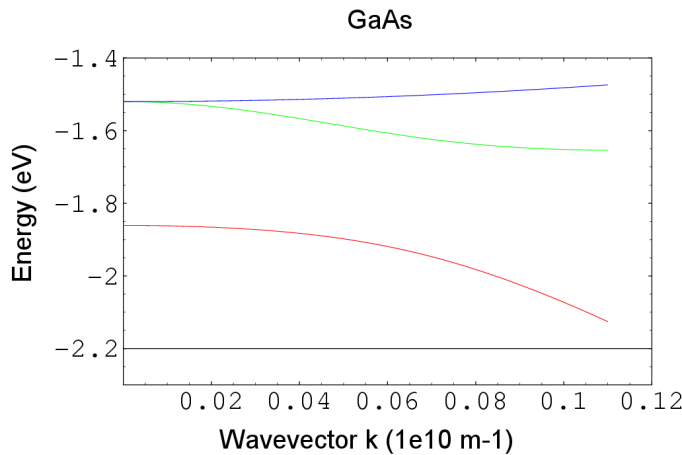
Figure 5.6: Computed valence band structure of the GaAs using the 8 band model

A striking feature is the electron-like dispersion, with a bare electron mass, of the heavy hole states. It means that the heavy hole band is not coupled to the conduction band. The correct dispersion of the heavy hole band can only be predicted when including the

effects of the remote bands. The absence of coupling is apparent from inspection of the $\mathbf{k} \cdot \mathbf{p}$ by remembering that the direction of quantification is arbitrary and therefore can be chose always parallel to the vector $\vec{k}$. In that case, $k = k_z$ and it is apparent that the states $|\frac{3}{2}, \pm\frac{3}{2}\rangle$ are not coupled to any other band. For an other direction of quantification, the same heavy particle is a linear combination of $|\frac{3}{2}, \pm\frac{3}{2}\rangle$ and $|\frac{3}{2}, \pm\frac{1}{2}\rangle$ states.

Effective masses can be obtained from this model through a Taylor expansion of the solution of equation 5.1.29 around $k = 0$. The values obtained are

$$\frac{1}{m_{\Gamma_6}} = \frac{1}{m_0} + \frac{4}{3}\frac{P^2}{E_G} + \frac{2}{3}\frac{P^2}{E_G + \Delta} \tag{5.1.31}$$

$$\frac{1}{m_{\Gamma_8}} = \frac{1}{m_0} - \frac{4}{3}\frac{P^2}{E_G} \tag{5.1.32}$$

$$\frac{1}{m_{\Gamma_7}} = \frac{1}{m_0} - \frac{2}{3}\frac{P^2}{E_G + \Delta} \tag{5.1.33}$$

$$\tag{5.1.34}$$

where the group theory notation has been used to distinguish the various band edges: Γ_6 corresponds to the conduction band, Γ_8 the light holes and Γ_7 the split-off band. The mirror effect of the bands is clearly apparent.

Comparison between this dispersion and the results of a pseudo-potential computation is shown in Fig. 5.7
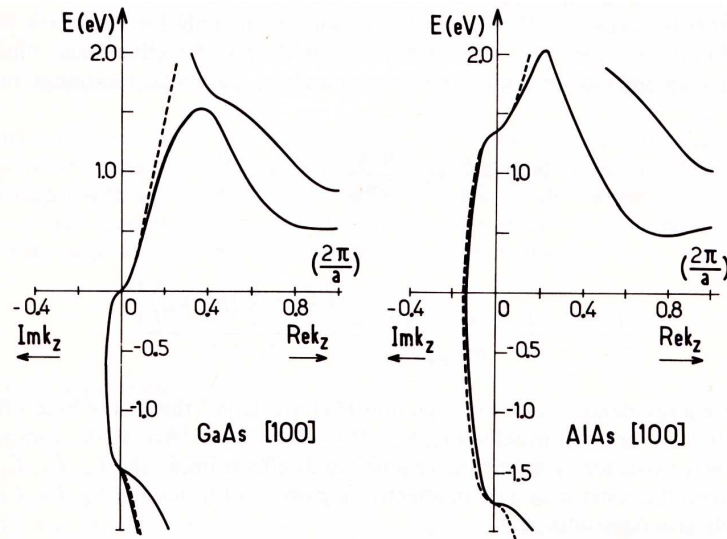
Figure 5.7: Comparison between the kp approximation and a pseudo-potential computation

The $k \cdot p$ approximation is very good as long as the wavevector remains close to the center of the Brillouin zone. In particular, it is unable to predict the minima at the edge of the Brillouin zone.

5.2 Computation of the absorption edge in bulk materials

From the comparison between the energy lost by the optical wave and the one gained by the quantum system, we had derived in equation 3.5.23 a relationship between the scattering rate given by Fermi's golden rule R and the absorbtion for an electric field $\mathcal{E}$.

$$\alpha = \frac{2R\hbar\omega}{\epsilon_0 n_{refr} c \mathcal{E}^2} \tag{5.2.35}$$

Rewriting the latter equation as a function of the potential vector $A_0 = \mathcal{E}/(2i\omega)$ and using for the matrix element the equation 4.2.3 we obtain:

$$\alpha(\omega) = 2\pi \frac{\hbar^2 q^2}{\epsilon_0 n_{refr} m_0^2 \omega c} \int \frac{1}{8\pi^3} \frac{dS |e \cdot M_{vc}|^2}{|\nabla_k (E_c - E_v)||_{E_c - E_V = \hbar\omega}} \tag{5.2.36}$$

If we assume that the matrix element is constant as a function of k, we can pull it in front of the integral, and the integral itself gives the value $\frac{1}{8\pi^3} \frac{4\pi k^2 m_r}{\hbar^2 k}$; writing the result as a function of the reduced electron-hole effective mass m_r we have:

$$\alpha(\omega) = \frac{q^2}{2\pi\epsilon_0 n_{refr} m_0^2 \omega c} \left(\frac{2m_r}{\hbar^2}\right)^{3/2} |\hbar e \cdot M_{vc}|^2 \sqrt{\hbar\omega - E_G} \tag{5.2.37}$$

In this approximation, the term $\alpha(\omega)\omega$ is proportional to $\sqrt{\hbar\omega - E_G}$, which is the reason it is displayed under this form in Fig. 4.7. The Matrix element $|e \cdot M_{vc}|$ is given by

$$\hbar|e \cdot M_{vc}| = \vec{e} \cdot \int_{crystal} d^3 r e^{i\vec{k}\vec{r}} u^*_{v\vec{k}}(\vec{r}) \vec{p} e^{-i\vec{k}\vec{r}} u_{c\vec{k}}(\vec{r}) \tag{5.2.38}$$

The integral can be carried over using the rule for the application of the $\vec{p}$ operator on the Bloch wavefunctions: $\vec{p} \rightarrow (\hbar\vec{k} + \vec{p})$ that yields:

$$\begin{aligned}
\hbar|e \cdot M_{vc}| &= \vec{e} \cdot \frac{1}{V_{crystal}} \int_{crystal} d^3 r e^{i\vec{k}\vec{r}} u^*_{v\vec{k}}(\vec{r}) e^{-i\vec{k}\vec{r}} (\hbar\vec{k} + \vec{p}) u_{c\vec{k}}(\vec{r}) \\
&= \vec{e} \cdot \frac{1}{V_{crystal}} (\int_{crystal} d^3 r (u^*_{v\vec{k}}(\vec{r}) \hbar\vec{k} u_{c\vec{k}}) + \int_{crystal} u^*_{v\vec{k}} \vec{p} u_{c\vec{k}}(\vec{r})) \\
&= \vec{e} \cdot \frac{1}{V_{cell}} \int_{cell} d^3 r u^*_{v\vec{k}} \vec{p} u_{c\vec{k}}(\vec{r}) \\
&= p_{cv}
\end{aligned} \tag{5.2.39}$$

assuming $\vec{e}//\vec{p}$. The first part of the integral is zero because of the orthogonality of the basis Bloch function. Because of the $\mathbf{k} \cdot \mathbf{p}$ formalism, we know the value of this integral that is rather constant for III-V semiconductors as the Kane energy $E_P = 2p_{cv}^2/m_0$ is about $20eV$. We may also express it in terms of a dipole matrix element r_{cv} using the relationship between the r and p matrix elements $(r_{cv} = \frac{-i}{m_0\omega_{cv}} p_{cv})$ and yield

$$|r_{cv}| = \frac{\hbar}{E_G} \sqrt{\frac{E_P}{2m_0}}. \tag{5.2.40}$$

To find the accurate values of the matrix element p_{cv} for a given polarization direction, one should take advantage from the the fact that the interband matrix element has the same form as the one used for the $\mathbf{k} \cdot \mathbf{p}$ derivation, by just identifying the light polarization direction $\vec{e}$ with the $\vec{k}$ and using directly the matrix shown in Fig. 5.4. The spin selectivity of the $|3/2, 3/2\rangle$ to the conduction band $|1/2, 1/2\rangle$ is already apparent in the the matrix.

Using $\mathbf{k} \cdot \mathbf{p}$ approach, we can also explain why the matrix element is a slowly varying function of k: as we move away from the k=0 condition, the states will be admixtures of the Bloch edge wavefunctions. The respective contribution will scale like the $\delta E/\Delta$ for the spin-split band and $\delta E/E_G$ for the condution band part.

Finally, one can rewrite Eq 5.2.37 using the relationship between p_{cv} and the Kane energy E_P. To be accurate, on also should consider that with the spin-orbit coupling in effect, $\frac{2}{3}$ of the oscillator strength will be at the first band edge, as shown by the ratio of the contribution to the effective masses of the bands. The absorption then writes:

$$\alpha(\omega) = \frac{q^2}{6\pi\epsilon_0 n_{refr} m_0 c} \left(\frac{2m_r}{\hbar^2}\right)^{3/2} \frac{E_P}{\hbar\omega} \sqrt{\hbar\omega - E_G} \qquad (5.2.41)$$

5.3   Effect of carriers

A key feature of a semiconductor is the possibility it offers to modify its free carrier density either by doping, electrical injection or optical pumping. Not only will these carriers modify the conductivity of the structure, they also greatly affect the absorption edge.

When computing the net rate of transition between in a general two level system, the net rate of transition writes:

$$w_{net} = w_{abs} - w_{stim} = w(n_1 - n_2) \qquad (5.3.42)$$

where w is the rate per carrier. We will modify the relations in a similar way for the semiconductors. We will assume that the probability of finding an electron at energy E in a band is given by a Fermi-Dirac distribution function such that

$$f_c = \frac{1}{exp(\frac{E-\mu_c}{kT}) + 1} \qquad (5.3.43)$$

$$f_v = \frac{1}{exp(\frac{E-\mu_v}{kT}) + 1}. \qquad (5.3.44)$$

In these equations, we choose to allow a different chemical potential for the electrons in the valence band and in the conduction band. As the thermalization of the electrons occur on a much faster time scale within the bands (typ 10ps) than between the bands (typ time 1ns), this approximation enables us to treat carrier injection in semiconductors. Note that the Fermi distribution for the valence band f_v is the one of the electrons, the one for holes being simply $f_v^{(h)} = 1 - f_v^{(e)}$.

As in the two-level system, we write the net absorption as the difference between absorption

(proportional to $f_v(1 - f_c)$) and stimulated emission (proportional to $f_c(1 - f_v)$), yielding

$$\alpha(\omega) = 2\pi \frac{\hbar^2 q^2}{\epsilon_0 n_{refr} m_0^2 \omega c} \int \frac{1}{8\pi^3} \frac{dS|e \cdot M_{vc}|^2}{|\nabla_k(E_c - E_v)||_{E_c - E_V = \hbar\omega}} \big(f_v(1 - f_c) - f_c(1 - f_v)\big)$$
$$= 2\pi \frac{\hbar^2 q^2}{\epsilon_0 n_{refr} m_0^2 \omega c} \int \frac{1}{8\pi^3} \frac{dS|e \cdot M_{vc}|^2}{|\nabla_k(E_c - E_v)||_{E_c - E_V = \hbar\omega}} \big(f_v(E_{k,v}(\hbar\omega)) - f_c(E_{k,c}(\hbar\omega))\big)$$

(5.3.45)

which can also be written in the parabolic case:

$$\alpha(\omega) = \frac{q^2}{6\pi\epsilon_0 n_{refr} m_0 \omega c} \Big(\frac{2m_r}{\hbar^2}\Big)^{3/2} \frac{E_P}{\hbar\omega} \sqrt{\hbar\omega - E_G} \big(f_v(E_{k,v}(\hbar\omega)) - f_c(E_{k,c}(\hbar\omega))\big) \quad (5.3.46)$$

where the energy dependence of the Fermi distribution has been explicited in the last equation in the kinetic energy terms $E_{k,(c,v)}$. The latter ones can be easily extracted from the fact that we are dealing with vertical transitions in k-space:

$$E_{k,v}(\hbar\omega) + E_{k,c}(\hbar\omega) = \hbar\omega - E_G \quad (5.3.47)$$

which for parabolic bands can be expressed as:

$$E_{k,c} = \frac{m_h^*}{m_e^* + m_h^*}(\hbar\omega - E_G) \quad (5.3.48)$$

$$E_{k,v} = \frac{m_e^*}{m_e^* + m_h^*}(\hbar\omega - E_G) \quad (5.3.49)$$

5.3.1 Burnstein shift

In the case of doping, we usually have that if the doping of type n then f_v is unity, in the case of p doping then f_c is zero. The net effect of doping is a shift of the bandgap as the band is filled by carrier.
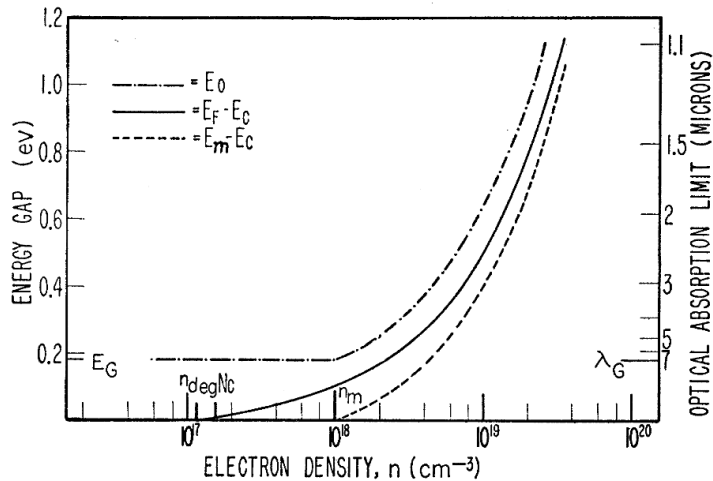
Figure 5.8: Burstein shift of InSb (very light electron mass of 0.013 m0) with n doping)

This phenomenon has been recently used to fabricate low loss waveguides for InAs-based QCLs at $\lambda = 3\mu m$, where InAs would normally be strongly absorbing.
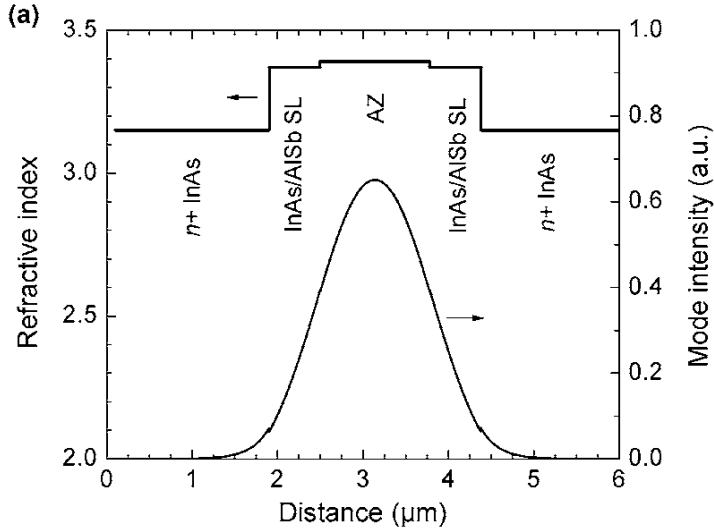
Figure 5.9: Waveguide including heavily doped InAs layers

It can be shown, using the Kramers-Konig relations and assuming parabolic bands, that the change in absorption edge with the presence of free carriers induces a change in refractive index that can be approximated by:

$$\Delta n(E) = -\frac{4\pi\hbar^2 q^2}{n_{refr}m_0^2}\frac{p_{cv}^2}{\bar{E}_G(\bar{E}_G^2 - E^2)}n_{e,h} \tag{5.3.50}$$

where $\bar{E}_G \approx E_G + kT$ is the energy at which the integrand in the KK relation has a maximum. The latter relation is valid far enough from the band edge.

5.3.2   Bandgap shrinkage

Coulomb interaction introduce a bandgap shrinkage proportional to the $n^{1/3}$ and is independent of effective mass. This term is difficult to compute accurately but should be taken into account for reliable computations of the effective bandgap.

5.4   Gain

In the case of non-equilibrium bands ($\mu_c \neq \mu_v$) then the possibility arises to observe a negative absorption, i.e. gain. The condition for the observation is that

$$f_v - f_c < 0 \tag{5.4.51}$$

which, when explicitely writing f_c and f_v, yields that

$$\exp\big(\frac{(\mu_c - \mu_v) - \hbar\omega}{kT}\big) > 1 \tag{5.4.52}$$

which implies that

$$(\mu_c - \mu_v) > \hbar\omega. \tag{5.4.53}$$

The separation between the quasi-Fermi levels must be larger than the photons. (It also means that the applied voltage on the diode must be larger than the photons, also!). This condition is referred as the Bernard-Durrafourg condition.

The gain as a function of injected carrier density may be directly computed by using Eq 5.3.46 and the neutrality condition:

$$n = p. \tag{5.4.54}$$

for undoped material, or more generaly

$$N_D^+ + N_A^- + n + p = 0 \tag{5.4.55}$$

Using the Fermi distributions and the neutrality condition for undoped material, the difference between the separation of the quasi-Fermi levels and the bandgap of GaAs can be obtained and is plotted in Fig 5.10. As shown in the latter, for these parameters the transparency is reached at a carrier density of about $1.1 \times 10^{18} cm^{-3}$.
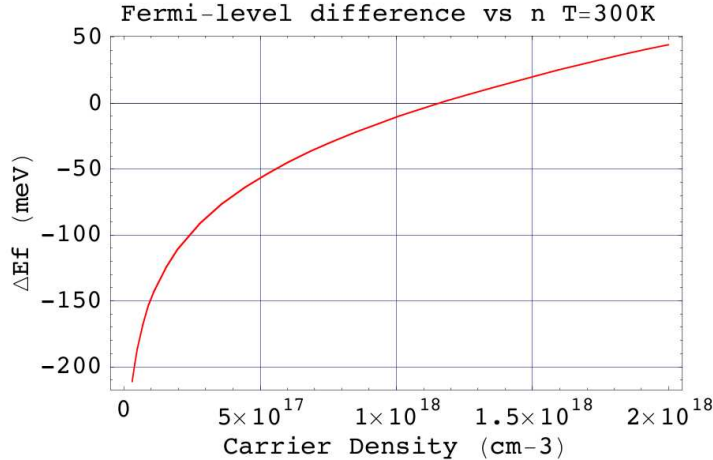
Figure 5.10: Separation of the quasi-Fermi levels and the bandgap of GaAs as a function of carrier density

Using the parameters of GaAs ($E_G = 1.5$ eV, $E_P = 22$eV, and the usual masses) the gain at T = 300K has been computed and is shown in Fig. 5.11.
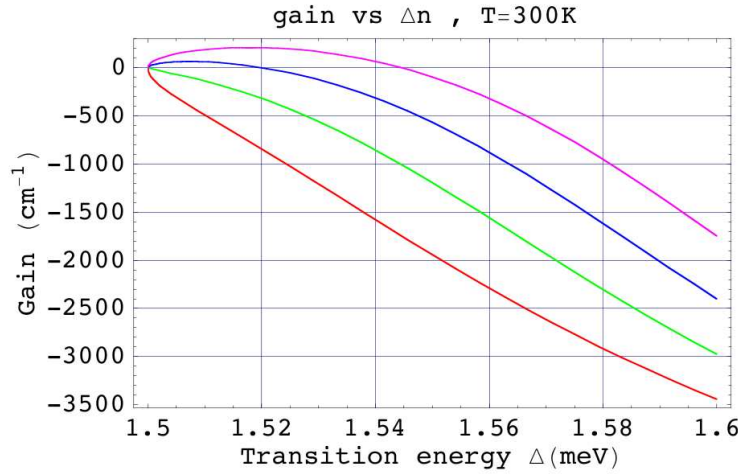
Figure 5.11: Computation of the gain for various carrier densities between 5×10^{17} to 2×10^{18}, as indicated

In Fig. 5.12, the energy range where the gain was displayed was broadened to show the energy range at which the change of absorption vanishes. The change in absorption with injected current, over this wide frequency range, is responsible for the large change in refractive index at the gain maximum.
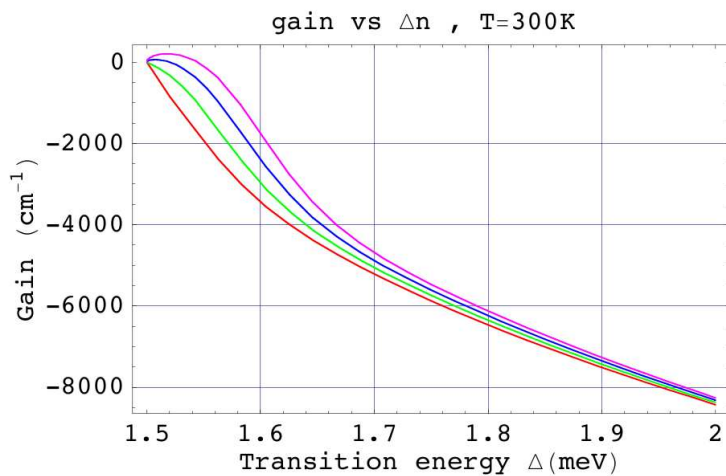
Figure 5.12: Computation of the gain for various injected densities, as indicated. The range is choosen to show the energy where the absorption is independent of carrier density

5.5   Spontaneous emission and luminescence

To compute the net absorption, we had to deal with the balance between the rate of upward transition and downward transitions. Let us write again the net transition rate as:

$$w_{net} = \rho_{BB} B_{cv}(f_v - f_c) \tag{5.5.56}$$

To derive an Einstein-like argument about the relationship between absorption and spontaneous emission, we will be interested in the case that the radiation illuminating ρ_{BB} the system is produced by a blackbody. We will write the transition rate using Fermi's golden rule:

$$B_{cv} = \frac{\pi}{2\hbar}|\langle i|H_{int}|j\rangle|^2 = \frac{\pi}{2\hbar}q^2\mathcal{E}^2 r_{cv}^2 \tag{5.5.57}$$

where we will associate the electric field produced by the single photon in the volume of our system, i.e. setting

$$\hbar\omega = \frac{1}{2}n_{refr}^2\epsilon_0\mathcal{E}^2 V. \tag{5.5.58}$$

We also use the relationship between the interband dipole matrix element r_{cv} and the Kane energy E_P

$$r_{cv}^2 = \frac{\hbar^2}{2m_0}\frac{E_P}{E_G^2}, \tag{5.5.59}$$

as a result, we obtain

$$B_{cv} = \frac{\pi q^2\hbar}{2n_{refr}^2\epsilon_0 m_0}\frac{E_P}{E_G}. \tag{5.5.60}$$

The blackbody electromagnetic energy density, usually expressed as a function of frequency, must be expressed in density of photon per unit energy, i.e.

$$\rho_{BB} = \frac{8\pi n_{refr}^3 h^2\nu^2 V}{h^3 c^3}\frac{1}{exp(-\frac{h\nu}{kT}) - 1}. \tag{5.5.61}$$

We then write a detailed balance between stimulated emission, absorption and spontaneous emission at thermal equilbrium:

$$\rho_{BB}B_{cv}f_v(1 - f_c) = \rho_{BB}B_{cv}f_c(1 - f_v) + A_{cv}f_c(1 - f_v) \tag{5.5.62}$$

Using the definitions of f_c, f_v as above, we obtain that A_{cv} and B_{cv} must be related by

$$A_{cv} = B_{cv}\frac{8\pi n_{refr}^3 h^2\nu^2}{h^3 c^3}. \tag{5.5.63}$$

The coefficient A_{cv} has to be interpreted as the rate at which a carrier in the band, having a hole to recombine with, will incur spontaneous emission. We define the inverse of $A_{cv}^{-1} = \tau_S$ as the spontaneous emission lifetime τ_S. Finally, using the value of B_{cv} derived from above, we have:

$$\frac{1}{\tau_S} = \frac{q^2 n_{refr}}{2\pi\hbar^2 c^3\epsilon_0 m_0}E_G E_P. \tag{5.5.64}$$

A typical value for the spontaneous lifetime is $\tau_S = 0.7ns$ for GaAs. As shown by the above equation, this time will drop as the energy of the gap increases.

5.5.1 Relationship between absorption and luminescence

Note that we can write the absorption coefficient α as:

$$\alpha = \frac{n_{refr}}{c} B_{cv}(f_v - f_c). \tag{5.5.65}$$

The Einstein relation between A_{cv} and B_{cv} allow us to write a very general relationship between the spontaneous emission and the absorption. The spontaneous emission rate at the photon energy $h\nu$

$$
\begin{aligned}
r_{spon} &= A_{cv}f_c(1-f_v) = B_{cv}(f_v - f_c)\frac{A_{cv}f_c(1-f_v)}{B_{cv}(f_v - f_c)} \\
&= \alpha(h\nu)\frac{c}{n_{refr}}\frac{8\pi n_{refr}^3 \nu^2}{hc^2}\frac{f_c(1-f_v)}{f_v - f_c} \\
&= \alpha(h\nu)\frac{8\pi n_{refr}^2 h^2\nu^2}{h^3 c^2}\frac{1}{exp(-\frac{h\nu}{kT}) - 1}
\end{aligned}
\tag{5.5.66}
$$

For large gap materials, and at reasonably low temperatures, $E_G >> kT$ and therefore

$$r_{spon} = \alpha(h\nu)\frac{8\pi n_{refr}^2 h^2\nu^2}{h^3 c^2}\exp(-\frac{h\nu}{kT}) \tag{5.5.67}$$

5.5.2 applications: luminescence lineshape

In general, we saw that for Bulk materials, the absorption has the form $\sqrt{\hbar\omega - E_G}$ with some weaker energy dependences. As a consequence of Eq. 5.5.67 the luminescence lineshape should conserve the $\sqrt{\hbar\omega - E_G}$ behavior at the low energy side and an exponential decrease at the high energy side.

$$\mathcal{L}(h\nu) \approx \sqrt{h\nu - E_G}\exp(-\frac{h\nu}{kT}) \tag{5.5.68}$$

The width of the curve should be approximatly $1.8kT$.
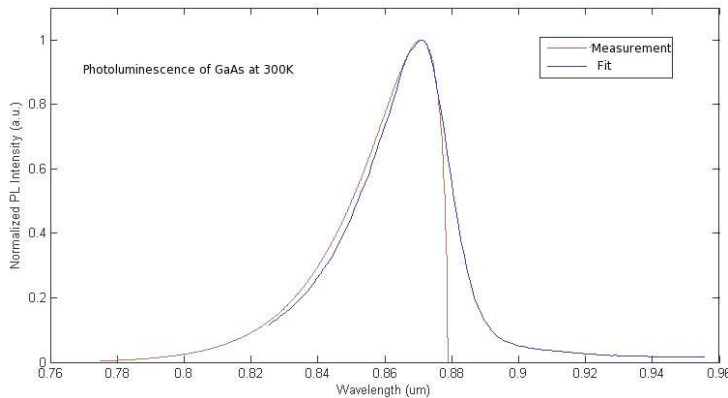
Figure 5.13: High energy tail of the photoluminescence of GaAs as a function of pumping intensity. The fitted temperature is indicated.

The photoluminescence of a undoped GaAs at room temperature is shown in Fig. 5.13 as a function of wavelength, along with a fit that uses an expression equal to Eq. 5.5.68 but expressed in wavelength units.

5.5.3 Electronic temperature

The measurement of the high energy tail of the distribution, because of the relative slow variation of the absorption, enables the measurement of the carrier temperature. This was recognized very early by Jagdeep Shah of Bell laboratories who first measured the shape of the luminescence as a function of optical pumping intensity. Result of such an experiment is shown in Fig. 5.14
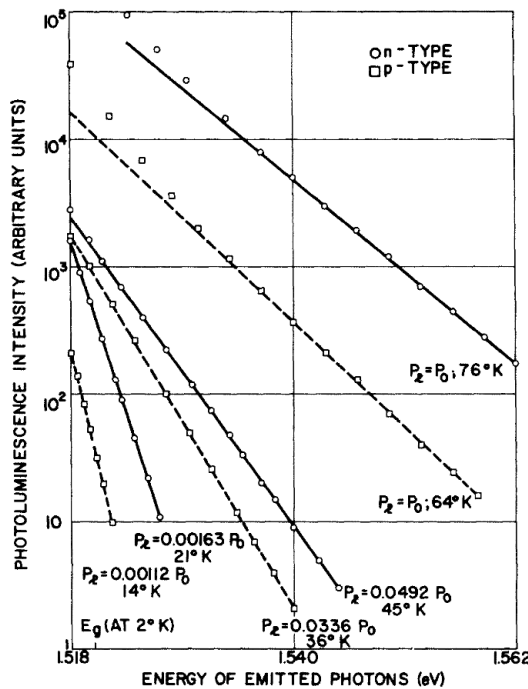
Figure 5.14: High energy tail of the photoluminescence of GaAs as a function of pumping intensity. The fitted temperature is indicated.

A plot of the carrier temperature as a function of pumping intensity demonstrated the key role of the optical phonon energy in the carrier energy dissipation:
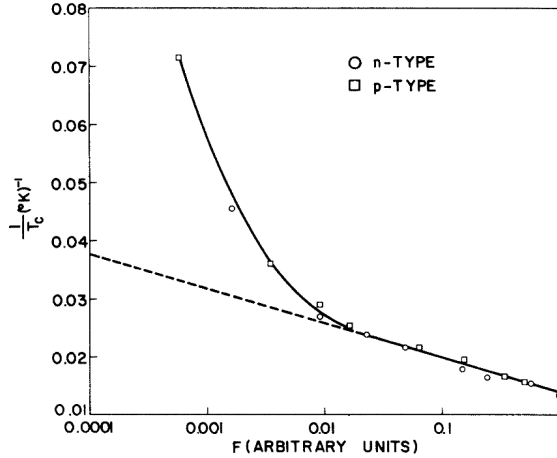
Figure 5.15: Electron temperature as a function of pumping flux. The activation energy found (33meV) is very close to the optical phonon energy (36meV)

This technique became a standard procedure for the measurement of the carrier temperature in all optoelectronic devices (lasers, transistors, etc...)

5.5.4   Gain measurement

An other interesting application of the relationship between luminescence and absorption is the possibility of measuring gain from the measurement of unamplified luminesence. In fact, assuming that f_c and f_v are characterized by quasi-Fermi chemical potentials μ_c and μ_v, the ratio $f_c(1 - f_v)/(f_v - f_c)$ appearing in Equ. 5.5.66 does yield:

$$\frac{f_c(1 - f_v)}{f_v - f_c} = \frac{1}{\exp\left(\frac{\hbar\omega - (\mu_c - \mu_v)}{kT}\right) - 1} \tag{5.5.69}$$

in which case the absorption is related to the luminescence by:

$$\alpha(h\nu) = r_{spon} \frac{h^3 c^2}{8\pi n_{refr}^2 h^2 \nu^2} \exp\left(\frac{\hbar\omega - (\mu_c - \mu_v)}{kT}\right) - 1 \tag{5.5.70}$$

and the latter equation can be used to measure the absorption (and therefore the gain) through a measurement of the unamplified luminescence as a function of injected current. This technique was first demonstrated by C. Henry from Bell Labs.
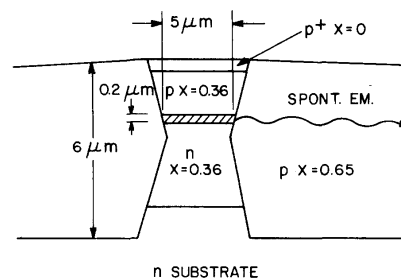
Figure 5.16: Schematic drawing of the luminescence measurement geometry
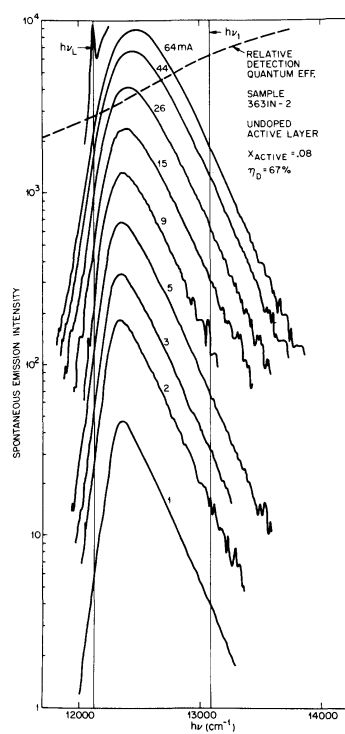
Figure 5.17: Luminescence as a function of injected current. The measurement of the gain is deduced from the ratio of these curves
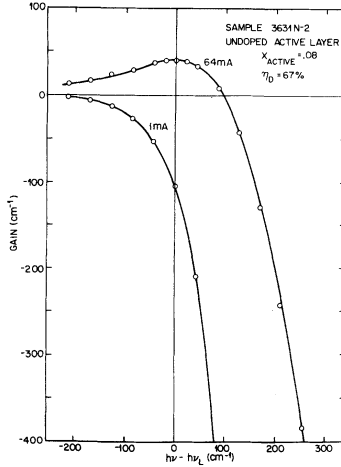
Figure 5.18: Measured gain at 1mA and 64mA injection current
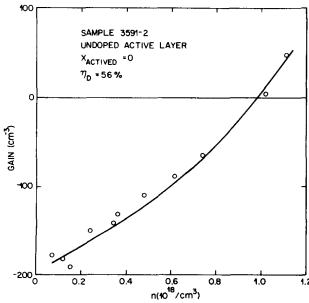
Figure 5.19: Gain at the laser wavelength versus carrier density

5.5.5   Bimolecular recombination

Let us consider the term $f_c(1 - f_v)$ at low injection levels, in the classical regime. we have

$$f_c = \frac{1}{\exp(\frac{E_c - \mu_c}{kT}) + 1} \approx \exp(-\frac{E_c - \mu_c}{kT})$$

$$1 - f_v = 1 - \frac{1}{\exp(\frac{E_v - \mu_v}{kT}) + 1} \approx \exp(\frac{E_v - \mu_v}{kT})$$

$$(5.5.71)$$

As a result, the product $f_c(1 - f_v)$ is given by

$$f_c(1 - f_v) \approx \exp\left(-\frac{\hbar\omega - (\mu_c - \mu_v)}{kT}\right). \tag{5.5.72}$$

We then want to compute the total recombination rate from all the carrier population. To this end, we integrate the spontaneous emission as a function of photon energy:

$$
\begin{aligned}
R_{spon} &= \int \frac{1}{\tau_S} \rho_j(h\nu) f_c (1 - f_v) dh\nu \\
&= \frac{1}{\tau_S} \exp\left(\frac{\mu_c - \mu_v}{kT}\right) \int_{E_G}^{\infty} \rho_j \exp\left(-\frac{h\nu}{kT}\right) dh\nu \\
&= \frac{\exp\left(\frac{\mu_c - \mu_v}{kT}\right)}{\tau_S} \frac{1}{2\pi^2} \left(\frac{2m_r}{\hbar^2}\right)^{3/2} \int_{E_G}^{\infty} \sqrt{h\nu - E_G} \exp\left(-\frac{h\nu}{kT}\right) dh\nu \\
&= \frac{\exp\left(\frac{\mu_c - \mu_v}{kT}\right)}{\tau_S} \frac{1}{2\pi^2} \left(\frac{2m_r kT}{\hbar^2}\right)^{3/2} \int_0^{\infty} \sqrt{u} \exp(-u) du.
\end{aligned}
\tag{5.5.73}
$$

The integral $\int_0^{\infty} \sqrt{u} \exp(-u) du = \frac{\sqrt{\pi}}{2}$. The above equation may be simplified by expressing the quasi-Fermi level implicitly through the electron and hole concentrations, always in the classical limit:

$$
\begin{aligned}
n &= N_c \exp\left(-\frac{E_c - \mu_c}{kT}\right) \\
p &= N_v \exp\left(\frac{E_v - \mu_v}{kT}\right)
\end{aligned}
\tag{5.5.74}
$$

where the quantum concentration $N_{c,v}$ is given by:

$$
N_{c,v} = 2\left(\frac{m_{c,v} kT}{2\pi\hbar^2}\right)^{3/2}
\tag{5.5.75}
$$

The product np yields (law of mass action)

$$
np = N_c N_v \exp\left(-\frac{(E_c - E_v) - (\mu_c - \mu_v)}{kT}\right)
\tag{5.5.76}
$$

That allows finally us to write the total spontaneous emission rate:

$$
R_{spon} = \frac{1}{\tau_{spon}} \frac{np}{N_c N_v} N_j
\tag{5.5.77}
$$

written usually as a function of the bimolecular recombination coefficient B

$$
R_{spon} = Bnp
\tag{5.5.78}
$$

As the value of B is given by:

$$
B = \frac{N_j}{N_c N_v \tau_{spon}}
\tag{5.5.79}
$$

B is both material and temperature dependent. The temperature dependence is $T^{-3/2}$ and the material dependence can be expressed using the known values of the quantum concentrations and of the spontaeous lifetime.

It should be remembered that the range of concentration in which this expression is valid: it assumes classical distribution (limitation towards the high concentrations) but does not include the excitonic effects and so is expected to fail at very low concentrations.

Chapter 6

Quantum wells and nanostructures

6.1 Envelope function approximation

The problem we will try and solve now is the one of a heterosructure, in which two materials A and B are sandwiched together. Of course such a material could be seen as a new material by itself, and its band solved by ab initio techniques, but such a computation is very heavy, time consuming and moreover does not give much physical insight into the result. The envelope function approximation solves this problem in a very efficient and elegant manner. It is widely used to predict the optical, electrical properties of semiconductor nanostructures.

6.1.1 Multiband case

At the core of the envelope function approximation is a generalization of the $\mathbf{k} \cdot \mathbf{p}$ approximation: it is postulated that the wavefunction can be written as a sum of slowly varying envelop functions $f_l^{A,B}(r)$ that will modulate the Bloch function of the material, namely:

$$\Psi(r) = \sum_l f_l^{A,B} u_{l,k_0}^{A,B}(r). \tag{6.1.1}$$

Behind the equation 6.1.1 is the idea that at each point, the wavefunction is described by a $\mathbf{k} \cdot \mathbf{p}$ decomposition and that this decomposition depends on the position. Furthermore, it is assumed that

1. the envelop function $f_l^{A,B}(r)$ is slowly varying compared to the Bloch wavefunction, if $f_l^{A,B}(r)$ is written in a Fourier decomposition, the wavevectors are close to the center of the Brillouin zone

2. the Bloch functions are identical in both materials, i.e. $u_{n,k_0}^A(r) = u_{n,k_0}^B(r)$. This also implies that the interband matrix element $\langle S|p_x|X \rangle$ is equal in both materials.

It allows us to write te wavefunction as

$$\Psi(r) = \sum_l f_l^{A,B} u_{l,k_0}(r). \tag{6.1.2}$$

Let us assume first a quantum well, in which a layer of material A is sandwiched into a barrier material B. Because of the in-plane translational invariance, the wavfuction may be written as plane waves:

$$f_l(r_\perp, z) = \frac{1}{\sqrt{S}} e^{ik_\perp r_\perp} \chi_l(z) \qquad (6.1.3)$$

where z is choosen as the growth direction and $k_\perp = (k_x, k_y)$ is the in-plane wavevector. Note that this convention there is confusion in the litterature as the sign $\perp$ may either mean perpendicular to the plane of the layers or to the growth axis. The Hamiltonian is then

$$H = \frac{p^2}{2m_0} + V_A(r)Y_A + V_B(r)Y_B \qquad (6.1.4)$$

where the functions $Y_A(z)$ and $Y_B(z)$ "turn on" the potential in the respective layers. We will develop our system close to k=0. To solve the system, we must:

1. Let H act upon $\Psi(r)$

2. multiply on the left by $u_{m0}^*(r)e^{-ik_\perp r_\perp}\chi_m^*(z)$

3. integrate over space

We have to use the following relations. As the envelop function is slowly varying, we may write

$$\int_{cell} d^3r f_l^* f_m u_l^* u_m = f_l^* f_m \int_{cell} d^3r u_l^* u_m = f_l^* f_m \delta_{lm} \qquad (6.1.5)$$

and take advantage of the fact that the band edge are eigen function of the Hamiltonian at (k=0):

$$\Big(\frac{p^2}{2m_0} + V^{A,B}(r)\Big)u_{m,0}(r) = \epsilon_{m,0}^{A,B}u_{m,0}(r). \qquad (6.1.6)$$

The derivation is rather tedious, but one should note the similarity with the normal $\mathbf{k} \cdot \mathbf{p}$ technique by considering the action of the operator $\mathbf{p}$ on the wavefunction:

$$p(e^{k_\perp r_\perp}\chi_l(z)u_l(r)) = (\hbar k_\perp - i\hbar\frac{\partial}{\partial z} + p)e^{ik_\perp r_\perp}\chi_l(z)u_l(r) \qquad (6.1.7)$$

and we then may consider the substitution

$$p \rightarrow (\hbar k_\perp - i\hbar\frac{\partial}{\partial z} + p) \qquad (6.1.8)$$

where it is understood that p then acts only on the Bloch part of the wavefunction. Using the above substitution into the Hamiltonian, one finally get the following set of diferential equation written in a matrix form:

$$\underline{D}(z, -i\hbar\frac{\partial}{\partial z})\chi = \epsilon\chi \qquad (6.1.9)$$

where the elements of the matrix $\underline{D}$ are given by the equation

$$
\begin{aligned}
D_{lm} = \Big(\epsilon_l^A Y_A + \epsilon_l^B Y_B + \frac{\hbar^2 k_\perp^2}{2m_0} - \frac{\hbar^2}{2m_0} \frac{\partial^2}{\partial z^2} \Big) \delta_{l,m} \\
+ \frac{\hbar k_\perp}{m_0} \langle l|p_\perp|m\rangle - \frac{i\hbar}{m_0} \langle l|p_z|m\rangle \frac{\partial}{\partial z}
\end{aligned}
\tag{6.1.10}
$$

and the matrix element $\langle l|p|m\rangle = \int_{cell} u_l^* p u_m d^3 r$.

6.1.2   One Band model

As an example, let us consider first a pure one band model. Setting

$$
\epsilon_l^A Y_A + \epsilon_l^B Y_B = V(z)
\tag{6.1.11}
$$

we obtain the Schrödinger equation:

$$
(-\frac{\hbar^2}{2m_0} \frac{\partial^2}{\partial z^2} + V(z))\chi(z) = \epsilon \chi(z)
\tag{6.1.12}
$$

This equation is of course the one of a free electron in a potential. As a consequence, it does not take into account the dispersion of the band. A much better model would be to replace m_0 in equation 6.1.12 by the band effective mass m_{eff}. For an isolated band such as the heavy hole band, it is a rather good approximation. Formally, it should be done by adding the effect of the remote bands in the matrix 6.1.10, the result of which is given (see Bastard) for a 8 band model with the remote bands as

$$
\begin{aligned}
\sum_{m=1}^{8} \Big(\big[\epsilon_m^A + V_m(z) + \frac{\hbar^2 k_\perp^2}{2m_0} - \frac{\hbar^2}{2m_0} \frac{\partial^2}{\partial z^2} \big] \delta_{l,m} + \frac{\hbar k_\perp}{m_0} \langle l|p_\perp|m\rangle - \frac{i\hbar}{m_0} \langle l|p_z|m\rangle \frac{\partial}{\partial z} \\
- \frac{\hbar^2}{2} \frac{\partial}{\partial z} \frac{1}{M_{lm}^{zz}} \frac{\partial}{\partial z} - \frac{i\hbar^2}{2} \sum_{\alpha=x,y} \big[k_\alpha \frac{1}{M_{lm}^{\alpha z}} \frac{\partial}{\partial z} + \frac{\partial}{\partial z} \frac{1}{M_{lm}^{z\alpha}} k_\alpha \big] + \frac{\hbar^2}{2} \sum_{\alpha,\beta=x,y} k_\alpha \frac{1}{M_{lm}^{\alpha\beta}} k_\beta \Big) \chi_m = \epsilon \chi_l
\end{aligned}
\tag{6.1.13}
$$

where effective mass parameters $M_{lm}^{\alpha\beta}$ are defined as

$$
\frac{m_0}{M_{lm}^{\alpha\beta}} = \frac{2}{m_0} \sum_\nu \langle l|p_\alpha|\nu\rangle \frac{1}{\epsilon - \epsilon_{\nu 0} - V_\nu(z)} \langle m|p_\beta|\nu\rangle
\tag{6.1.14}
$$

One sees that for a one band model, neglecting the in-plane dispersion, the term $\frac{\hbar^2}{2} \frac{\partial}{\partial z} \frac{1}{M_{lm}^{zz}} \frac{\partial}{\partial z}$ is the only one remaining and will then change the effective mass. Boundary conditions can be derived and be shown to force the continuity of the wavefunction and of the quantity

$$
\frac{1}{m(z)} \frac{\partial \chi}{\partial z}
\tag{6.1.15}
$$

which is proportional to the probability current.

Using this model, on immediatly obtain the confinement energy in quantum wells, that will express themselves by a increase of the apparent conduction band and valence band energy. This effect will be stronger for electrons that are lighter than for the heavier holes.
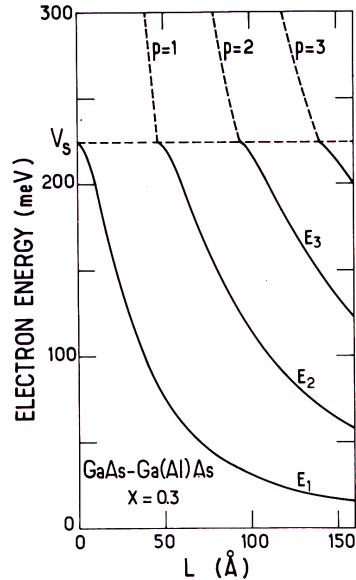
Figure 6.1: Computed confinement energy of electrons in the conduction band as a function of well width.
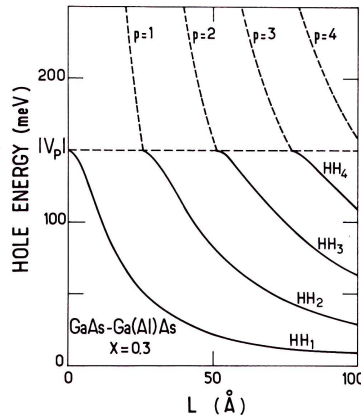
Figure 6.2: Computed confinement energy of the valence band as a function of well width.

6.1.3 Two band model

For the conduction band, a very nice model is the one in which one keeps one valence band, creating a two-band model. For simplicity, let us look at the states at $k_\perp = 0$ and neglect

the free electron term. We obtain the system of equation given by:

$$V_c(z)f_c - \frac{i\hbar}{m_0}p_{cv}\frac{\partial}{\partial z}f_v = \varepsilon f_c \tag{6.1.16}$$

$$\frac{-i\hbar}{m_0}p_{cv}^*\frac{\partial}{\partial z}f_c + V_v(z)f_v = \varepsilon f_v \tag{6.1.17}$$

Extracting f_v from the second equation yields:

$$f_v = \frac{1}{V_v(z) - \epsilon}\frac{i\hbar}{m_0}p_{cv}^*\frac{\partial}{\partial z}f_c \tag{6.1.18}$$

replacing into the first equation, after substitution, the following reslult is obtained.

$$-\frac{\hbar^2|p_{cv}|^2}{m_0}\frac{\partial}{\partial z}\frac{1}{\varepsilon - V_v(z)}\frac{\partial}{\partial z}f_c + V_c(z)f_c = \varepsilon f_c. \tag{6.1.19}$$

Recalling the definition of the Kane energy $E_P = \frac{2}{m_0}p_{cv}^2$ and defining an energy-dependent effective mass:

$$\frac{1}{m(\varepsilon, z)} = \frac{1}{m_0}\frac{E_P}{\varepsilon - V_v(z)} \tag{6.1.20}$$

we obtain finally a Schrödinger-like equation

$$-\frac{\hbar^2}{2}\frac{\partial}{\partial z}\frac{1}{m(\varepsilon, z)}\frac{\partial}{\partial z}f_c + V_c(z)f_c = \varepsilon f_c. \tag{6.1.21}$$

This model is very useful to model the electronic states in the conduction band with the inclusion of the non-parabolicity. It is very widely used in the study of intersubband transitions.
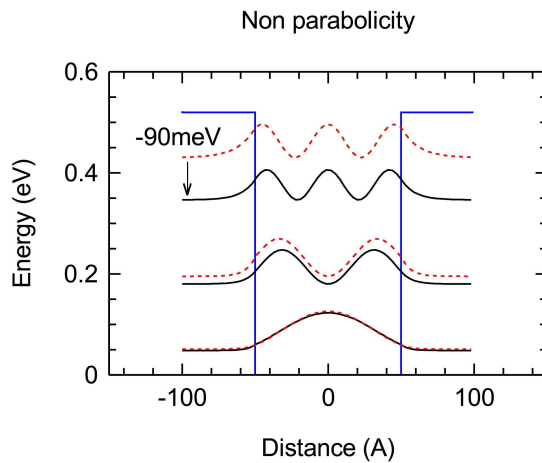
Figure 6.3: Energy states of a quantum well computed with a two-band model, and compared with a one-band model (dashed lines). The growing importance of non-parabolicity as one moves away from the gap is clearly apparent.

6.1.4   Full model: the valence band

To be accurate, the full $\mathbf{k\cdot p}$ envelope function model must be solved, that is the set of 8 differential equations defined by the equation 6.1.9. Solving the full model is essential in the valence band because no simplified model can easily be used if some degree of accuracy is sought. It is observed that:

- It is usualy convienient to use the growth direction as the quantization direction for the angular momentum.

- The confinement potential lifts the degeneracy between the heavy and light hole bands, because their different mass induce a different confinement energy

- The in-plane dispersion is highly non-parabolic because of the coupling between the bands induced by the in-plane momentum. In particular, this coupling prevents any crossing between the light-hole derived and the heavy hole-derived band (see dahsed lines)

- In some cases, the mass is inverted: the bottom of the LH1 band has a electron-like character over some portion of reciprocal space because of the repulsion and its proximity to the HH2 state.

This effect is shown schematically in Fig. 6.4. As a result, the computed band structure is usually fairly complex, and yield results such as the ones shown in Fig. 6.5
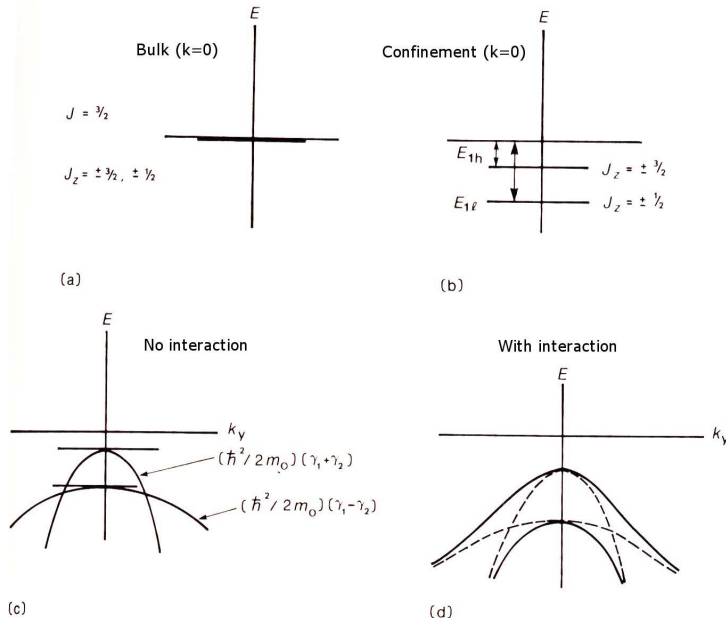
Figure 6.4: Schematic description of the origin of the valence band dispersion in the quantum well showing schematically the effects of confinement and interactions.
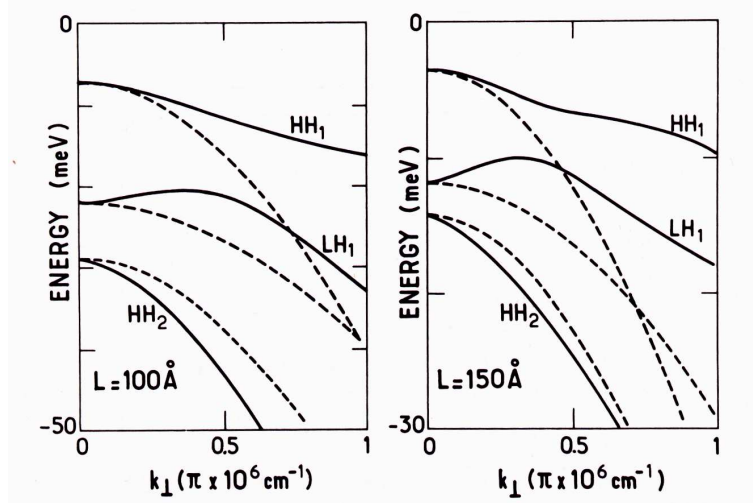
Figure 6.5: Dispersion of the state of a quantum well in the valence band.

6.2   Absorption: interband case

The states computed using the envelope function approximation can now be used as a basis for the computation of the absorption in the system. Let us use here the dipole interaction Hamiltonian (the reason for using it will appear later) so that

$$H_{int} = -q\mathcal{E} \cdot r \tag{6.2.22}$$

and let us consider the transition from a valence band state given by

$$|nk_\perp\rangle = \frac{1}{\sqrt{A}}\chi_n(z)e^{ik_\perp r_\perp}u_v(r) \tag{6.2.23}$$

to a conduction band

$$|mk'_\perp\rangle = \frac{1}{\sqrt{A}}\chi_m(z)e^{ik'_\perp r_\perp}u_c(r) \tag{6.2.24}$$

where $r = (r_\perp, z)$ is the position and $r_\perp$ is the in-plane coordinate and A the sample's area. The matrix element is then

$$\langle mk'_\perp|\mathcal{E} \cdot r|nk_\perp\rangle = \frac{1}{A}\int_{space} d^3r \chi_m^*(z)e^{-ik'_\perp r}u_c^*(r)\mathcal{E} \cdot r\chi_n(z)e^{iqr}e^{ik_\perp r}u_v(r). \tag{6.2.25}$$

The above integral can be simplified by:

- Breaking the integral into a sum of elementary cells $\sum_{i_x,i_y,i_z}$ over which the integral is carried over

- Assuming that the envelope functions are slowly varying and therefore can be pulled out in front of the integrals.

We then obtain:

$$\langle mk'_\perp|\mathcal{E}\cdot r|nk_\perp\rangle = \frac{1}{A}\sum_{i_z}\chi_m^*(z)\chi_n(z_i)\frac{a_z}{N_xN_y}\sum_{i_x,i_y}e^{i(k_\perp+q-k'_\perp)r_{\perp,i}}$$
$$\frac{1}{V_{cell}}\Big[\int_{cell}d^3r'u_c^*(r')\mathcal{E}\cdot r'u_v(r)e^{i(k_\perp+q-k'_\perp)r'} \qquad (6.2.26)$$
$$+\mathcal{E}\cdot r'\int_{cell}d^3r'u_c^*(r')u_v(r)e^{i(k_\perp+q-k'_\perp)r'}\Big].$$

that can then further be simplified (note that the second integral is zero because the Bloch functions are orthogonal):

$$\langle mk'_\perp|\mathcal{E}\cdot r|nk_\perp\rangle = \delta(k_\perp+q-k'_\perp)r_{cv}\int_{-\infty}^{\infty}\chi_{m,c}^*\chi_{n,v} \qquad (6.2.27)$$

The corresponding scattering rate, computed using Fermi's golden rule, writes:

$$w_{v\to c} = \frac{\pi}{2\hbar}q^2|r_{cv}|^2|\langle m,c|n,v\rangle|^2. \qquad (6.2.28)$$

As in the three dimentional case, it should be summed in k-space for all available states that satisfy the k-selection rule, and multiplied by the corresponding Fermi distributions. We obtain for one pair of subband:

$$w_{v\to c} = \frac{\pi}{2\hbar}q^2|r_{cv}|^2|\langle m,c|n,v\rangle|^2\frac{m_r}{\pi\hbar^2}\Theta(\hbar\omega-(E_G+\epsilon_{c,m}+\epsilon_{v,n}))f_{v,n}(1-f_{c,n}) \qquad (6.2.29)$$

Notes on this result:

- The scalar product $|\langle m,c|n,v\rangle|^2$ will be zero for quantum well states of opposite parity in symmetric quantum wells.

- In general, this term will be very small for states with different level index.

- The matrix element r_{cv} depends on the polarisation direction and on the nature of the valence band Bloch states.

Let us consider the last point a little more in detail. For example, let us assume we are looking at a transition between a state $|\frac{3}{2},\frac{3}{2}\rangle$ and the conduction band $|i\S\uparrow\rangle$. Using the relation between the dipole matrix element and the momentum matrix element:

$$r_{cv} = \frac{-i\hbar}{m_0E_G}p_{cv} \qquad (6.2.30)$$

we can then use the Kane matrix $\mathbf{k}\cdot\mathbf{p}$ 5.4 to obtain the value of the matrix element, that would be $\frac{1}{\sqrt{2}}p_{cv}$ for this heavy-hole to conduction band transition in the TE polarization direction. One can check that considering a light hole to conduction band transition would lead to a coefficient equatl to $\frac{1}{\sqrt{6}}$.

Table II. — *Selection rules for interband (inter-subband) transitions obtained from the absolute value of the matrix element* $\langle S\uparrow | \boldsymbol{\varepsilon}.\boldsymbol{p} | u_\alpha \rangle$, $\alpha = \Gamma_8$, $\Gamma_7.\boldsymbol{k}_\perp = \boldsymbol{0}$.

Polarization	ε_x	ε_y	ε_z	Type of transitions
Propagation parallel to $\hat{z}$	$\dfrac{\Pi}{\sqrt{2}}$	$\dfrac{\Pi}{\sqrt{2}}$	impossible	$HH_n \to E_m$
Propagation parallel to $\hat{x}$	impossible	$\dfrac{\Pi}{\sqrt{2}}$	forbidden	$HH_n \to E_m$
Propagation parallel to $\hat{y}$	$\dfrac{\Pi}{\sqrt{2}}$	impossible	forbidden	$HH_n \to E_m$
Propagation parallel to $\hat{z}$	$\dfrac{\Pi}{\sqrt{6}}$	$\dfrac{\Pi}{\sqrt{6}}$	impossible	$LH_n \to E_m$
Propagation parallel to $\hat{x}$	impossible	$\dfrac{\Pi}{\sqrt{6}}$	$\dfrac{2\Pi}{\sqrt{6}}$	$LH_n \to E_m$
Propagation parallel to $\hat{y}$	$\dfrac{\Pi}{\sqrt{6}}$	impossible	$\dfrac{2\Pi}{\sqrt{6}}$	$LH_n \to E_m$
Propagation parallel to $\hat{z}$	$\dfrac{\Pi}{\sqrt{3}}$	$\dfrac{\Pi}{\sqrt{3}}$	impossible	$(\Gamma_7)_n \to E_m$
Propagation parallel to $\hat{x}$	impossible	$\dfrac{\Pi}{\sqrt{3}}$	$\dfrac{\Pi}{\sqrt{3}}$	$(\Gamma_7)_n \to E_m$
Propagation parallel to $\hat{y}$	$\dfrac{\Pi}{\sqrt{3}}$	impossible	$\dfrac{\Pi}{\sqrt{3}}$	$(\Gamma_7)_n \to E_m$

Figure 6.6: Interband selection rules for quantum wells
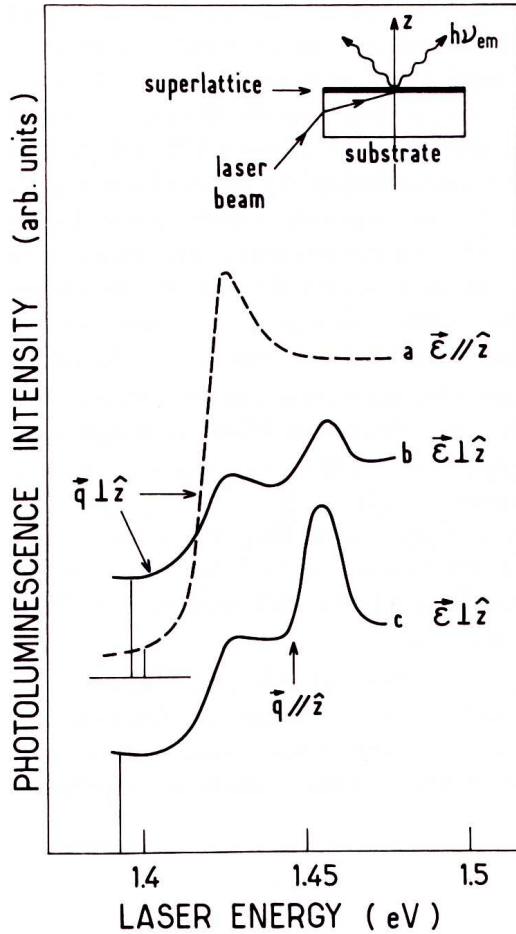
Figure 6.7: Quantum well absorption in TE and in TM, showing the absence of HH transition in TM

Finally, the absorption can be obtained from the scattering rate by computing the ratio of the absorbed power divided by the incident one. For a quantum well at an incident angle of θ, the result yield:

$$\alpha = \frac{\hbar\omega w_{v\to c}}{\frac{1}{2}\epsilon_0 nc\mathcal{E}^2 \cos(\theta)} = \frac{q^2 m_r \hbar\omega}{\hbar^3 \epsilon_0 n_{refr} c \cos(\theta)} |\eta_q \cdot r_{cv}|^2 |\langle m, c|n, v\rangle|^2 \qquad (6.2.31)$$

assuming the whole beam is intercepted by the quantum well.In the above equation, the absorption is number, and represents the fraction of the beam absorbed by the quantum well system. For situation where the incidence angle is $\theta = \pi/2$, the latter assumption is not possible and one then defines an absorption coefficient given by:

$$\alpha = \frac{q^2 m_r \hbar\omega}{\hbar^3 \epsilon_0 n_{refr} c} |\eta_q \cdot r_{cv}|^2 |\langle m, c|n, v\rangle|^2 \frac{\Gamma}{d_{qw}} \qquad (6.2.32)$$

where d_{qw} is the thickness of the quantum well (but can be defined in an other manner as the period length for a superlattice) and the overlap factor of the quantum well with the intensity of a guided modeΓ is defined by:

$$\Gamma = \frac{\int_{-d_{qw}/2}^{d_{qw}/2} E^2 dz}{\int_{-\infty}^{\infty} E^2 dz} \tag{6.2.33}$$

Note that the product $d_{qw}\Gamma$ is almost indepdent of d_{qw} as long as the quantum well is much smaller than the width of the guided mode.

6.2.1 Interband spectroscopy: notes on the techniques

Comparison between the different techniques used.

- Absorption

- Photoluminescence

- Photoluminesence excitation
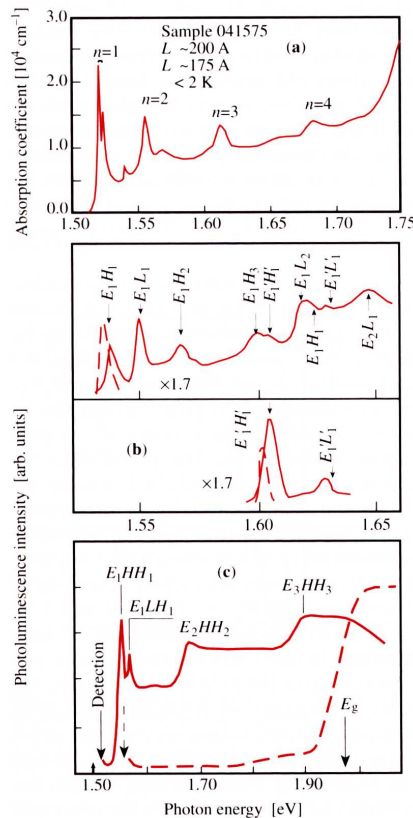
Fig. 7.16a–c. Comparison between absorption and PLE spectra in GaAs/AlGaAs quantum well (QW) samples measured at low temperature. (a) Absorption spectra in a 20 nm well showing structures due to excitonic absorption peaks (labeled n = 1, 2, etc.) [7.45]. (b) PLE spectra from a sample containing two QWs with widths of 5 and 10 nm (shown in *lower* and *upper panels* respectively). The *broken curves* show the PL from these two wells [7.46]. (c) PLE spectra from a p-doped well. The broken curve was obtained by setting the spectrometer to admit only excitonic emission (indicated by the *broken vertical arrow*). The *vertical arrow* labeled E_g marks the energy gap of the AlGaAs barrier layer. The *solid curve* is the PLE spectrum obtained when the spectrometer was set at the energy of the electron-to-neutral-acceptor emission (indicated by the *solid vertical arrow*) [7.47]

Figure 6.8: Comparison between absorption, PL and PL excitation (From Cardona's book)
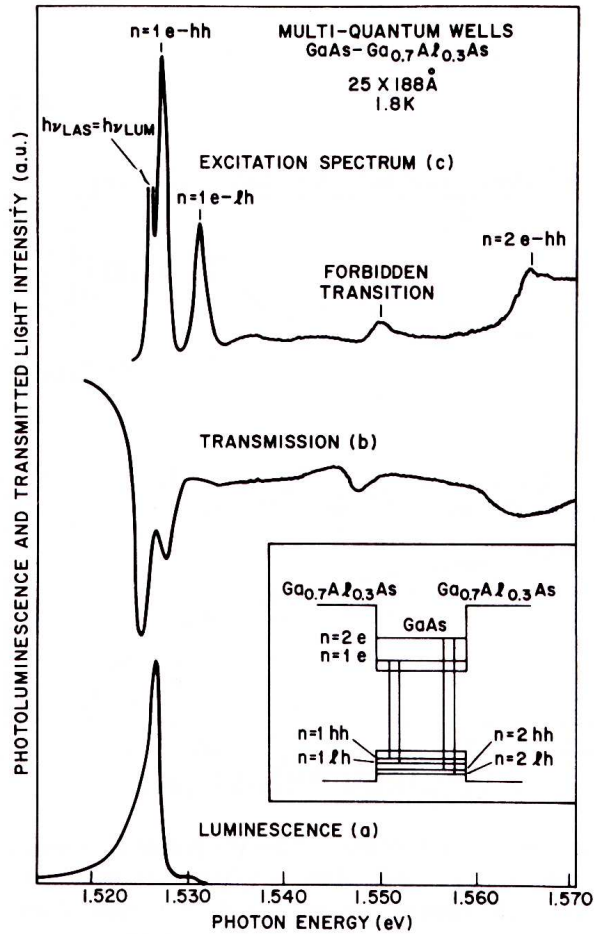
Figure 6.9: Comparison between absorption, PL and PL excitation (From Weisbusch and Winter)

6.2.2 Note on the QW absorption

Let us assume the transition between a pair of subband in a quantum well. The absorption for normal incidence $\theta = \pi/2$ (considering only the heavy hole transitions first):

$$\alpha = \frac{q^2 m_r^{hh} \hbar \omega}{\hbar^3 \epsilon_0 n_{refr} c} |r_{cv}^{hh}|^2 |\langle m, c | n, v \rangle|^2 \tag{6.2.34}$$

We should first note that the overlap factor $|\langle m, c | n, v \rangle|^2 \approx 1$ for a transition between two ground states. Then, we shall use the relationship between the dipole matrix element and the momentum matrix element

$$r_{cv} = \frac{-i\hbar}{m_0 E_G} p_{cv} \tag{6.2.35}$$

and we have, for a transition between hh1 and E1:

$$|r_{cv}|^2 = \frac{\hbar^2 E_P}{4m_0 E_G^2} \tag{6.2.36}$$

For the same transition, we may also express the joint density of state effective mass as:

$$m_{r,hh}^{-1} = m_e^{-1} + m_{hh}^{-1} \tag{6.2.37}$$

For the heavy hole state, we will use the in-plane mass of the $|\frac{3}{2}, \frac{3}{2}\rangle$ state that gives (see the kp matrix Fig. 5.4) as

$$m_{hh}^{-1} = -m_0^{-1} + \frac{P^2}{E_G} = -m_0^{-1} + m_0^{-1}\frac{E_P}{2E_G} \tag{6.2.38}$$

For the electron effective mass, we have:

$$m_e^{-1} = m_0^{-1} + \frac{2E_P}{3m_0 E_G} + \frac{E_P}{3m_0(E_G + \Delta)} \tag{6.2.39}$$

that then yields for the reduced mass:

$$m_{r,hh}^{-1} = m_0^{-1}\Big(\frac{7}{6}\frac{E_P}{E_G} + \frac{E_P}{3m_0(E_G + \Delta)}\Big) \approx \frac{3E_P}{2m_0 E_G} \tag{6.2.40}$$

Substituting both reduced mass and matrix element by the above expressions in the absorption yields:

$$\alpha_{hh} = \frac{2q^2}{3 \times 4\hbar\epsilon_0 n_{refr} c} = \frac{2}{3}\frac{1}{n_{refr}\pi\alpha_{fine}} \tag{6.2.41}$$

where $\alpha_{fine} \approx 1/137$ is the fine structure constant. For a refractive index of $n_{refr} = 3.6$, the absorption corresponds to $\alpha_{hh} = 4.26 \times 10^{-3}$. The effect of the refractive index is only there when measuring thick samples; for a very thin quantum well suspended in vaccum the absorption would simply be equal to $2\pi\alpha_{fine}/3$. It is interesting to note that not only this results does not depend on the detail of the quantum well such as its thickness or barrier height; it does not even depend on the value of the Kane energy E_P.

In most samples, the transition between LH1 and E1 is very close to the HH1 E1 transition and, because of excitonic effects, it is not possible to find a plateau of absorption between these two values. For this transition, the light hole mass (assuming the $|\frac{3}{2}, \frac{1}{2}\rangle$ basis state) :

$$m_{lh}^{-1} = -m_0^{-1} + \frac{P^2}{3E_G} = -m_0^{-1} + m_0^{-1}\frac{E_P}{6E_G} \tag{6.2.42}$$

The reduced mass is, in turn:

$$m_{r,lh}^{-1} = m_0^{-1}\Big(\frac{5}{6}\frac{E_P}{E_G} + \frac{E_P}{3m_0(E_G + \Delta)}\Big) \approx \frac{5E_P}{6m_0 E_G} \tag{6.2.43}$$

Similarely, the matrix element r_{cv} is given by

$$|r_{cv}|^2 = \frac{\hbar^2 E_P}{12 m_0 E_G^2} \tag{6.2.44}$$

Again, combining the two, we obtain:

$$\alpha_{lh} = \frac{q^2}{10 \hbar \epsilon_0 n_{refr} c} = \frac{2}{5} \frac{1}{n_{refr} \pi \alpha_{fine}} \tag{6.2.45}$$

The sum of the absorption caused by the lh and the hh state is then

$$\alpha_{hh,lh} = \frac{16}{15} \frac{1}{n_{refr} \pi \alpha_{fine}} \tag{6.2.46}$$

which is equal to 6.8×10^{-3} for a refractive index of $n_{refr} = 3.6$. The data in the litterature yield value somewhat larger. As an example, the data from Stolz et al for various well width in InGaAs/AlInAs samples yield a value of (0.82-0.89%), and an analysis of the absorption in InGaAs/InP quantum wells of Sugawara yields 0.85%. A enhancement given by the Sommerfeld factor, equal to 2 close to the bandgap, is perhaps the reason for the discrepancy. If it is true, the value for very low mass materials such as InAs should yield lower values. Indeed, values for the GaAs-based quantum wells reported by Masselink, with heavier masses and where excitonic effects ar more prevalents, are closer to 1% absorption.

Additionally, measurement of such small absorption factor are always difficult experiments. In particular, baseline issues become critical. The presence of standing wave brought about by the reflection on the surface will equally skew the results.
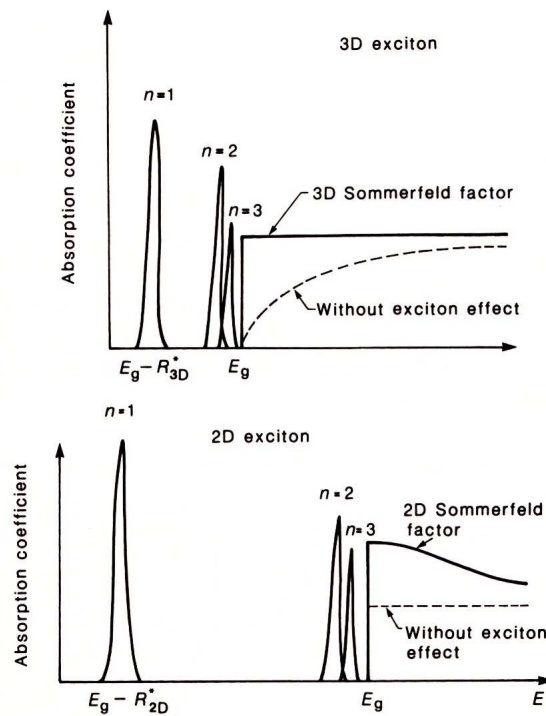
Figure 6.10: Sommerfeld factor for the exciton: 3D versus 2D case (Weisbuch and Winter).
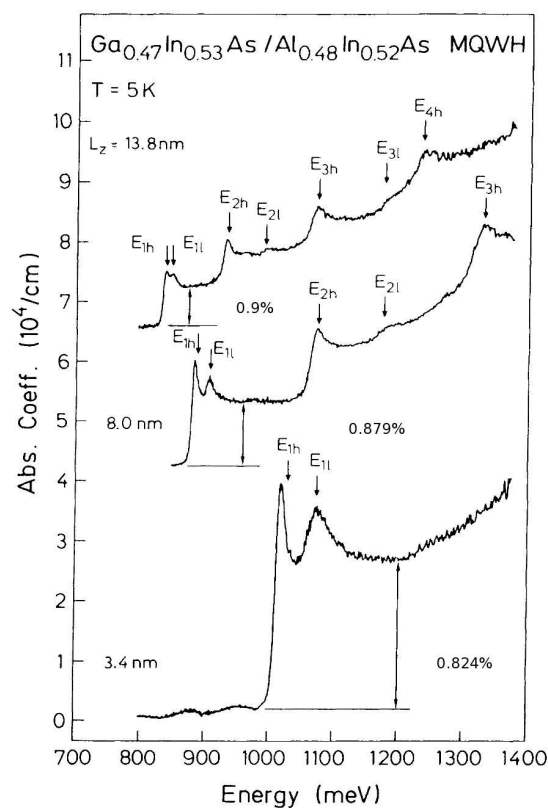
Figure 6.11: Absorption for quantum wells of various thicknesses

6.2.3 Effect of strain

The use of strained layers has been a very important milestone in the development of quantum well lasers.
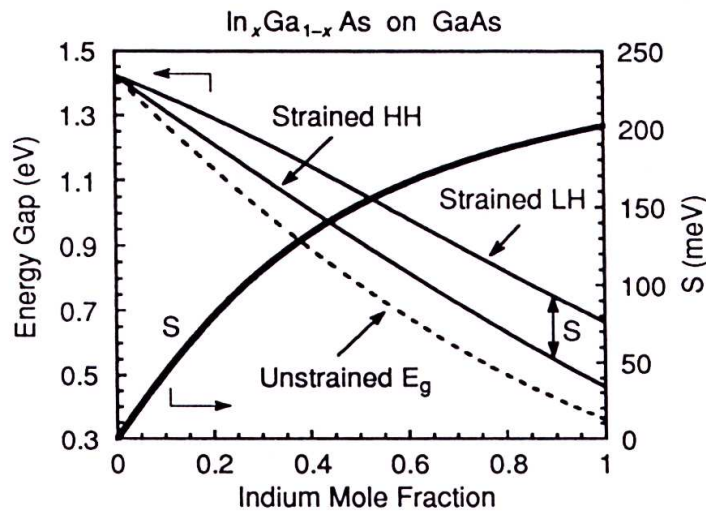
Figure 6.12: Effect of the material strain on the band structure. The strain anisotropy will split the valence band degeneracy between the HH and LH states by a value S

In the early nineties, it was realized that even thought lattice matching had to be preserved at all costs for the growth of quantum well lasers when thick layers were involved, one could grow very thin layers pseudo-morphically, i.e. in such a way that the grown material adapts its lattice to the one of the substrate. The result is a material in which very large amount of strain can be incorporated, corresponding to a lattice mismatch as high as 2%. The resulting strain is very anisotropic, as the material is constrained in the plane of the layer but can adapt its lattice spacing along the growth axis. The effect of this anisotropic strain is to split the valence band maximum and split the heavy hole and light hole bands by a value S, as indicated on figure 6.12. As the HH states derived from the $|\frac{3}{2}, \frac{3}{2}\rangle$ are heavy along the growth axis but light in the plane, the effective density of state in the plane is strongly reduced.
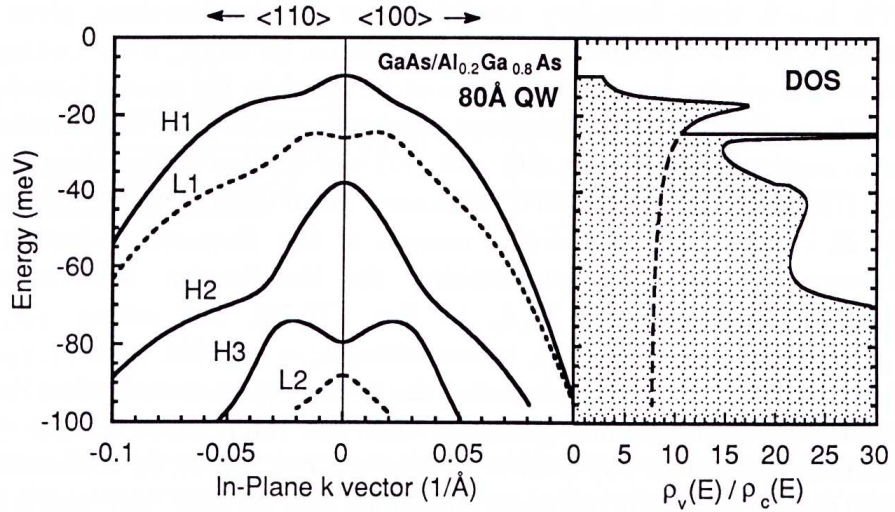
Figure 6.13: Valence band dispersion and density of state for a unstrained 8nm thick GaAs quantum welll
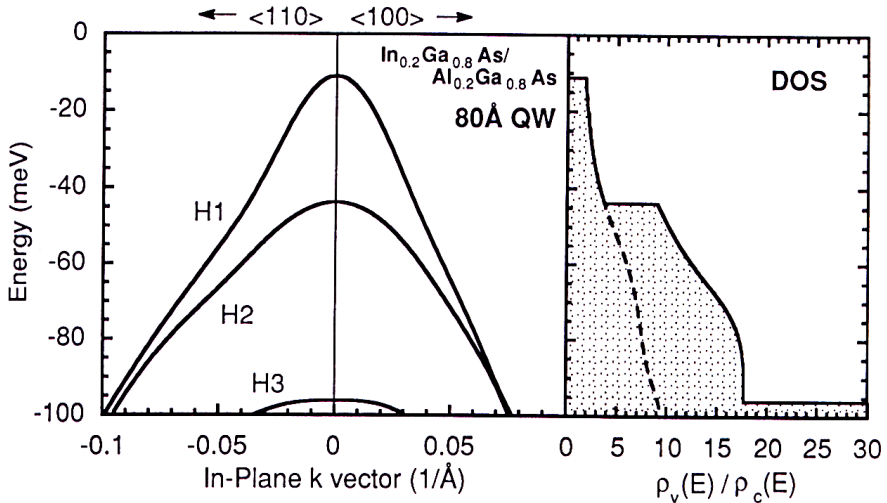
Figure 6.14: Valence band dispersion and density of state for a strained 8nm thick InGaAs quantum welll with 20% Indium

The figures 6.13 and 6.14, showing the dispersion along with the effective density of state, show the significant reduction in the density of state of the valence band that can be obtained by about 1% strain in the quantum well. As a result, the density of carrier needed to reach transparency, and as a result the transparency current density, are very strongly reduced, as shown in Fig. 6.15, 6.16, 6.17.
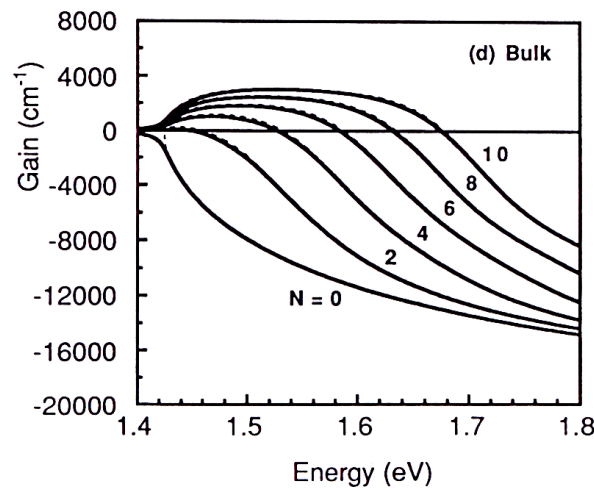
Figure 6.15: Computation of the gain for various carrier densities (indicated in units of $10^{18} cm^{-3}$): bulk GaAs.
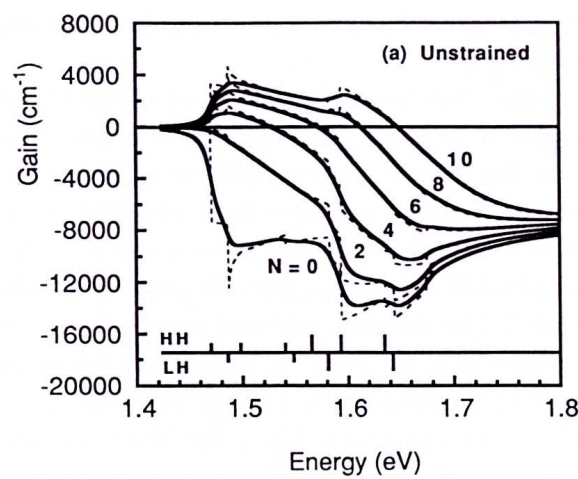
Figure 6.16: Computation of the gain for various carrier densities (indicated in units of $10^{18} cm^{-3}$): unstrained GaAs QW.
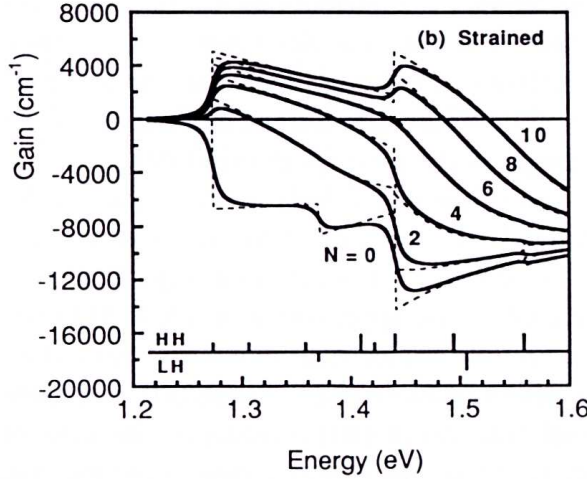
Figure 6.17: Computation of the gain for various carrier densities (indicated in units of $10^{18} cm^{-3}$): a strained 8nm thick InGaAs quantum welll with 20% Indium

6.3   Intersubband absorption

6.3.1   First approach: dipole in a one-band model

We use the same approach as above, using again the dipole interaction Hamiltonian. We now consider a transition between two conduction band states:

$$|nk_\perp\rangle = \frac{1}{\sqrt{A}}\chi_n(z)e^{ik_\perp r_\perp}u_c r \tag{6.3.47}$$

to a conduction band

$$|mk'_\perp\rangle = \frac{1}{\sqrt{A}}\chi_m(z)e^{ik'_\perp r_\perp}u_c r \tag{6.3.48}$$

where, again $r = (r_\perp, z)$ is the position and $r_\perp$ is the in-plane coordinate and A the sample's area. The matrix element is then

$$\langle mk'_\perp|\mathcal{E}\cdot r|nk_\perp\rangle = \frac{1}{A}\int_{space} d^3r \chi_m^*(z)e^{-ik'_\perp r}u_c^*(r)\mathcal{E}\cdot r\chi_n(z)e^{iqr}e^{ik_\perp r}u_c(r). \tag{6.3.49}$$

As above, we procceed the same way as for the interband case and we:

- Break the integral into a sum of elementary cells $\sum_{i_x,i_y,i_z}$ over which the integral is carried over

- Assume that the envelope functions are slowly varying and therefore can be pulled out in front of the integrals.

We then obtain:

$$\langle mk'_\perp|\mathcal{E}\cdot r|nk_\perp\rangle = \frac{1}{A}\sum_{i_z}\chi_m^*(z_i)\chi_n(z_i)\frac{a_z}{N_xN_y}\sum_{i_x,i_y}e^{i(k_\perp+q-k'_\perp)r_{\perp,i}}$$
$$\frac{1}{V_{cell}}\Big[\int_{cell}d^3r'u_c^*(r')\mathcal{E}\cdot r'u_c(r)e^{i(k_\perp+q-k'_\perp)r'} \tag{6.3.50}$$
$$+\mathcal{E}\cdot r'\int_{cell}d^3r'u_c^*(r')u_c(r)e^{i(k_\perp+q-k'_\perp)r'}\Big].$$

In this case, it is the first integral that vanishes and the second part that remains:

$$\langle mk'_\perp|\mathcal{E}\cdot r|nk_\perp\rangle = \delta(k_\perp+q-k'_\perp)\sum_{i_z}\chi_m^*(z)\chi_n(z_i)a_z\mathcal{E}\cdot r' \tag{6.3.51}$$

that can be converted into an integral that finally yields:

$$\langle mk'_\perp|\mathcal{E}\cdot r|nk_\perp\rangle = \delta(k_\perp+q-k'_\perp)\mathcal{E}_z\int_{-\infty}^{\infty}dz\chi_m^*(z)z\chi_n(z) \tag{6.3.52}$$

As in the interband case, the matrix element should be inserted in Fermi's golden rule;

$$w_{v\to c} = \frac{\pi}{2\hbar}q^2|\langle m,c|z|n,v\rangle|^2. \tag{6.3.53}$$

As in the interband case, it should be summed in k-space for all available states that satisfy the k-selection rule. Since the subbands are paralell in this one-band model, absorption exists only when the pair of subband is separated by exactly the photon energy:

$$\alpha(\hbar\omega) = \frac{\pi}{2\hbar}q^2|\langle m,c|z|n,v\rangle|^2.\delta(E_m-E_n-\hbar\omega)(n_n-n_m) \tag{6.3.54}$$

6.3.2 Absorption in a quantum well: a two-band model

The problem arising with the previous model is that it does not allow the introduction of non-parabolicity. It is valid then only for confinement energies much smaller than the bandgap $(E_n, E_m << E_G)$. One could be tempted to use the same approach when computing the absorption in the multiband case, taking as the matrix element the envelope function of the electron. This approach was used in some of the works, but lead to difficulties since, strickly speaking, the envelope functions of the conduction bands are no longer orthogonal to each other $(\langle\chi_m|\chi_n\rangle \neq \delta_{nm})$.A much better approach is to compute the matrix element directly in the multiband model. If one wants to treat conduction band state, an effective two-band model is perfectly valid. Let us then assume a two-component wavefunction:

$$\Psi_1 = f_c^{(1)}u_c + f_v^1u_v \tag{6.3.55}$$
$$\Psi_2 = f_c^{(2)}u_c + f_v^2u_v \tag{6.3.56}$$

Let us then evaluate the matrix element p_z:

$$\langle\Psi_1|p_z|\Psi_2\rangle = \langle f_c^{(1)}u_c + f_v^{(1)}u_v|p_z|f_c^{(2)}u_c + f_v^{(2)}u_v\rangle$$
$$= \langle f_c^{(1)}u_c|p_z|f_c^{(2)}u_c\rangle + \langle f_c^{(1)}u_c|p_z|f_v^{(2)}u_v\rangle + \langle f_v^{(1)}u_v|p_z|f_c^{(2)}u_c\rangle + \langle f_v^{(1)}u_v|p_z|f_v^{(2)}u_v\rangle. \tag{6.3.57}$$

Let us consider the first term, it yields:

$$\langle f_c^{(1)} u_c | p_z | f_c^{(2)} u_c \rangle = \langle f_c^{(1)} | p_z | f_c^{(2)} \rangle \langle u_c | u_c \rangle + \langle f_c^{(1)} | f_c^{(2)} \rangle \langle u_c | p_z | u_c \rangle$$
$$= \langle f_c^{(1)} | p_z | f_c^{(2)} \rangle \tag{6.3.58}$$

Similarely, the second term will yield

$$\langle f_c^{(1)} u_c | p_z | f_v^{(2)} u_v \rangle = \langle f_c^{(1)} | f_c^{(2)} \rangle p_{cv} \tag{6.3.59}$$

Using similar derivations for the third and fourth terms, the result can be summarized in a matrix form:

$$p = \begin{pmatrix} p_z & p_{cv} \\ p_{cv}^* & p_z \end{pmatrix} \tag{6.3.60}$$

acting on the components (f_c, f_v) of the wavefunction. Dropping the diagonal terms as $p_z << p_{cv}$, we finally obtain:

$$\langle \Psi_1 | p_z | \Psi_2 \rangle = \langle f_c^{(1)} | f_v^{(2)} \rangle p_{cv} + \langle f_v^{(1)} | f_c^{(2)} \rangle p_{cv}^* \tag{6.3.61}$$

Using the relationship between f_c and f_v given by the equation 6.1.18 and using the definition of the energy-dependent effective mass 6.1.20, we finally obtain:

$$\langle \Psi_1 | p_z | \Psi_2 \rangle = \langle f_c^{(1)} | \left(-i\hbar \frac{\partial}{\partial z} \right) \frac{m_0}{m(E,z)} + \frac{m_0}{m(E,z)} \left(-i\hbar \frac{\partial}{\partial z} \right) | f_c^{(2)} \rangle \tag{6.3.62}$$

In this picture, both intersubband and interband transitions are treated on the same footing.

6.3.3   Experimental results

As mentionned above, the dipole matrix element for intersubband transition is non-zero only for the z-component of the electric field. As a result, a number of geometries have been developed to measure the absorption, as shown in Fig. 6.18.
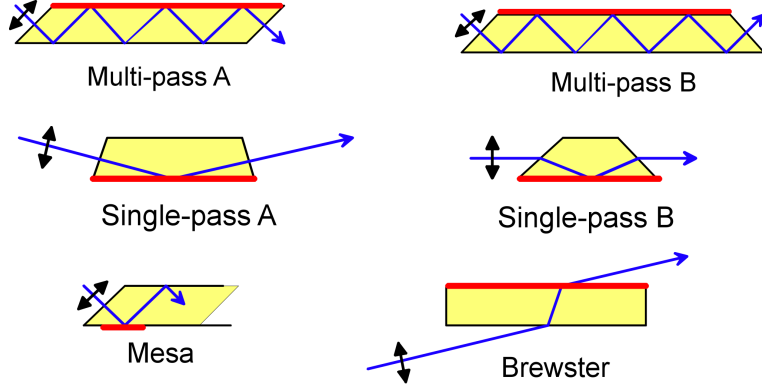
Figure 6.18: Experimental geometries allowing the measurements of intersubband transitions

An exemple of absorption between two subband is shown in Fig. 6.19.
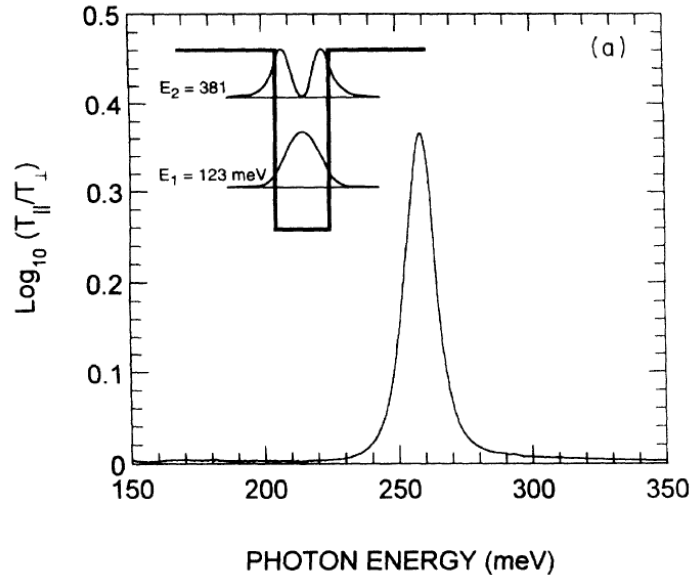
Figure 6.19: Intersubband absorption between two bound states

In contrast to interband transition, where the interband matrix element r_{cv} is the dominant term, the atomic-like nature of the joint density of state as well as the tailorability of the potential enables the fabrication of complex energy ladder structures.
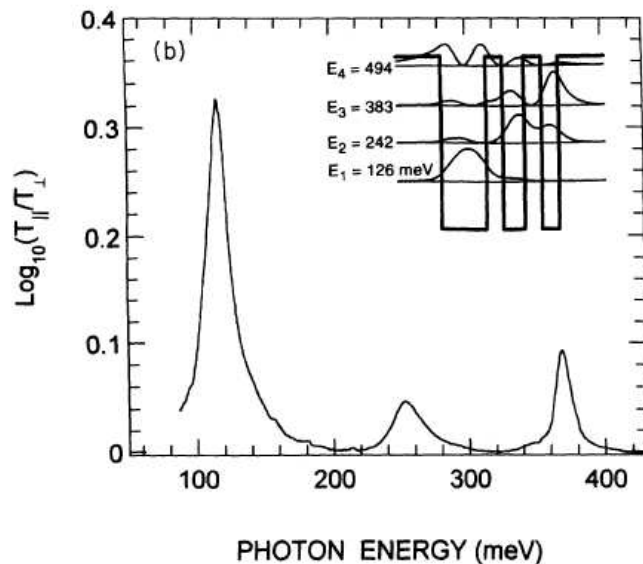
Figure 6.20: Intersubband absorption in a multiquantum well designed for triply resonant non-linear susceptibility

When the excited state is in a continuum, the absorption is broadened.
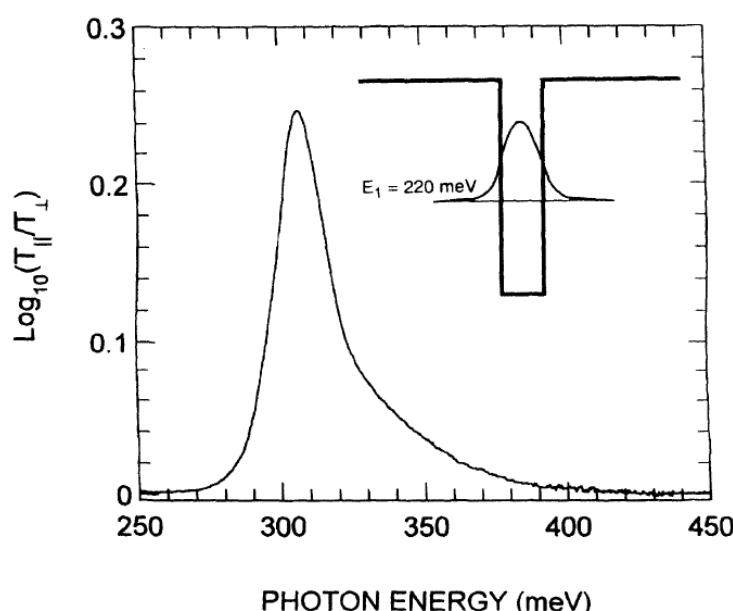
Figure 6.21: Intersubband absorption from a bound state to a continuum

Such quantum well absorption is the basis for the so-called Quantum Well Infrared Photo-conductors (QWIP) devices.

It is even possible to create quasi-bound states in the continuum using Bragg reflection, as shown in Fig. 6.22.
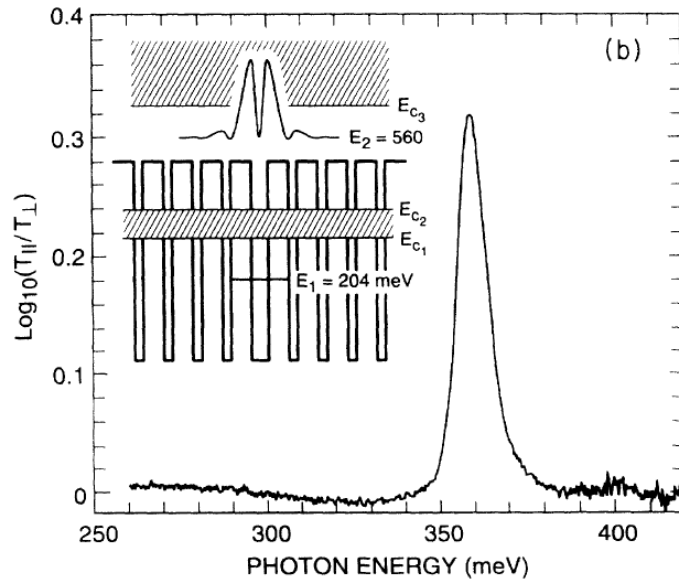
Figure 6.22: Bound-to-quasibound transition. The confinement of the upper state is created by Bragg electronic Bragg reflection

6.3.4 Intersubband absorption: multiband problem

Intersubband transitions are also possible in the valence band. However, the situation is much more complex because transitions with an interband character (i.e. where the Bloch part of the wavefunction is changed, such as a transition between HH1 and LH1 states) will coexist with transitions with a more intersubband character (like a transition between HH1 and HH2). The matrix element is in general dependent on the in-plane wavevector, further complicating the analysis. However, a multiband $k \cdot p$ analysis yields spectra that fit very well the epxerimental data.
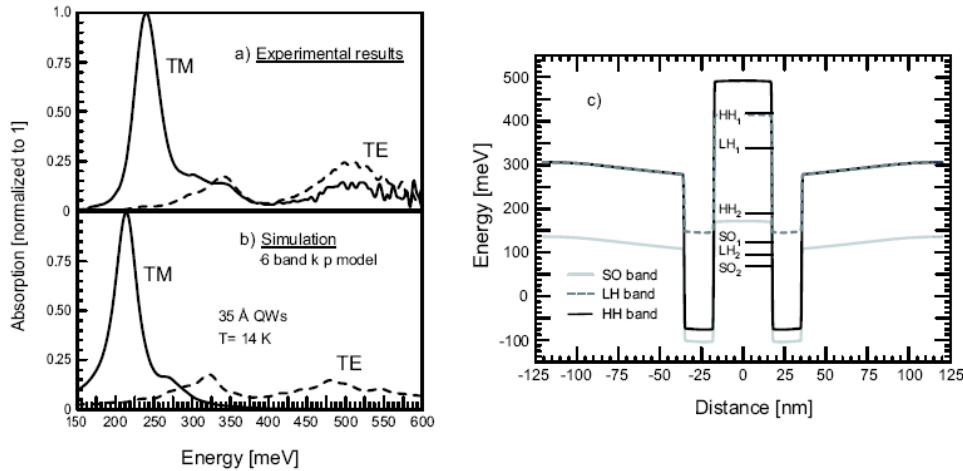
Figure 6.23: Intersubband absorption measurements for both light polarization directions TE and TM in a SiGe quantum well. Due to the presence of states with different Bloch wavefunctions, the absorption is allowed for both polarization directions. a) Experimental result. b) Computed absorption using a 6 bands $k \cdot p$ approach. c) Band structure of the quantum well, indicated the location of the different confined states as well as their main character (HH, LH, SO)

Chapter 7

Electric and Magnetic Fields

7.1 Franz-Keldish effect

The electric field $\mathcal{E}$ is applied on a bulk semiconductor of gap E_G. If we want to consider the most general situation the complete Schroedinger equation must be solved (not taking into account excitonic contribution):

$$\left(-\frac{\hbar^2}{2m_r}\nabla^2 - eFz \right) \psi_n(\mathbf{r}) = E_n\psi_n(\mathbf{r}) \tag{7.1.1}$$

The solution of this equation can be expressed as a combination of Airy functions. The oscillatory character of the Airy functions introduces oscillations in the absorption above bandgap.

The low energy absorption edge is modified according to the following formula:

$$\alpha_{FK} = \alpha(\omega, \mathcal{E}) \simeq \frac{8\pi^2|p_{cv}|^2}{\omega m_0^2 nc} \frac{\mathcal{E}}{E_G - \hbar\omega} exp\left[-\frac{4}{3F}\left(\frac{2m_r(E_G - \hbar\omega)}{\hbar^2} \right)^{3/2} \right] \tag{7.1.2}$$

Absorption now extends below E_g and the profile is modified (see continuous line Fig.7.1)
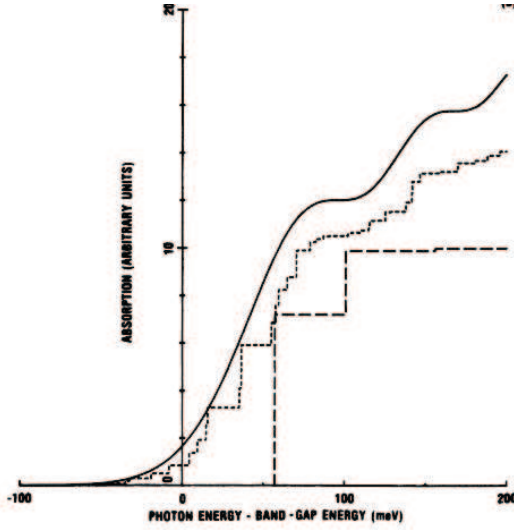
Figure 7.1: Absortpion edge calculated for bulk (continuous line) and quantum well for an applied electric field of 100 kV/cm

If excitonic effects are introduced, the absorption profile is modified according to the following formula:

$$\alpha(\omega) = \alpha_{FK} \left(\Gamma(1 - \frac{1}{\sqrt{\epsilon}})exp\left(\frac{1}{\sqrt{\epsilon}}ln\left(\frac{8\epsilon^{3/2}}{\mathcal{E}} \right) \right) \right)^2 \tag{7.1.3}$$

The main effect on the excitonic resonance is the blurring of the excitonic absorption peak as a function of the applied electric field.

7.2   Quantum confined Stark effect

The quantum confined Stark effect arises from the application of a DC electric field on a quantum well system. Two main configuration are analyzed: the electric field is parallel to the growth axis of the well or it is perpendicular to the growth axis.

7.2.1   Transverse QCSE

Interband case

When the applied electric field is sufficiently low, a perturbative approach can be followed. Let us evaluate the effect of an electric field $\vec{F}$ on a quantum well of width L. We consider the ground state in the conduction band and the first heavy hole state in the valence band. If we label the states as $|\psi_n^v\rangle$, $|\psi_m^c\rangle$ we can write the correction to the energy levels due to the perturbation $W = -eFz$. At the first order the energy correction to the levels will be zero because the quantum well is symmetric and the centroids of the wavefunctions will have the same expectation value:

$$\Delta E^I_{Stark} = \langle\psi^c_2|W|\psi^c_1\rangle - \langle\psi^v_2|W|\psi^v_1\rangle = e\mathcal{E}(\langle\psi^v_2|z|\psi^v_1\rangle - \langle\psi^c_2|z|\psi^c_1\rangle) = 0 \qquad (7.2.4)$$

We then consider the second order correction $E^{II}_n = \sum_{i\neq n}\frac{|\langle\psi_i|W|\psi_n\rangle|^2}{E_n - E_i}$: only the nearest levels will be included in the calculation and the energy correction will then be:

$$\Delta E^{II}_{Stark} = -e^2F^2\left[\frac{|\langle\psi^c_2|z|\psi^c_1\rangle|^2}{E^c_2 - E^c_1} + \frac{|\langle\psi^v_2|z|\psi^v_1\rangle|^2}{E^v_2 - E^v_1}\right] \qquad (7.2.5)$$

The application of an electric field results in a redshift of the transition: the effective bandgap of the quantum well is reduced. If we employ the infinite well approximation where the energy levels are expressed by $E_n = n^2\frac{\hbar^2\pi^2}{2m^*_{e,hh}L^2}$ and the matrix element is $z_{21} = \frac{16}{9}\frac{L}{\pi^2}$ we can express this energy shift in terms of:

$$\Delta E^{II}_{Stark} = -\frac{e^2F^2}{\pi^4\hbar^2}\left(\frac{16}{9}\right)^2\frac{2}{3}(m^*_e + m^*_{hh})L^4 \qquad (7.2.6)$$

where the strong dependence from the well width is explicit.
The excitonic resonance is not blurred but can be shifted for high values of the applied electric fields (see Fig. 7.3): this effect is at the basis of the electroabsorption modulators.

Intersubband case

In the intersubband case, we will obviously have zero shift at first order because of the symmetric profile of the quantum well. At the second order the calculation is analogous to what seen in the previous paragraph, by taking into account only the ground state and the first excited state of the quantum well. The shift in the intersubband case reads (evaluated for the conduction band):

$$\Delta E^{II}_{StarkISB} = 2e^2\mathcal{E}^2\frac{|\langle\psi^c_2|z|\psi^c_1\rangle|^2}{E^c_2 - E^c_1} = \frac{2^{10}}{3^5}\frac{e^2\mathcal{E}^2}{\pi^6\hbar^2}L^4 m^*_e \qquad (7.2.7)$$

Note that in this case the shift is positive: the ground state of the QW is lowered and the first excited state is lifted up. The intersubband transition in a symmetric quantum well will blue shift as a function of the applied electric field F. The range of validity of the perturbative treatment is given by $\Delta E_{QCSE} \ll E^0_2 - E^0_1 \simeq \frac{\hbar^2}{2m_e a^2}$. For a typical value of 100 kV/cm for the applied electric field, we obtain $\frac{\Delta E_{QCSE}}{E^0_2 - E^0_1} = 0.1$ for a L=12 nm wide quantum well. First order QCSE can be observed in asymmetric quantum wells or in coupled quantum well systems, like the quantum cascade laser

7.2.2 Longitudinal QCSE

In the longitudinal QCSE the main effect is the blurring of the excitonic resonance as observed in the bulk: this is expected since in the plane of the quantum well the carriers are free to move as in the bulk.

7.2.3   Quantum Well exciton resonance in an electric field
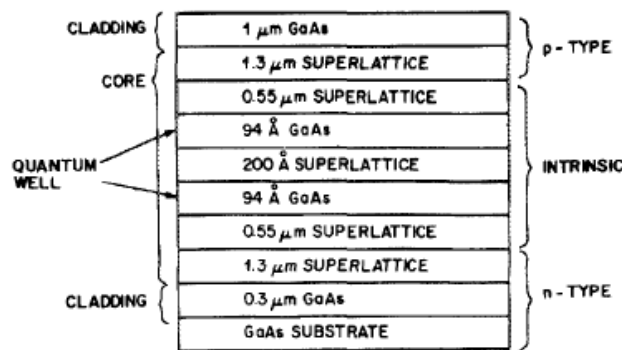
Figure 7.2: GaAs/AlGaAs multiquantum well structure
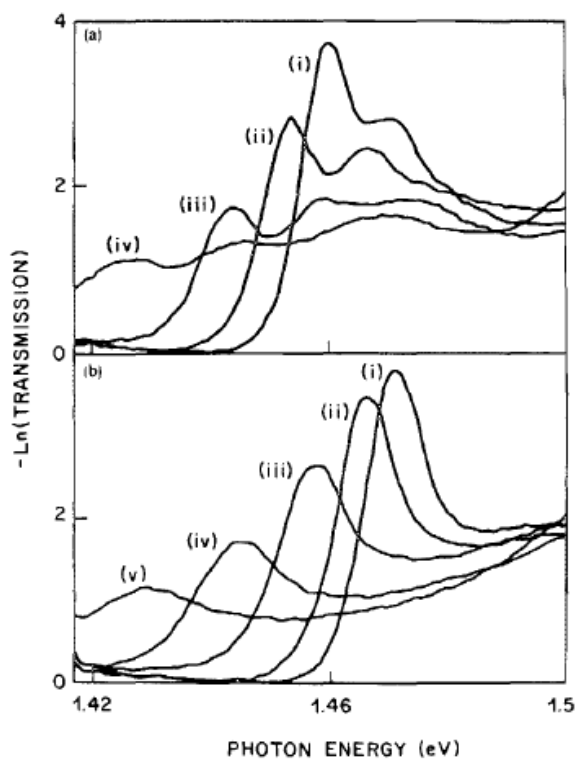
Figure 7.3: Absorption for increasing electric field (i) to (iv), with the light polarization in the plane of the layer (a) and perpendicular to the plane of the layers (b)

7.2.4 Piezo-electric fields in Nitride Quantum wells

7.2.5 Application: EA modulator
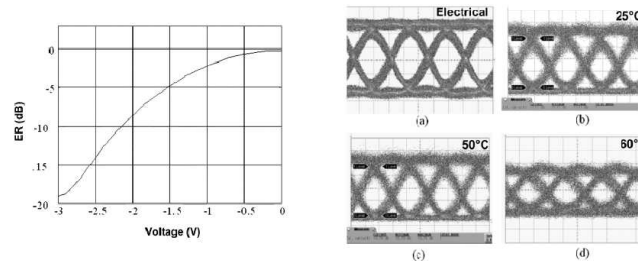
Figure 7.4: High frequency modulation experiments with a 40Gb/s electromodulator. Left: absorption versus applied voltage. Right: eye diagram for increasing frequency

7.2.6 QCSE in Ge quantum wells

An interesting application of QCSE in a Ge/SiGe quantum well structure. Althought the bandgap is indirect, the QCSE effect is strong because of the proximity of the Γ point of the band structure.
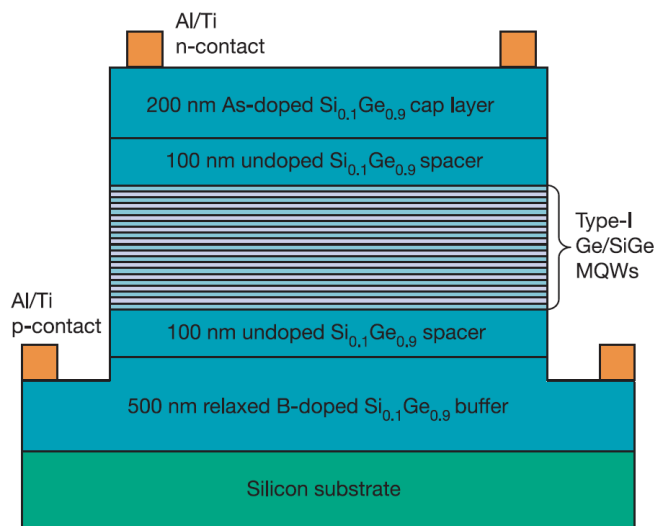
Figure 7.5: SiGe sample description
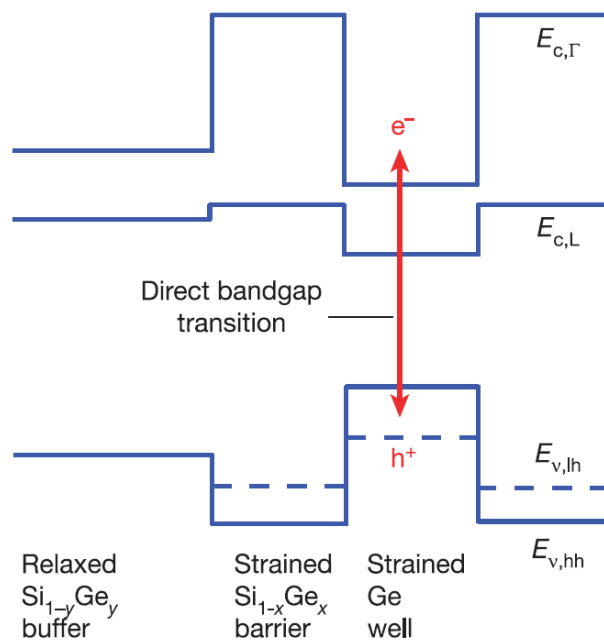
Figure 7.6: Band alignement of the various bands of the Ge/SiGe quantum wells structure
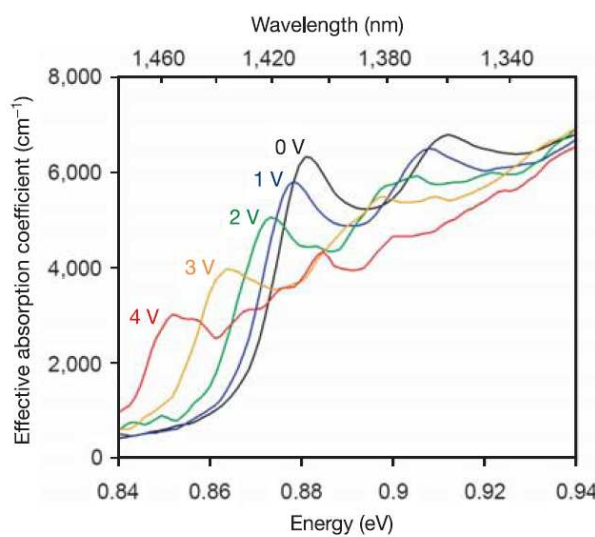
Figure 7.7: Results: absorption versus applied field, for increasing applied voltages

7.3 Cyclotron resonances

7.3.1 Classical approach

Let us describe first a purely classical model, where a carrier with charge q and effective mass m is subject to a damping term, an a.c. electric field with angular frequency ω and a static magnetic field $\vec{B}$ along the z-direction:

$$\frac{dm\vec{v}}{dt} + \frac{m\vec{v}}{\tau_m} = q(\vec{\mathcal{E}} + \vec{v} \times \vec{B}). \tag{7.3.8}$$

The cyclotron frequency ω_c is defined as (q has the sign of the particle charge)

$$\omega_c = \frac{qB}{m} \tag{7.3.9}$$

The d.c. Drude conductivity is:

$$\sigma_0 = \frac{nq^2\tau_m}{m} \tag{7.3.10}$$

A tensor of conductivity can be derived from the relationship between $\vec{j} = nq\vec{v}$ and the electric field $(j = \sigma\mathcal{E})$:

$$\sigma_{xx} = \sigma_{yy} = \sigma_0\tau_m^{-1}\frac{\tau_m^{-1} + i\omega}{(\tau_m^{-1} + i\omega)^2 + \omega_c^2}$$

$$\sigma_{xy} = -\sigma_{yx} = \sigma_0\tau_m^{-1}\frac{\omega_c}{(\tau_m^{-1} + i\omega)^2 + \omega_c^2} \tag{7.3.11}$$

$$\sigma_{zz} = \sigma_0\tau_m^{-1}\frac{1}{\tau_m^{-1} + i\omega}$$

Let us consider a now a light with circular (right) polarization; the electric field $\mathcal{E}_x = -i\mathcal{E}_y$. The conductivity σ_+ is:

$$\sigma_+ = \frac{j_x}{\mathcal{E}_x} = \sigma_{xx} + \sigma_{xy}\frac{E_y}{E_x} = \sigma_0\tau_m^{-1}\frac{\tau_m^{-1} + i\omega - i\omega_c}{(\tau_m^{-1} + i\omega)^2 + \omega_c^2} = \frac{\sigma_0\tau_m^{-1}}{\tau_m^{-1} + i(\omega + \omega_c)} \tag{7.3.12}$$

Similarely, the conductivity for the left polarized light writes:

$$\sigma_- = \frac{\sigma_0\tau_m^{-1}}{\tau_m^{-1} + i(\omega - \omega_c)} \tag{7.3.13}$$

We note that the conductivity σ_+ will have a resonance for $\omega = |\omega_c|$ while the same resonance will happen for holes and σ_-. The sharpness of the resonance will depend on the product $\omega\tau_m$.

7.3.2 Quantum model

For the quantum model, one starts with the usual Hamiltonian with the substitution for the momentum:

$$\vec{p} \rightarrow (\vec{p} - q\vec{A}) \tag{7.3.14}$$

The magnetic field is along the z direction, with a component in the y direction. We choose the gauge such that the potential vector is written as:

$$\vec{A} = (Bz\sin\theta, Bx\cos\theta, 0) \tag{7.3.15}$$

The total Hamiltonian for a quantum well is then

$$H = \frac{p_z^2}{2m} + V_{conf}(z) + \frac{1}{2m}\left(-i\hbar\frac{\partial}{\partial x} + qB_\perp z\right)^2 + \left(-i\hbar\frac{\partial}{\partial y} + qB_\| x\right)^2 + g^*\mu_B \sigma \cdot B \tag{7.3.16}$$

where the component of the field parallel to the growth axis

$$B_\| = B\cos\theta \tag{7.3.17}$$

and the component in the plane

$$B_\perp = B\sin\theta \tag{7.3.18}$$

have been used. The spin operator has the eigenvalues $\pm\frac{1}{2}$ and the coupling with the magnetic field is given by the Landé factor g^*. In general, the Hamiltonian 7.3.16 is not solvable exactly, and in particular is not separable as the in-plane component of the field is mixed with the confinement. In the case that the in-plane component can be neglected, the resulting Hamiltonian is:

$$H_\perp = \left[\frac{p_x^2}{2m} + \frac{1}{2m}\left(\hbar k_y + qB_\| x\right)^2\right]\phi_n(x) = E_n\phi_n(x) \tag{7.3.19}$$

which, as is apparent, can be mapped onto a Harmonic oscillator. The solutions are the celebrated Landau levels with energy:

$$E_n = \hbar|\omega_c|\left(n + \frac{1}{2}\right) \tag{7.3.20}$$

7.3.3 Determination of the effective mass

7.3.4 Application: InSb THz detector

7.3.5 Application: p-Ge laser

A p-Ge laser is a unipolar laser based on the motion of electrons in crossed electric and magnetic fields

7.4 Interband recombinaison in Magnetic Fields

In the first order, the bands are shifted by the zero point energy of the Landau levels. The situation is much more interesting in confined structures, especially quantum dots where the shift of the levels with magnetic field can be used to probe the eigenstates

Chapter 8

Second-order processes and quasi-particles

8.1 Interband absorption in indirect materials

In Si, Ge, AlAs, GaP, the minimum of the conduction band does not occur at the Γ point, while the maximum of the valence band does occur at this location. As a result, interband transitions at the bandgap involve always a momentum transfer. This one can be provided by any elastic or quasi-elastic process in principle. In practice, however, the most efficient process is the emission and absorption of zone-edge optical or acoustical phonons.
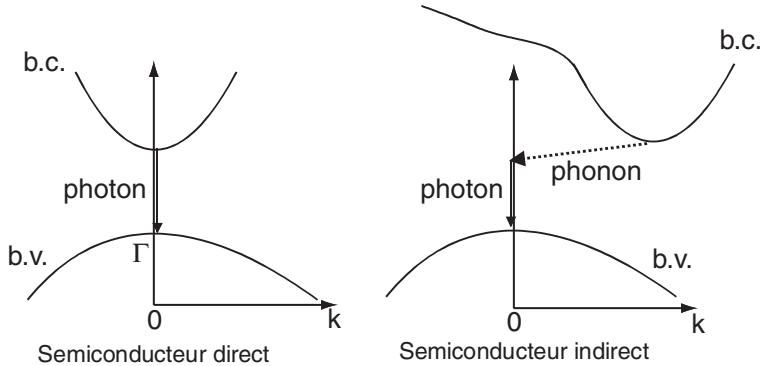
Figure 8.1: Schematic band structure diagram of a direct and indirect semiconductor

The rate at which such process occur can be computed using a second-order, time-dependent perturbation theory well described by Feynman diagrams. The rate of such process can be written as:

$$R_{ind} = \frac{2\pi}{\hbar} \sum_{k_c, k_v} |\sum_i \frac{\langle f|H_{eo}|i\rangle \langle i|H_{ep}|0\rangle}{E_{io} - \hbar\omega}|^2 \delta(E_c(k_i) - E_v(k_v) - \hbar\omega \pm E_p). \qquad (8.1.1)$$

In the above equation, H_{eo} is the coupling between the electron and the incident optical radiation; H_{ep} the coupling between the electron and the phonon population. The sum runs

over all possible intermediate states $|i\rangle$. The latter is either in the conduction band (if the virtual absorption occurs before the emission/absorption of phonon) or in the valence band (in the opposite case). The energy

$$E_c(k_i) - E_v(k_v) - \hbar\omega \pm E_p \tag{8.1.2}$$

and total momentum

$$k_v + q = k_c \tag{8.1.3}$$

is conserved in the process, q being the momentum of the phonon. In the latter equation

1. The δ function insures that at the end of the process, the energy is conserved.

2. Two classes of process exist: one in which a phonon is absorbed, one in which one is emitted. Obviously only the latter subsists at T = 0.

3. As the conduction band minimum is at the edge of the Brillouin zone, the momentum of the phonon q is much larger than the thermal wavevector of either initial or final state. As a result, the process does not conserve the wavevector of the electron or hole.

4. Therefore, we have to run the integral on both initial an final states with each a density of state with an energy dependence $\mathcal{D}_\sqsubseteq(E) = \sqrt{-E_v}$ and a final state $\mathcal{D}_\rfloor(E) = \sqrt{E_c - E_{ig}}$. We expect then a energy dependence as $(E - E_{ig} \pm E_p)^2$.

Taking also into account the dependence of the matrix elements in the phonon numbers:

$$\alpha(\omega) = \frac{\pi K}{8\omega} |P_{va}|^2 |H_{ac}|^2 N_c N_v n_{ph} x^2 \theta(x) + (n_{ph} + 1) y^2 \theta(y) \tag{8.1.4}$$

where the phonon occupation number is

$$n_{ph} = \frac{1}{\exp(\frac{\hbar\omega_{ph}}{kT}) - 1} \tag{8.1.5}$$

As a result the absorption edge is quadratic energy dependence, and is strongly temperature dependence.
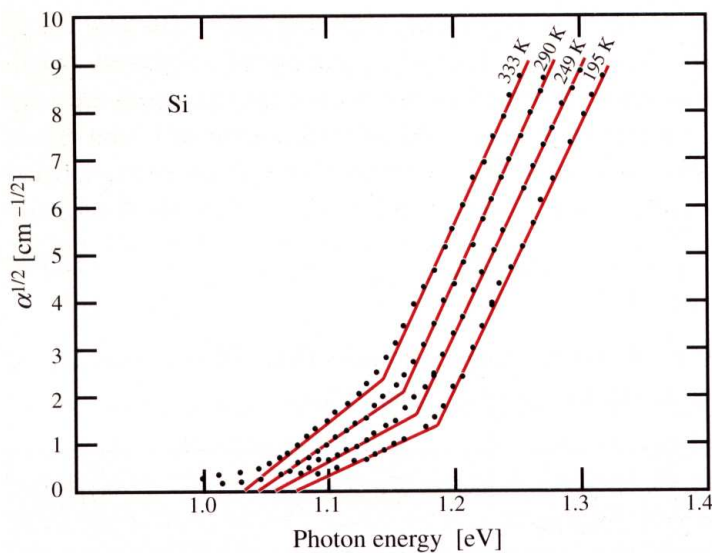
Figure 8.2: Plot of the square root of the absorption coefficient of Silicon as a function of photon energy for various temperatures, as indicated

The log plot of the absorption of the Germanium shows both the fundamental indirect gap at an energy of 0.65-0.75eV and the fundamental one at 0.85eV.
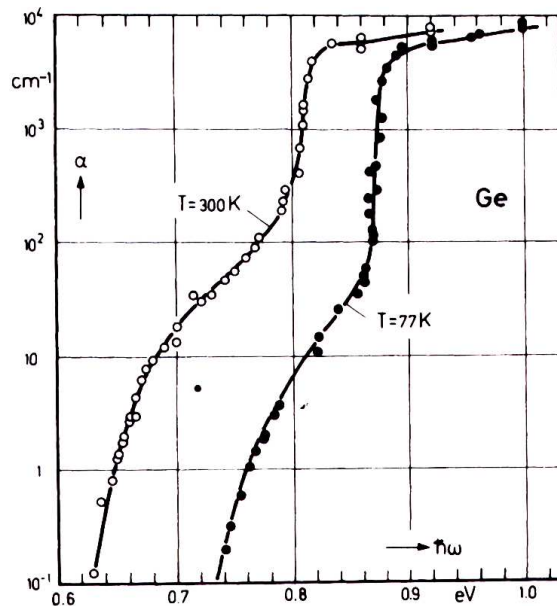
Figure 8.3: Log plot of the absorption of Germanium showing both the indirect fundamental gap and the higher energy direct gap

Interestingly, the very low absorption (and emissivity) of the indirect materials do not forbid *a priori* the fabrication of relatively efficient emitters. Of course, those can be realized only if the minority carrier lifetime can be brought by the reduction of other scattering mechanisms (impurities, deep trap, surface states) to a level comparable to the radiative lifetime, equal to about 14ms for Silicon at room temperature. Recent results along this line have shown efficiencies of more than 1%. However, a laser is believed to be impossible as the cross section for absorption is larger than the one for emission.

8.2   Free-carrier absorption

Free carriers are responsible for non-resonant light absorption. These phenomena are important parasitic mechanism in optoelectronic devices.

8.2.1   Classical model

We had derived in the third chapter the classical response of an electron gas. Assuming this classical model with no restoring force

$$\chi(\omega) = -\frac{\omega_p^2}{\omega}\frac{1}{\omega + 2i\gamma} \tag{8.2.6}$$

The imaginary part of the susceptibility is then:

$$\chi"(\omega) = \frac{\omega_p^2}{\omega}\frac{2\gamma}{\omega^2 + 4\gamma^2} \tag{8.2.7}$$

It can be related to the absorption coefficient $\alpha(\omega)$:

$$\alpha(\omega) = \frac{4\gamma\omega_p^2}{cn(\omega^2 + 4\gamma^2)} \tag{8.2.8}$$
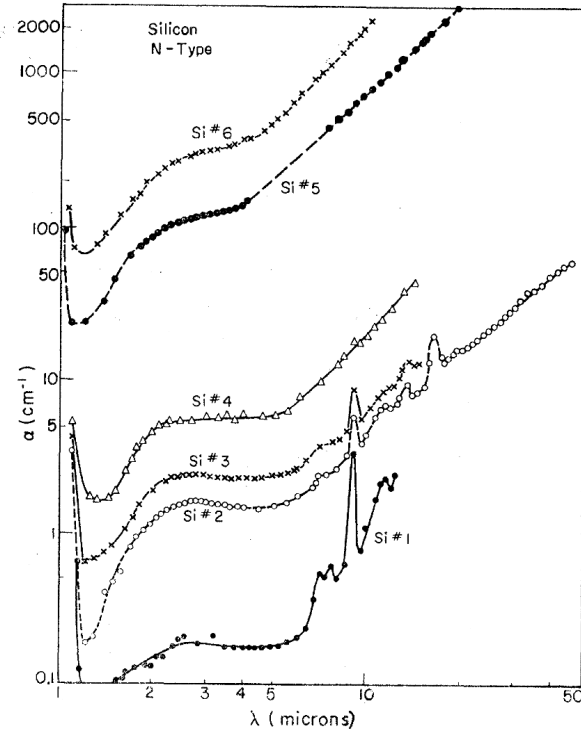
Figure 8.4: Room temperature free carrier absorption in silicon, for various carrier densities. #1: $1.4 \times 10^{16} cm^{-3}$ #2 $8.0 \times 10^{16} cm^{-3}$. #3 $1.7 \times 10^{17} cm^{-3}$ #4 $3.2 \times 10^{17} cm^{-3}$ #5 $6.1 \times 10^{18} cm^{-3}$ #6 $1.0 \times 10^{19} cm^{-3}$

This relationship predicts a ω^{-2} or λ^2 dependence of the free carrier absorption; the latter is approximately observed in experiments, as shown for the example of Silicon (if one neglects an impurity band present in the $\lambda = 2 - 5\mu m$)in Fig. 8.4. In other materials, a dependence in λ^p with $2 < p < 3$ is observed and is attributed to the variation of the damping term with frequency. Note that the specific choice made of the damping term in equ. 3.1.1 implies that the Drude scattering time is now $\tau_m = \frac{1}{2\gamma}$.

As for the case of the interband absorption in indirect materials, the absorption can be computed more rigorously using second-order perturbation theory.

$$S(i \rightarrow j) = \frac{\pi}{\hbar}|\sum_n \frac{\langle f|H_{op}|n\rangle\langle n|H_{ph}|i\rangle}{E_i - E_n} + \frac{\langle f|H_{ph}|n\rangle\langle n|H_{op}|i\rangle}{E_i - E_n}|^2\delta(E_{tot}) \qquad (8.2.9)$$

where the sum should be in principle carried over all processes: impurity, optical and acoustical phonons.

8.3 Excitons

When a electron-hole pair is created by absorption of a photon inside a semiconductor, the pair experiences an attractive Coulomb force. The latter is responsible for the creation of

a bound state called an exciton. The exciton can be loosely described by a Hydrogen-like system where electrons and holes orbit around their center-of-mass. One distinguish in the literature two type of excitons, depending essentially on the ratio of the exciton radius to the lattice spacing. When the attraction is so strong that the radius of the exciton is of the same order as the lattice spacing, one refers to a Frenckel exciton. Because of the small effective mass and the dielectric constant of the semiconductors, the exciton in a semiconductor is rather of the Wannier type, where the exciton radius is of many lattice periods.

8.3.1   Elementary treatement

Applying an effective mass description of the electron and hole, one easily maps the system onto a Hydrogenoid particule with reduced mass $\mu^{-1} = (m_e^*)^{-1} + (m_h^*)^{-1}$. The energy spectrum is the one of the Hydrogen atom:

$$E_n = -\frac{\mathcal{R}^*}{n^2} \tag{8.3.10}$$

where the renormalized Rydberg energy $\mathcal{R}^*$ is given by

$$\mathcal{R}^* = \frac{\mu}{m_0}\frac{\epsilon_0^2}{\epsilon^2}\mathcal{R} \tag{8.3.11}$$

were ϵ is the semiconductor dielectric constant. As the energy E_n is negative, the exciton features will appear as discrete eatures inside the material's bandgap.Both effective mass and dielectric constant are strongly dependent on the material's effective mass. As a result, and as shown in Fig. 8.5, the binding energy of the exciton grows strongly with the material bandgap. In large bandgap materials such as GaN, excitonic features are observed up to room temperature, whereas in narrow gap materials such as InAs they are difficult to observe even at cryogenic temperature.
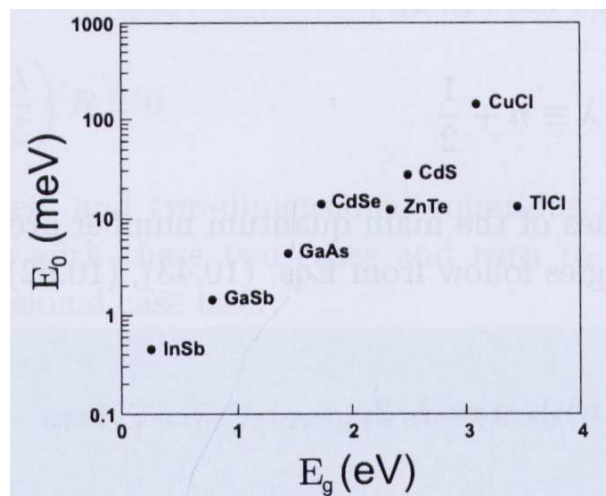
Figure 8.5:

8.3.2 Excitons in confined structures

Because they are states that cover a large number of lattice spacing, the excitons are well described by an envelope function formalism, where the two particule wavefunction is written as:

$$\Psi(r_e, r_h) = \sum_{k_e, k_h} C(k_e, k_h)\psi_{k_e}(r_e)\psi_{k_h}(r_h) \tag{8.3.12}$$

However, because the exciton is a localized state, it is more conveniently written in terms of a Wannier functions $a_n(r; R_i)$ of site R_i rather than in terms of the Bloch functions. Wannier functions and Bloch functions are defined by the set of reciprocal relations:

$$a_n(r; R_i) = \frac{1}{\sqrt{N}} \sum_k \exp(-ikR_i)\psi_{nk}(r) \tag{8.3.13}$$

$$\psi_{nk}(r) = \frac{1}{\sqrt{N}} \sum_{R_i} \exp(ikR_i)a_n(r, R_i). \tag{8.3.14}$$

The exciton wavefunction then writes:

$$\Psi(r_e, r_h) = \frac{1}{\sqrt{N}} \sum_{R_e, R_h} \Phi(R_e, R_h)a(r_e; R_e)a(r_h; R_h) \tag{8.3.15}$$

The exciton wavefunction is solution of the equation

$$\left[-\frac{\hbar^2}{2m_e}\nabla^2_{r_e} - \frac{\hbar^2}{2m_e}\nabla^2_{r_h} - fracq^2 4\pi\epsilon|r_e - r_h|\right]\phi(r_e, r_h) = -E\phi(r_e, r_h). \tag{8.3.16}$$

This is a hydrogen-like Hamiltonian that can be solved using the center-of-mass coordonates:

$$R = \frac{m_e r_e + m_h r_h}{m_e + m_h} \tag{8.3.17}$$

and a relative coordinate

$$r = r_e - r_h. \tag{8.3.18}$$

The two resulting equations are

$$-\frac{\hbar^2}{2M}\nabla^2_R\Psi(R) = E_R\Psi(R) \tag{8.3.19}$$

$$\left(-\frac{\hbar^2}{2\mu}\nabla^2_r\Psi(r) - \frac{q^2}{4\pi\epsilon r}\right)\phi(r) = E_r\phi(r) \tag{8.3.20}$$

where the reduced mass μ and the total mass $M = m_e + m_h$ have been used. The solutions of the center of mass equation are readily obtained:

$$\Psi_k(r) = \frac{1}{\sqrt{N}}\exp(-KR) \tag{8.3.21}$$

$$E_R = \frac{\hbar^2 K^2}{2M} \tag{8.3.22}$$

The solution for the relative motion follows the usual Hydrogen solution, where the wave-function is written as a product of a radial function and the spherical harmonics:

$$\phi_{n,l,m}(r) = R_{n,l}(r)Y_{l,m}(\theta,\phi) \qquad (8.3.23)$$

where $R_{n,l}$ are teh Laguerre polynomials and $Y_{l,m}(\theta,\phi)$ the spherical harmonics. The energy spectrum is then given by the same expression as shown above:

$$E_r(n) = E_r(\infty) - \frac{\mathcal{R}^*}{n^2} \qquad (8.3.24)$$

where the renormalized Rydberg energy is given by:

$$\mathcal{R}^* = \frac{\mu q^4}{2\hbar^2\epsilon^2} \qquad (8.3.25)$$

which the result already obtained in the preceding paragraph.

8.3.3 Quantum well

A interesting case is the one of the exciton confined in dimension in a quantum well. The envelope function for the exciton $\phi(r)$ follows now the Schrödinger equation:

$$\frac{\hbar^2\nabla_r^2}{2m_r}\phi(r) + V_{eff}(r)\phi(r) = (E - \frac{\hbar^2 K^2}{2M} - \epsilon_1^{(c)} - \epsilon_1^{(v)} - E_G)\phi(r) \qquad (8.3.26)$$

where the effective interaction potential now writes

$$V_{eff}(r) = \int dz_1 dz_2 \frac{q^2|\chi_1^c(z_1)|^2|\chi_1^v(z_2)|^2}{4\pi\epsilon\sqrt{r^2 + (z_1-z_2)^2}} \approx \frac{q^2}{4\pi\epsilon r} \qquad (8.3.27)$$

in the limit of the perfect two-dimensional case, valid when the exciton radius is much larger than the quantum well width. The equation is the one of a two-dimentional Hyrdrogen atom. The energies of the latter are defined by:

$$E_n = -\frac{\mathcal{R}^*}{(n-1/2)^2}. \qquad (8.3.28)$$

As a result, the excitonic confinement of the ground state is *multiplied by a factor of 4* compared to the bulk case. As a result, excitonic features are now observable in quantum wells at room temperature.

Chapter 9

Quantum dots

9.1 Basic ideas

We have seen that the gain in semiconductor laser is proportional to the product of the density of state and the Fermi distribution difference:

$$g(E) = C\mathcal{D}_j(\hbar\omega)(f_c(\hbar\omega) - f_v(\hbar\omega)) \tag{9.1.1}$$

where C is a prefactor that contains the matrix element and fundamental constants. Changing the dimensionality of the active region, i.e.going from a bulk material to a quantum well and finally a quantum wire and dot, because of the change in the density of state, has a strong influence on the maximum gain. Proposed already by Arakawa and Sakaki in their celebrated paper in 1982, they showed that in general the reduction of dimensionality had a very strong influence on lowering the threshold current density and decreasing the temperature coefficient of the gain. As shown schematically in Fig. 9.1, the density of state is narrowed by the reduction of the dimensionality.
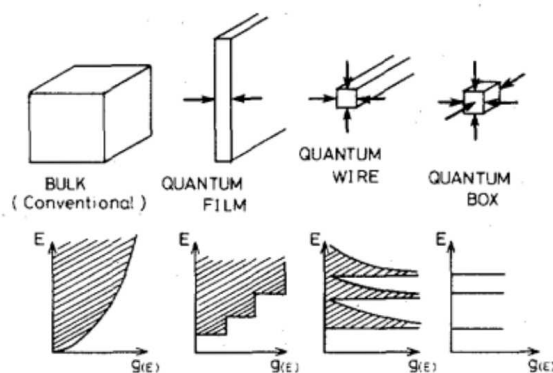
Figure 9.1: Comparison of the density of state for bulk, quantum wells, quantum wires and quantum dots.(Asada, IEEE JQE 1986)

As shown in Fig. 9.2 the gain should be greatly improved for a given carrier density when decreasing the dimensionality of the active region.
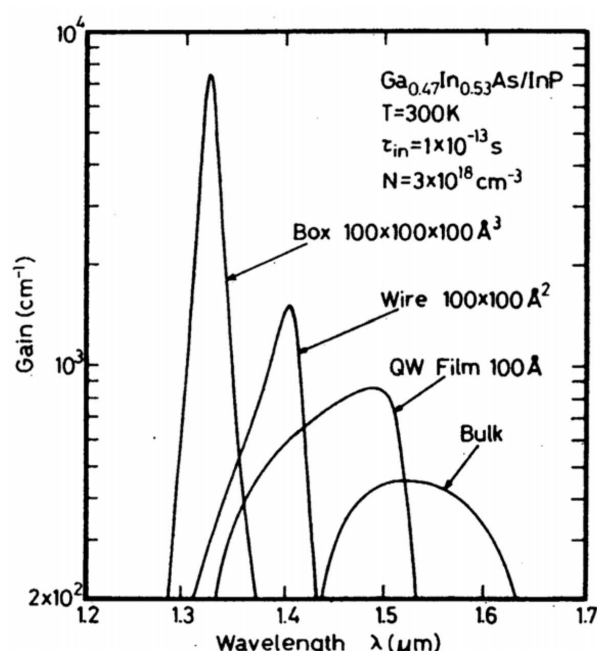
Figure 9.2: Comparison of the computed gain for bulk, quantum well, quantum wire and quantum dot material.(Asada, IEEE JQE 1986)

The temperature dependence of the threshold should be greatly improved, with a gain independent of the temperature in the limit of the quantum dots, as shown in Fig. 9.3
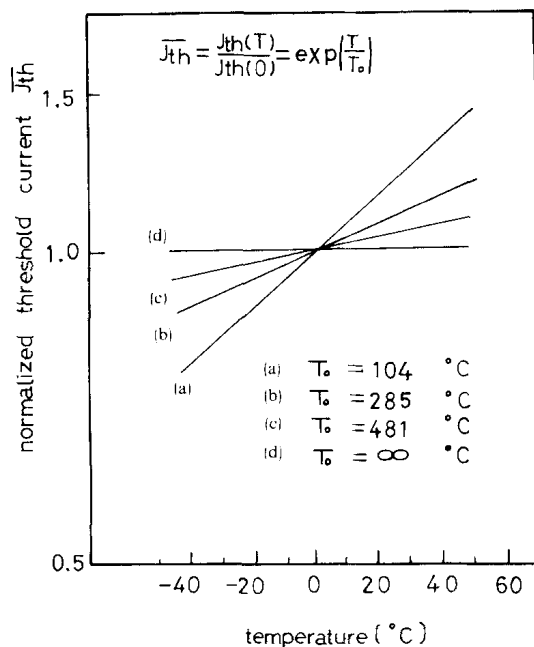
Figure 9.3: Comparison of the temperature dependence of the threshold current for bulk (a), quantum well (b), quantum wire (c) and quantum dot material (d).(Arakawa and Sakaki, APL 1982)

9.2 Fabrication issues

The problem of fabricating quantum dots with good size uniformity, crystalline quality and purity is a very difficult technical challenge. A large number of techniques have been used. At this point, the most successful is the self-assembly of dots by Stransky-Krastanow mode of 3D growth. This technique enables the fabrication of a relatively large density of dots with excellent purity and crystallographic quality and with reasonable size uniformity.
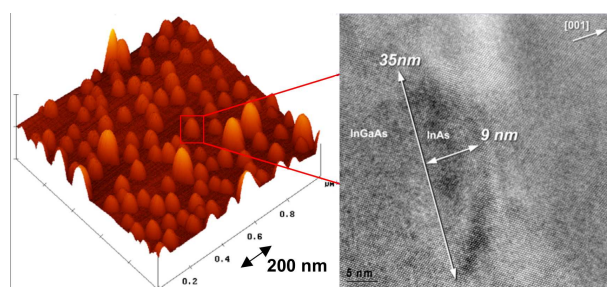
Figure 9.4: Atomic force microscopy image and transmission electron microscopy image of self-assembled quantum dots (data courtesy of Andrea Fiore)

9.3 Quantum dot luminescence

The luminescence of self-assembled quantum dots is shown in Fig. 9.5 as a function of pump intensity.
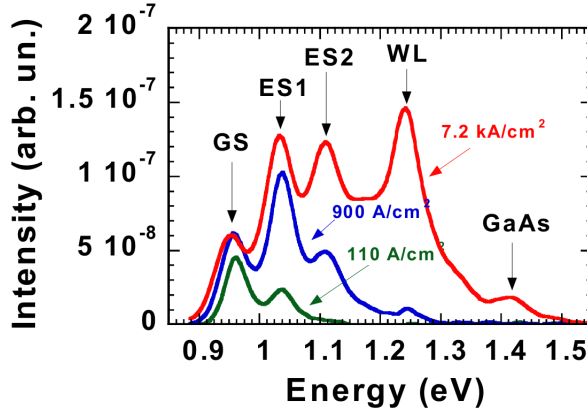
Figure 9.5: Luminescence of self-assembled quantum dots as a function of (data courtesy of Andrea Fiore)

The data show clearly the apparition of successive excited states as the pump intensity is increased. Those can be computed by an envelope function computation, taking into account strain and the three dimensional confinement. The broadening of the curve is almost completely caused by the size variation of the dots. The system is thus completely inhomogenously broadened.

9.4 Quantum dot lasers

The light versus current characteristics of a laser based on an active region with quantum dots is shown in Fig. 9.6. As compared to a quantum well material, the quantum dot has a very diffent behavior. The three essential physical differences are:

1. The active region is inhomogenously broadened

2. The capture time in the dot and interlevel scattering in each dot is significantly longer (about x10) than in quantum well structures

3. The total density of state per dot layer is much smaller than the one of a single quantum well

As a result, the devices exhibit in general a much lower gain (but can also show very low transparency current for the same reason). They also exhibit spectral hole burning features. Finally, the longer capture time and interlevel scattering time is detrimental to the slope efficiency and maximum modulation frequency.
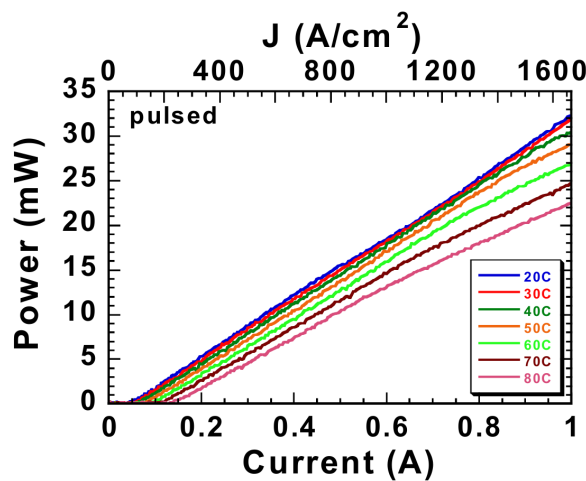
Figure 9.6: Optical power versus injected current characteristics of a quantum dot laser. (data courtesy of Andrea Fiore)

However, for the same reasons, these active region may have very interesting applications for optical amplifiers and superluminescent diodes. They can also exhibit very low values of the linewidth enhancement factor.